UNIVERSITÀ DEGLI STUDI
DI MODENA E REGGIO EMILIA

Dottorato di ricerca in Neuroscienze
in convenzione con l'Università degli Studi di Parma

Ciclo XXXII

H3.3A and H3.3B: unraveling the regional distribution and cellular expression of H3.3 histone variant isoforms in different physiological conditions

H3.3A e H3.3B: distribuzione regionale ed espressione cellulare delle isoforme della variante istonica H3.3 in diverse condizioni fisiologiche

Candidato: Dr.ssa Eleonora Daini

Relatore (Tutor): Prof. Michele Zoli

Correlatore (Co-Tutor): Dr.ssa Antonietta Vilella

Coordinatore del Corso di Dottorato: Prof. Michele Zoli

TABLE OF CONTENTS

Table of abbreviations

AA	Amino acid
Ab	Antibody
ac	Acetylation
αC	α-helix in the C-terminal
aCg	Anterior cingulate cortex
Ala, A	Alanine
APC	Allophycocyanin
Arc	Arcuate nucleus
ASF-1	Anti-silencing function-1
Asp, A	Aspartic acid
ATRX	Alpha-thalassemia/mental retardation X-linked syndrome protein
BAM	Border-associated macrophage
BDNF	Brain derived neurotrophic factor
BSA	Bovine serum albumin
bp	Base pair
CA1	Cornu Ammonis 1
CA3	Cornu Ammonis 3
CAF-1	Chromatin assembly factor 1
CAMKIIα	Calmodulin-dependent protein kinase II
CBX	Cerebellum
CC	Corpus callosum
CD206	Cluster of differentiation 206
CENP-A	Centromere protein-A
Cg	Cingulate cortex
CNS	Central nervous system
Coc	Cocaine
CpG	Cytosine-phosphate-guanine
CPu	Caudate-putamen
CR	Calretinin
CSDS	Chronic social defeat stress
C-tail	Carboxy-terminal tail
CTX	Cortex
Cys, C	Cysteine
DA	Dopamine
DAB	Diaminobenzidine
DAPI	4′,6-diamidino-2-phenylindole
DAXX	Death domain-associated protein
DBE	Dibenzyl ether
DCM	Dichloromethane

DCX	Doublecortin
DG	Dentate gyrus
DMSO	Dimethyl sulfoxide
DNMT1	DNA methyltransferase 1
EE	Enriched environment
ESC	Embryonic stem cell
EtOH	Ethanol
EDTA	Ethylenediaminetetraacetic Acid
FACS	Fluorescence-activated cell sorting
FACT	Facilitates chromatin transcription
FBS	Fetal bovine serum
FMO	Fluorescence minus one
FosB	Murine osteosarcoma viral oncogene homolog B
FSC	Forward scatter
Fw	Forward
GDNF	Glial-cell-derived neurotrophic factor
GFAP	Glial fibrillary acidic protein
GFP	Green fluorescent protein
Gln, Q	Glutamine
Glu, E	Glutamic acid
Gly, G	Glycine
gr	Granular layer
GS	Glutamine synthetase
H	Height
HA	Hemagglutinin
HAT	Histone acetyltransferase
HB	Helices bundle
Hb	Habenula
HBSS	Hank balanced salt solution
HDAC	Histone deacetylase
HFD	Histone fold domain
Hip	Hippocampus
HIRA	Histone regulator A
HJURP	Holliday junction recognition protein
hr	Hour
HRP	Horseradish peroxidase
Hyp	Hypothalamus
Iba1	Ionized calcium-binding adapter 1
IF	Immunofluorescence
IHC	Immunohistochemistry
Ile, I	Isoleucine
ir	Immunoreactivity

ISWI	Imitation switch
KD	Knock-down
KI	Knock-in
KO	Knock-out
L1	Loop1
Lmol	Lacunosum moleculare layer
LS	Lateral septum
LTP	Long-term potentiation
Lys, K	Lysine
me	Methylation
Men	Meninges
MeOH	Methanol
Met, M	Methionine
MGV	Mean grey value
mH2A	MacroH2A
min	Minute
miR	MicroRNA
mol	Molecular layer
NAc	Nucleus accumbens
NaN_3	Sodium azide
NAP-1	Nucleosome assembly protein-1
NDR	Nucleosome depleted region
NeuN	Neuronal nuclei
NHEJ	Non-homologous end joining
NPY	Neuropeptide Y
NS	Normal serum
N-tail	Amino-terminal tail
O/N	Overnight
obj	Objective
oligo(dA)	Oligodeoxyadenylated
p	Phosphorylation
PB	Permeabilization buffer
PBS	Phosphate buffered saline
PCR	Polymerase chain reaction
PE	Phycoerythrin
PENK	Proenkephalin
PFA	Paraformaldehyde
poly(A)	Poly adenylation
PTM	Post-translational modification
PV	Parvalbumin
RC	Replication-coupled
Rev	Reverse

RI	Replication-independent
RNA pol II	RNA polymerase II
RT	Room temperature
Rt	Reticular thalamus
S100B	S100 calcium-binding protein B
SAHF	Senescence-associated heterochromatic foci
Sal	Saline
SB	Staining buffer
SD	Standard deviation
SE	Standard environment
SEM	Standard error of the mean
Ser, S	Serine
SGZ	Sub-granular zone
SN	Substantia nigra
SP1	Specific protein 1
SS	Somatostatin
SSC	Side scatter
STED	Stimulated emission depletion
SWI/SNF	Switch/sucrose non-fermentable
SWR1	Swi2/Snf2-related ATPase
TAE	Tris-acetate EDTA
TF	Transcription factor
TH	Tyrosine hydroxylase
Thal	Thalamus
Thr, T	Threonine
TREM2	Triggering receptor expressed on myeloid cells 2
UTR	Untranslated regions
Val, V	Valine
VPL	Ventral posterolateral thalamic nuclei
VTA	Ventral tegmental area
WT	Wild type
W	Width
Φ	Hydrophobic amino acid

Abstract

Histone variants play a fundamental role in the complex scenery of epigenetic dynamics and chromatin remodeling; their replication-independent (RI) incorporation into chromatin and rapid turnover have recently suggested their involvement in central nervous system (CNS) pathophysiology and plasticity, though their precise role is still to be elucidated. The H3.3 histone variant, highly expressed in the brain, is encoded by two different intron-containing genes namely *H3f3a* and *H3f3b*. Although the coded proteins, H3.3A and H3.3B respectively, are identical, knocking out *H3f3b* generates a more severe phenotype compared to *H3f3a*, suggesting the lack of a complete functional overlap. This different impact may derive from a differential cell-type expression and regional distribution in the CNS. In order to investigate the functional role of H3.3 variant expression in the CNS it is therefore necessary to clarify the localization and cellular expression of the two isoforms. This will permit to define whether H3.3A and H3.3B turnover, alone or together, participates to molecular mechanisms that lead to neuroplasticity in specific neuronal circuits and associated functions.

In this project, hemagglutinin (HA)-tagged H3.3A (WT/HA-fH3.3A) and HA-tagged H3.3B (WT/HA-fH3.3B) mice were used to perform a detailed analysis of H3.3 isoform distribution in CNS white and grey matter regions, by using semi-quantitative immunohistochemistry (IHC). Moreover, cell-specific expression of these proteins was assessed by using specific antibodies against microglia, astrocytes, oligodendrocytes and neurons through double immunofluorescence (IF) stainings and high-resolution confocal microscopy. H3.3A and H3.3B have a widespread though different region-specific distribution and, as concerns their cellular expression, they are mostly, though not exclusively, expressed by neurons. Additionally, stimulated emission depletion (STED) microscopy was employed to assess H3.3A and H3.3B co-localization with H2A.Z variant. Next, we investigated the possible changes in H3.3 expression in various physiological conditions, including ageing and exposure to an enriched environment (EE), a procedure that models the neurotrophic and neuroprotective impact of high educational attainment in humans. In this latter model, an increased expression of H3.3B variant in specific brain areas and cell types was observed. Innovative techniques such as tissue clearing and light sheet microscopy allowed us to obtain an overall view of H3.3 isoform distribution in the whole brain after EE exposure. Additionally, fluorescence-activated cell sorting (FACS) analysis revealed an increment in H3.3B expression in microglial cells in EE housed mice with respect to SE housed mice.

Finally, sub-chronic cocaine (Coc) treatment was able to increase the number of H3.3B expressing cells in the nucleus accumbens (NAc).

Our results demonstrate for the first time a different regional distribution and cellular expression of the two H3.3 isoforms in the mouse CNS as well as their changes in physiological and pharmacological conditions. This opens up a path to the generation of cell population-specific conditional knock-out (KO) mice to elucidate H3.3 isoform contribution to the functions of precise cerebral circuits.

Riassunto

Le varianti istoniche svolgono un ruolo fondamentale nel complesso scenario dell'epigenetica e del rimodellamento della cromatina; l'evidenza della loro incorporazione replicazione-indipendente all'interno della cromatina e di un turnover rapido hanno recentemente portato a ipotizzare un loro coinvolgimento nella fisiopatologia e plasticità del sistema nervoso centrale (SNC), ma rimane ancora da chiarire quale parte svolgano in questi processi. La variante istonica H3.3, altamente espressa nel cervello, è codificata da due diversi geni chiamati *H3f3a* e *H3f3b*. Sebbene le proteine che ne derivano, rispettivamente H3.3A e H3.3B, siano identiche, inattivando *H3f3b* si genera un fenotipo più grave rispetto a *H3f3a*, il che suggerisce la mancanza di una completa sovrapposizione funzionale. Questi diversi fenotipi potrebbero derivare da una diversa espressione cellulo-specifica e distribuzione regionale nel SNC delle due isoforme. Al fine di comprendere il ruolo funzionale dell'espressione della variante H3.3 nel SNC è necessario dunque chiarire la localizzazione e l'espressione cellulare delle due isoforme. Questo consentirà di definire se il turnover di H3.3A e H3.3B, singolarmente o insieme, è alla base di processi neuroplastici e alterazioni funzionali in specifici circuiti neuronali.

In questo progetto di tesi sono stati usati topi H3.3A (WT/HA-fH3.3A) e H3.3B (WT/HA-fH3.3B) che esprimono un tag di emoagglutinina per eseguire un'analisi dettagliata della distribuzione delle isoforme di H3.3, nelle regioni di sostanza bianca e grigia del SNC, tramite immunoistochimica semi-quantitativa. È stata inoltre valutata l'espressione cellulo-specifica di queste proteine mediante l'utilizzo di anticorpi diretti contro microglia, astrociti, oligodendrociti e neuroni grazie a tecniche di doppia immunofluorescenza e microscopia confocale ad alta risoluzione. H3.3A e H3.3B hanno una differente distribuzione nel SNC, per entrambe molto diffusa ma eterogenea, e, per quanto riguarda la loro espressione cellulare, sono per la maggior parte, ma non esclusivamente, espresse dai neuroni. Inoltre, la co-localizzazione di H3.3A e H3.3B con la variante H2A.Z è stata studiata tramite l'utilizzo di microscopia STED. In seguito, abbiamo studiato i possibili cambiamenti nell'espressione di H3.3 in diverse condizioni fisiologiche, quali l'invecchiamento e l'esposizione ad ambiente arricchito, una procedura che mima gli effetti neurotrofici e neuroprotettivi di un livello elevato di istruzione negli uomini. In quest'ultimo modello, è stato osservato un incremento nell'espressione di H3.3B in specifiche aree cerebrali e specifici tipi cellulari. Tecniche innovative quali la chiarificazione dei tessuti e la microscopia a foglio di luce hanno permesso di ottenere una visione d'insieme della localizzazione dell'isoforma H3.3B, nell'intero cervello, in seguito all'esposizione ad ambiente arricchito.

Analisi FACS, eseguite su animali stabulati in ambiente arricchito, hanno rivelato un incremento di espressione di H3.3B in cellule microgliali corticali. Infine, il trattamento sub-cronico con cocaina si è rivelato in grado di aumentare il numero di cellule esprimenti H3.3B nel nucleo accumbens.

I nostri risultati descrivono per la prima volta la precisa distribuzione regionale ed espressione cellulare delle due isoforme di H3.3 nel SNC di topo così come i loro cambiamenti in varie condizioni fisiologiche e farmacologiche. Questo studio apre la strada alla generazione di topi knock-out condizionali per specifiche popolazioni cellulari al fine di comprendere il contributo delle isoforme di H3.3 in specifici circuiti cerebrali.

1. Introduction

1.1. Histones, nucleosomes and chromatin

Knowledge about chromatin has made remarkable progresses from Flemming's identification of a stainable substance inside eukaryotic cells, Kossel's extraction of basic nuclear proteins called by him "histones" and Miescher's isolation of the first chromatin preparation or "nuclein", in 1882, 1884 and 1891 respectively [1]. It is now known that chromatin is the combination of two nuclear elements namely DNA and histones, positively charged proteins necessary for DNA compaction; in fact, to fit inside the nucleus the genetic material needs to be coiled several times to achieve ultimately the chromosome conformation. The basic unit of chromatin is the nucleosome; in each nucleosome 146-147 base pair (bp) of DNA are wrapped around histones approximately 1.7 times while 10-90 bp of linker DNA separate one nucleosome from the other [2, 3]. There are 5 major histone families: H1/H5, H2A, H2B, H3 and H4; four of them, namely H2A, H2B, H3 and H4 are the components of the nucleosome whereas H1 binds to both DNA coils of the nucleosome and the linker DNA and it is called linker histone for that [3, 4]. Each nucleosome is composed of eight histone proteins: two H2A-H2B and two H3-H4 dimers. The two H3-H4 dimers assemble, in the center of the nucleosome, to form a highly stable tetramer while the two H2A-H2B dimers dock at the edges of the core particle after H3-H4 deposition (Fig. 1, a). Due to some amino acids (AAs) of H2A and H2B, each side of the nucleosome disc presents a negatively charged surface called acidic patch which is a very unique region in these basic proteins [5, 6].

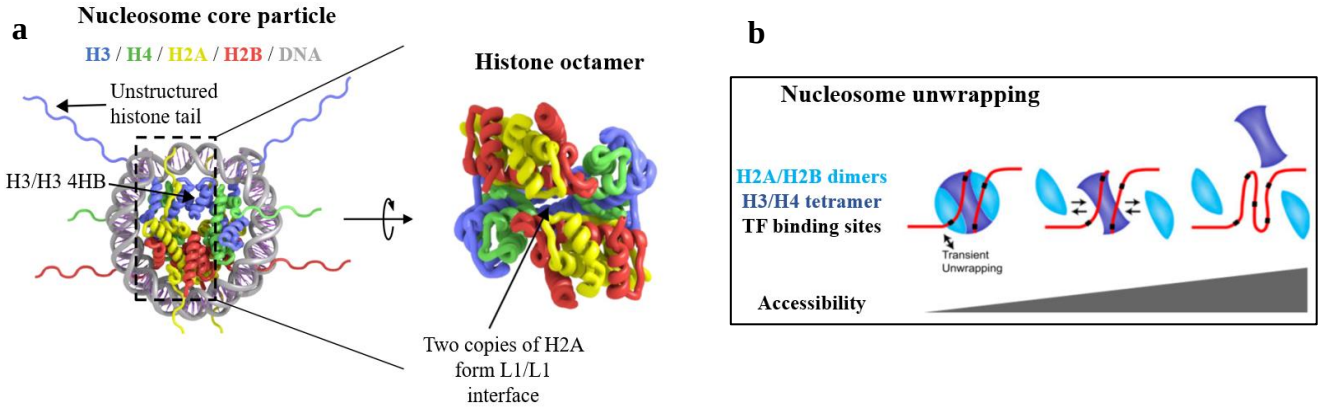

Fig. 1: a) Nucleosome structure. The two H2A-H2B dimers are at the edges of the DNA wrap whereas H3-H4 tetramer is in the center. H3/H3 interaction is mediated by the four helices bundle (HB) whereas H2A/H2A is mediated by their Loop1 (L1) region (modified from [26]). **b) Nucleosome turnover modulates DNA accessibility**. Nucleosome dissociation occurs more easily for H2A-H2B than for H3-H4, the unwrapping exposes DNA modulating the access to transcription factor (TF)-binding sites (modified from [5]).

There are several levels of organization of the chromatin structure which, according to Woodcock and Dimitrov [7], can be summarized in three major categories addressed as primary, secondary and tertiary. The first one is the linear arrangement of nucleosomes on DNA (e.g., 10 nm fiber or "beads on a strings") while the secondary structure (e.g., the 30 nm fiber with 6-11 nucleosomes per turn) is given by the interaction between nucleosomes, i.e., by the folding of the primary structure. Finally, the interaction of secondary structures forms the tertiary level; these chromatin higher-order structures culminate with chromosomes [3, 7].

Chromatin, at all organization levels, is extremely dynamic and each level, as well as their conformational changes, is implied in the control of DNA replication and transcription [8]. In fact, even if nucleosomes are stable structures, histone interactions with DNA are constantly changing; nucleosome shifting and/or eviction influenced by environmental stimuli, cell cycle phase or transcriptional needs, allows DNA exposure favoring gene expression along with DNA recombination and repair [9]. Additionally, histone turnover, that has been reported *in vivo*, may contribute to TF-binding site exposure; because of weaker intranucleosomal contacts, H2A-H2B turnover is faster than H3-H4 turnover which, in turn, requires a near complete unwrapping (Fig. 1, b) [10]. This is one of the many reasons why H3-H4 turnover is often considered as associated with activation of transcription [5].

137 years have passed from chromatin discovery but *in vivo* chromatin organization and dynamics, as well as how they correlate with transcriptional changes, are still not fully elucidated. What is known is that among the many factors influencing secondary structure changes (e.g., presence of H1 and ions) histone modifications and histone variants certainly play a crucial role.

1.2. Epigenetic inheritance and transcription

In 1956, the biologist Conrad Waddington demonstrated that changes in flies phenotype (thorax and wings structure) derived from exposure to specific environmental stimuli (temperature or chemicals) could be inherited by their progeny [11]. Observing this phenomenon, he coined the term epigenetics which literally means "above genetics". The sense of this term, once referred to all modifications influencing the phenotype but not the genotype, has recently narrowed. Epigenetic modifications can generate differences in gene expression without mutating the DNA sequence; these alterations are stable and can be heritable, in fact they can be considered as a sort of "cellular memory" [12]. Three are the key actors in the complex epigenetic landscape: i) covalent modifications of DNA bases such as DNA methylation, ii) post-translational modifications (PTMs) of histone tail AAs and iii) histone variants [13].

DNA methylation

DNA methylation in mammals is mediated by the DNA methyltransferase 1 (DNMT1) enzyme and occurs mainly in cytosines of the cytosine-phosphate-guanine (CpG) sequences; DNA methylation is essential for the stable maintenance and propagation of a silent chromatin state, especially through mitotic cell division and during embryogenesis. Epigenetic processes such as DNA methylation are implicated in the maintenance of X-inactivation and parental imprinting hallmarks [12, 13]. In fact, in vertebrates, loss of methylation induces apoptosis and embryonic lethality. *De novo* methylation after development is rare and usually associated with cancer [12]. However, a direct proof that epigenetics comprises more than just covalent modification of DNA bases derives from the presence of an epigenetic inheritance in organisms like flies and yeast which lack DNA methylation [14].

PTMs of histone tails

Almost the 25-30% of the total mass of a histone protrudes from the chromatin polymer surface generating what is commonly called histone tail (Fig. 1, a). The precise position of histone tails, in higher-order fibers, is still not clear but, being exposed, they provide a substrate for potential interactions with other proteins like histone modifying enzymes and chromatin remodelers. In fact, amino-terminal tails (N-tails) can be subjected to modifications such as acetylation (ac), methylation (me), phosphorylation (p), ubiquitination and ADP-ribosylation after the protein synthesis [15-17]. PTMs of histone N-tails, influencing contacts between DNA and histones and among histones, are involved in chromatin remodeling and in the regulation of gene transcription; for instance, *in vitro* evidence showed that acetylation loosens high-order structures favoring DNA exposure. Moreover, N-tails marks can be read by several proteins so that the ensemble of histone protruding nucleotides and their PTMs is commonly called the “histone code”; to properly interpret this code we need to consider that these marks may act in a sequential or combinatorial way on one or different tails [15-17]. Combination of multiple modifications may trigger different outcomes altering chromatin structure (*cis* mechanism) or generating a substrate for the binding of different effector proteins (*trans* mechanism) [15-18]; this histone code readout can explain exceptions to the common knowledge on chromatin organization which considers the addition of positive (e.g., ac) or negative (e.g., me) charges as relaxing or condensing chromatin, respectively. For instance, the phosphorylation of H1 and H3 tails is implicated in mitosis-related chromosome condensation but the phosphorylation of H3 Serine (Ser, S) 10 residue (H3S10p) is linked to the induction of c-jun, c-fos and c-myc [16].

The acetylation of lysine (Lys, K) residues is mostly associated with the activation of transcription (e.g., H3K9ac) while, depending on the residue and the number of methyl molecules added, transcriptional activity can be either activated (e.g., H3K4me3) or repressed (e.g., H3K9me3) by methylation [13].
Finally, epigenetic marks play a fundamental role not only in the propagation of gene activity states but also in the maintenance of genome stability through the silencing of centromeres and telomeres and transposable elements, respectively allowing the correct association to microtubules and avoiding insertional mutagenesis.

All these processes can occur during both development and cell proliferation but also in adult life by random changes or under environmental influences; in fact, some external and/or internal stimuli can revert or rouse epigenetic modifications [12]. A single enzyme (i.e., DNMT) is responsible for DNA methylation propagation whereas, as concerns histone modifications, multiple enzymes belonging to different complexes recognize and catalyze the reactions; these marks are stable but reversible. While during gametogenesis and embryogenesis epigenetic reprogramming occurs, the extent of histone marks retention between generations is still unknown [13]. Moreover, after the replication, old and new histones distribute randomly in daughter strands with little, but however existing, chance to produce strands with no marks at all. So, how histone marks are retained through a single or multiple rounds of cell division could not be explained only with the histone code hypothesis [14].

Histone variants

Histones can be distinguished in subclasses based on their primary AA sequence and their N-tail PTMs, but the major distinction concerns their regulation with respect to the cell cycle [19]. For decades, histone synthesis has been considered as tightly associated with DNA synthesis; this assumption came from the observation that inhibition of DNA synthesis caused the blockade of histone synthesis and from the absence of histone mRNAs in G1 cultured cells. Over the years, this shortsighted vision has changed and along with these “S-phase histones” another class of proteins, addressed as “basal histones”, was first discovered *in vitro*; these new histones are not necessarily coupled with S phase, are less inhibited by DNA-synthesis inhibition and represent approximately the 10% of the total histone synthesis [20].
Histones whose expression is strongly correlated with DNA synthesis are now called canonical or replication histones whereas “basal histones” are now addressed as replacement variants [19, 21]. Since canonical histones (H2A, H2B, H3 and H4) are incorporated into chromatin in a replication-dependent manner (replication-coupled, RC), they are highly expressed in a rather small period coincident with S

phase and therefore are responsible for packaging newly synthetized genome and filling the gaps behind the replication fork. On the contrary, the deposition of histone replacement variants, being replication-independent (RI), may occur throughout the cell cycle so that they can accumulate even after DNA replication, especially during cellular differentiation and development [5, 6, 9].
Histone replacement variants possess a slightly different primary sequence and a very different gene arrangement compared to their canonical counterparts; the organization pattern of canonical histones is similar for chickens, mice and humans where these genes are intron-free and arranged in nontandemly clustered cassettes [9, 19, 22]. On the contrary, histone variants genes are solitary, not grouped in clusters [6] and possess "intervening sequences", so that they are intron-containing [19]. Finally, mature mRNA of RI variants is polyadenylated while canonical histones present a unique stem-loop 3' end [23].

Together with nucleosome shifting and/or eviction mediated by ATP-dependent chromatin remodelers and with PTMs, the replacement of canonical histones with variants is an effective mechanism to influence nucleosome-DNA interplay, to make DNA more accessible to TFs and to allow RNA polymerase II (RNA pol II) translocation. RNA pol II binding occurs preferentially on H2A-H2B depleted nucleosomes and pol-mediated elongation contributes to the exchange of these dimers [5, 24]. While *in vitro* RNA pol II alone is able to evict H2A-H2B dimer during transcription, complexes such as facilitates chromatin transcription (FACT) seems to help RNA pol II in displacing H2A-H2B dimer *in vivo* [25]. Normally, both heterodimers, especially H3-H4 dimers, are exchanged and incorporated together to avoid nucleosome instability [9].

Specific complexes are responsible for RC incorporation of canonical histones and RI incorporation of variants into chromatin and, as previously stated, their deposition can have major influence on gene expression. For instance, chromatin assembly factor 1 (CAF-1) is responsible for the deposition of H3-H4 but not of dimers with variants of H3 [9, 14]. Additionally, histone variants can be modified on their N-tails but these marks are not entirely the same as those of canonical histones suggesting that histones are probably modified when assembled and that histone modifying enzymes are able to identify different chromatin targets [14].

Notably, variant synthesis and incorporation into chromatin independently of DNA replication suggests their potential relevance to both transcription and epigenetic formation and maintenance.

1.3. H4 and H2B limited evolutionary specialization

Eukaryotic histones derive from archaeal histones, first identified in the Euryarchaeal lineage (*M. fervidus*). These archaeal histones are quite different from the eukaryotic ones since they present a single histone fold domain (HFD) with three α-helices, two intervening loops and no N- or Carboxy-terminal tails (C-tails). These ancient histones called HMfA and HMfB (from histone *M. fervidus* A and B) can assemble in both homodimers and heterodimers to form a tetramer which protects and packages 60 bp of DNA. Apparently, H3 and H4 are more similar to HMfA and HMfB and are therefore thought to have evolved before H2A and H2B; the origin of these two latter histones represented the shift from tetramers to octamers, probably due to the need of increasing packaging, dependent on the increment in genome size. Linker histones and histone tails are other evolutionary acquisitions to achieve higher levels of compaction. Generally speaking, histone proteins are highly conserved throughout evolution, especially canonical H3 and H4 [6, 19].

H4 is the most slowly evolving histone; it has remained constant without any evident AA changes in fungi, plants and animals. In these species it is also not possible to distinguish between canonical and RI variants while, in mammals, they are only the products of the alternative processing of the same transcript. So H4 does not exhibit any true RI variant whereas, from all other histones, different variants have evolved probably to fulfill distinct roles in transcription; H4 conservation may be necessary since, being a central protein in the nucleosome, it makes close contacts with all other histones and changes in its sequence may disrupt these contacts [6].

On the contrary, a lot of H2B variants developed in mammals but, as for H4, H2B evolutionary specialization is limited to few functions; in fact, most of H2B variants are testis-specific (e.g., H2B.1) and specialized for gametic functions (e.g., SubH2Bv is associated with rodent and bovine acrosome formation) [6]. Recently, a new variant named H2B.E has been characterized; with only 5 AAs different from H2A, it seems to regulate olfactory neuron function in mice. Moreover, H2B.1 and H2B.E genes do not exhibit the typical histone variant organization but are located in gene clusters as canonical histones; the only other variant with this peculiarity is the testis-specific H2A variant (H2A.1) [26]. H2B has very conserved structure with an α-helix in the C-terminal (αC) which protrudes from the nucleosome disc and favors its interaction with the DNA; this might explain the lack of evolutionary changes concerning its sequence [6].

1.4. H2A and its replication independent variants

The H2A histone family comprehends the most diverse replacement variants; they may be found in most eukaryotic lineages (e.g., H2A.Z and H2A.X), only in vertebrates, (e.g., macroH2A (mH2A)), or only in mammals (e.g., H2A.B (H2A.Bbd)) [5, 6]. H2A proteins interact with each other inside the nucleosome through their L1 region (Fig. 1, a); the only other histone capable of self-interactions is H3 which, however, does not exhibit this particular loop. On the other hand, the C-tail is in contact with H3-H4 dimer and is called docking domain for that. The major structural differences between canonical H2A and its variants and among the different variants reside right in these two regions [6].

mH2A is the only histone containing, on its C terminus, a non-histone globular domain (~20 kDa) with strong homology to RNA viruses, eubacteria, archaea and eukaryotic proteins [5, 6]; this feature, called macro domain, makes mH2A three times the size of H2A. The non-globular part of this variant is approximately 60% identical to the canonical histone and allows the binding of specific complexes such as histone deacetylases (HDACs) [5, 9]. This RI variant has been found only in vertebrates (mH2A.1.1, mH2A.1.2, mH2A.2) and in very few invertebrates. *In vitro*, mH2A favors heterotypic (mH2A/H2A) nucleosome formation while H2A.Z and H2A.B display no preference [27]. *In vivo*, a mH2A enrichment on large transcriptionally silent loci, senescence-associated heterochromatic foci (SAHF), XY body in male meiosis and in the inactivated X chromosome (Barr body) can be observed, even if this variant is not required for X inactivation [5, 6]. Incorporation of mH2A into SAHF is mediated by the same chaperone responsible for H3.3 deposition, namely histone regulator A (HIRA), and by anti-silencing function-1a (ASF-1a) [9, 28]; additionally, mH2A inhibits switch/sucrose non-fermentable (SWI/SNF) family recruitment, ATP-remodeling complexes involved in canonical H2A-H2B dimers exchange [5, 29]. Altogether, these features, along with a rather high stability and the C-terminal domain interference with TF binding, point to a generally repressive role for this variant [5, 6].

H2A.X possesses a C-terminal extension, not present in the canonical H2A, with an hydrophobic residue (Φ) at the end of a Ser-Glutamine (Gln, Q)-Glutamic acid (Glu, E)/Aspartic acid (Asp, D) consensus sequence (SQ(E/D)Φ) crucial for the repair of DNA double-strand breaks and for chromatin condensation. H2A.X is generally deposited at disrupted nucleosomes and phosphorylated in the Ser residue of the consensus sequence [6, 9]. The spread in phosphorylation arising from this event is a marker for DNA damage and may be crucial, for the engagement and retention of chromatin remodelers, to promote DNA repair through non-homologous end joining (NHEJ) [6, 26].

In its non-phosphorylated state H2A.X is widely distributed independently of DNA lesion: for instance, H2A.X in male mammals is also capable of maintaining X and Y chromosomes transcriptionally silent in the meiotic prophase [6].

H2A.Z represents almost the 15% of total H2A and, contrary to H2A.X, it separated (and remained distinct) from canonical H2A in a single evolutionary event; it is, however, comparably conserved between species and is the most evolutionarily conserved among H2A proteins suggesting, along with the ancient specialization, a peculiar and unique role of this variant [6]. H2A.Z diverges by approximately 40% from H2A and its presence in the nucleosome seems to weaken the interaction with H3-H4 dimers, because of an AA substitution (Gln to Glycine, Gly or G) in the docking domain compromising three hydrogen bonds [5, 9]. Other structural divergences between H2A and H2A.Z are in the L1 and L2, responsible for self-interactions and DNA contacts, respectively [6]. Additionally, H2A.Z is more prone to stimulate imitation SWI (ISWI)-mediated (ATP-dependent remodeler) remodeling activity, presenting an extended acidic patch on its surface [5]. There are two H2A.Z isoforms (H2A.Z.1 and H2A.Z.2) differing by a single Ser-Threonine (Thr, T) substitution (Ser38Thr) in the HFD preceding the L1 [26].
H2A.Z functions are quite controversial. In *S. cerevisiae*, two principal roles for Htz1, homolog of H2A.Z, have been described: Htz1 may act as i) activator of transcription (in fact, 200 genes have been identified as requiring H2A.Z for their expression) and ii) barrier for heterochromatin spreading (in fact, loss of H2A.Z favors heterochromatin formation mediated by Sir proteins). In *D. melanogaster*, H2Av is involved in the silencing of euchromatin, however this variant is not completely an H2A.Z homolog but possesses some H2A.X features such as the SQ(E/D)Φ sequence [9]. As concerns mammals, some *in vitro* evidence suggests that H2A.Z presence tends to stabilize the nucleosome; in fact, transcriptional activation of c-myc occurs along with H2A.Z displacement in the transcribed region [5, 30]. *In vivo* H2A.Z is distributed in both eu- and heterochromatin but seems to have mostly a destabilizing effect. Swi2/Snf2-related ATPase (SWR) complex, responsible for exchanging H2A with H2A.Z, acts predominantly at nucleosome depleted regions (NDRs) generally located at promoters of active genes but not onto free DNA [5, 9]. Interestingly, this complex comprises subunits present also in yeast NuA4 and fly Tip60 which are histone acetyltransferases (HATs) [9].
H2A.Z enrichment can be also found in gene bodies in mammals or in enhancer and in promoters of polycomb-silenced genes in embryonic stem cells (ESCs). In humans, H2A.Z plays a role in activation, initiation and elongation of transcription; in fact, this variant is important for RNA pol II recruitment and is exchanged prior to the loading of the enzyme; moreover, H2A.Z-H2B dimers aid transcriptional

elongation since they can dissociate more easily. Even if H2A.Z has a predominately positive role in transcription, it is also able to negatively regulate genes such as *p21* or mitosis silenced genes. Unfortunately, the specific pattern of distribution of H2A.Z enrichment in particular genomic sites, is still unclear. Yet, the dual effect exerted by H2A.Z on transcription may be explained by H2A.Z ability to render genome more accessible, facilitating the binding of both activating and repressive complexes. Moreover, N-tails PTMs (e.g., when H3K56 is acetylated, Ino80 and SWR1 remove H2A.Z from the nucleosome) and number of H2A.Z copies in the nucleosome (heterotypic A/Z or homotypic Z/Z) may contribute to this discrepancy [5, 9]. To further complicate this picture, an isoform, derived from alternative splicing of the *H2A.Z* gene, has been recently discovered in human brain tissues. Even if only a minor part of this histone is associated in nucleosomes, *in vivo* and *in vitro* evidence suggests that, because of its truncated C-tail, this H2A.Z.2.2 isoform has the potential to generate the least stable nucleosome known so far [26, 31].

The most recently discovered RI variant is H2A.B which, unlike H2A.Z, has evolved very rapidly [5, 32]. This variant is also called H2A.Bbd after Barr body deficiency but, despite its name, it positively correlates with transcriptionally active sites and its deposition seems to occur only in the absence of mH2A [6, 9, 32]. Even if the overall "relaxing" properties of this variant are consistent with those of H2A.Z, H2A.B sequence diverges from both H2A.Z and H2A possessing a shorter docking domain [6]. The lack of 19 AAs in its C terminus, along with other differences, makes this variant only 50% identical to H2A and confers particular physical properties to nucleosomes containing this variant; generally speaking, H2A.B nucleosome stability is lower and, therefore, its exchange occurs faster than that of H2A [5]; H2A.B containing-nucleosomes are associated only with 118-130 bp of DNA [26]. In mice, the presence of H2A.B containing-nucleosomes allows the formation of chromatin fibers which are only partially compacted because of an Asp residue not present in humans where, in fact, H2A.B counteracts compact chromatin fibers formation [5]. Mechanisms for *in vivo* deposition of this variant are still unclear but some *in vitro* evidence suggests nucleosome assembly protein 1 (NAP-1) as responsible for both the assembly and disassembly of H2A.B dimers. In yeast, NAP-1 has been also found associated with H2A.Z-H2B dimers [9].

H2A family presents other minor RI variants which are testis-specific (H2A.1) or involved in pericentric chromatin organization in spermatids (H2A.L); these variants are late evolutionary acquisitions typical of certain mammals [26]. As concerns functional evolutionary specialization, H3 comes right after H2A.

1.5. H3 replacement variants

Histone H3 is highly conserved throughout evolution but different H3 variants can be found in all eukaryotes suggesting an early divergence [33]. In fact, along with H3.1 and H3.2 which are the canonical histones, different species have developed different RI variants. As mentioned before, variants can be expressed ubiquitously or in a tissue-specific manner and in somatic or germinal cells; in mammals, H3.3 and centromere protein-A (CENP-A) variants are the major constituents of somatic cells while H3t is testis specific [34].

Differences between H3 family members can be found in their globular C-terminus which is an HFD with four α-helices (αN, α1, α2, α3) [33]; the modest diversities between canonical H3s (H3.1 and H3.2 differs only in the AA 96, Cysteine (Cys, C)/Ser respectively) (Fig. 2, b) and between canonical H3 and their variants (except for CENP-A) are however able to generate functionally distinct proteins [18].

The central localization of H3 inside the nucleosome and the presence of Cys in H3 protein core confer high stability to H3-H4 tetramer; Cys, especially the one in position 110 (α2 helix), have been proposed to form disulfide bonds, under oxidative conditions, between H3 proteins in the same nucleosome. For these reasons, canonical H3s are likely to be associated with heterochromatin and transcriptional silencing while, due to changes in the HFD sequence, variants functions can be diverse [18]. Moreover, since the chaperone-recognition region is located in the globular HFD, different complexes are responsible for RC and RI incorporation; H3 is deposited into chromatin in H3-H4 dimers and CAF-1 is the chaperone responsible for H3.1 and H3.2 but not H3.3 or CENP-A incorporation [34]. Another chaperone, ASF-1 can interact with both H3 and H3.3 but, differently from CAF-1, its binding region recognizes H3-H4 dimers but not the tetramer suggesting that the interaction is mediated by common AAs [35].

The incorporation of histone variants represents an alternative strategy to mark chromatin and CENP-A (in humans, CenH3 in eukaryotes, CID in *Drosophila*) has been the first variant to be implicated in the legacy of a chromatin state [14]. CENP-A is present in most eukaryotes and specialized in chromatin packaging at centromeres but, being a RI variant, it can be incorporated independently of centromere DNA replication [6, 9]. Apparently, in centromeric chromatin, blocks of CENP-A-containing nucleosomes are arranged in the external surface of the chromosome while H3 is concentrated on the inside and usually hypoacetylated (inactive chromatin) [36].

Compared to H3, CENP-A sequence is completely different in the N-tail and shares only 50% identity in the HFD; in particular, it lacks a Gln residue in the α1 and has a longer L1 (DNA contact region) resulting in more precise contacts/higher specificity. The L1 region alone is responsible for the centromeric localization and the N-tail of CENP-A presents docking signals for kinetochore proteins. Unlike other H3 RI variants, CENP-A is rapidly evolving since it is subjected to positive selection driven by L1 and N-tail DNA-binding specificity in meiotic competition [6]. CENP-A deposition into centromeric chromatin is not mediated by a canonical CAF but by a unique component of CAF-1 complex called Holliday junction recognition protein (HJURP) which recognizes the L1 and α2 helix of the HFD [37].

H3t, the human testis-specific H3 variant, differs from H3.1 by only 4 AAs [38]. Besides being necessary for chromatin reorganization during spermatogenesis [39], little is known concerning H3t functions but it is possible, for this variant, to mark specific chromatin states/regions. Proof of H3t existence in somatic cells is feeble but Govin and colleagues [38] suggest its expression as a potential pathophysiological response to certain stimuli.

Along with the five RC and RI variants found in mammals (H3.1, H3.2, H3.3, H3t and CENP-A), two primate-specific variants, namely H3.X and H3.Y, have been recently identified. They are expressed at low levels and they differ from canonical H3s in some functionally relevant residues (e.g., Ser10 and Ser28, which are usually post-translationally modified); notably, their coding sequences are more similar to H3.3 than to H3.1 and H3.2, especially in the region surrounding AAs 87-90, which is important for chaperone binding. Little is known about these variant functions but they are expressed in the human brain, with thalamus (Thal) as an exception, as in other tissues, and knocking down (KD) H3.Y alters the expression of cell cycle- and cell growth-related genes [40].

1.5.1. H3.3 variant and its dual nature: H3.3A and H3.3B

H3.3 was first identified by Zweidler and Franklin in the late ‘70s [19, 20]. As previously mentioned, H3.3 diverged very early from canonical H3s and its evolution is very slow; H3.3 sequence is in fact identical (e.g., in humans, mouse, *Xenopus* and *Drosophila*) or slightly different in many metazoan species [33]. *S. cerevisiae* and some other eukaryotes express only H3.3 but not the canonical H3.1/H3.2 highlighting the biological value of this variant [6].

H3.3 protein differs from H3.2 by only four AAs: Alanine (Ala, A) 31, Ser87, Valine (Val, V) 89, Methionine (Met, M) 90 in H3.2 are replaced by Ser31, Ala87, Isoleucine (Ile, I) 89 and Gly90 in H3.3 (Fig. 2) [18, 19]. Three out of four different AAs (87-89-90) are in the HFD and allow RI incorporation [5]; in fact, mutations in any of these AAs prevent H3.3 RI deposition. On the contrary, H3 N-tail is essential for *in vivo* RC but not RI deposition, so that potentially both H3 and H3.3-containing tetramers can be incorporated during DNA replication [41].

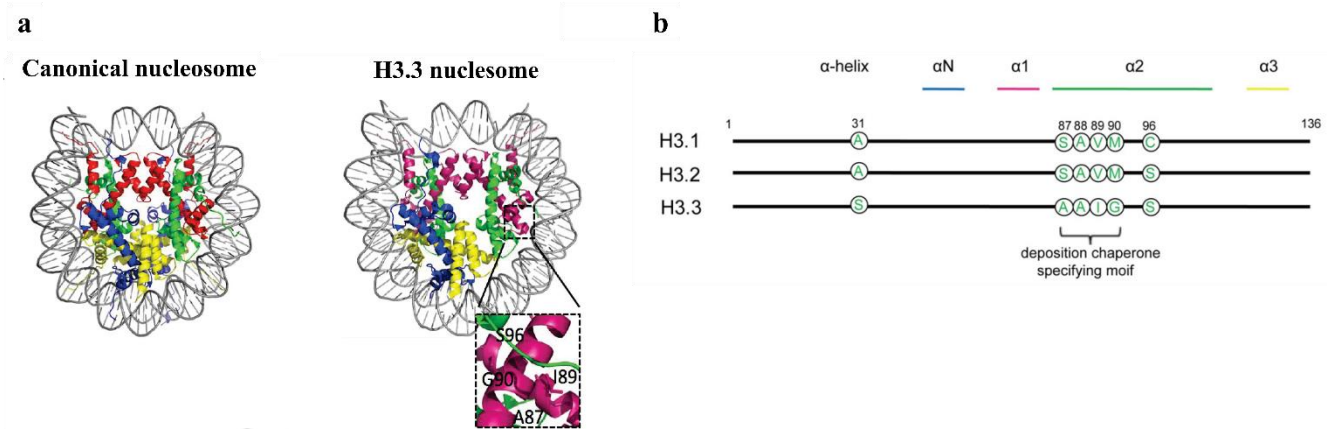

Fig. 2: a) Canonical and H3.3 nucleosome crystal structures. The red color represents H3 while H3.3 is purple, green marks H4, blue H2A, yellow H2B and the DNA is grey. In the dashed squared panel, the principal AAs different in H3.3 with respect to H3 are represented (modified from [99]). **b) Aligned sequences of mammalian H3.1, H3.2, and H3.3 histones**. Different AAs, four between H3.3 and H3.2 and five between H3.3 and H3.1, and major domains are marked (modified from [100]).

Even if H3.3 incorporation requires an almost complete DNA unwrapping and consequently exposure of TF binding sites, this variant exhibits a dual nature [42]. Ahmad and Henikoff [41], by means of H3.3-green fluorescent protein (GFP) fusion construct, were the first to hypothesize a link between H3.3 and the transcriptional state demonstrating an H3.3 enrichment in ribosomal repeat genes with active transcription. In yeast, where canonical H3s are absent, H3.3-H4 tetramers are rapidly removed and redeposited after RNA pol II passage while in *D. Melanogaster*, where both H3s and H3.3 are present, the variant is displaced and reloaded at transcription sites.

In mammals, H3-H4 tetramers exchange is not fully dependent on the transcriptional status. Precise reasons why H3.3 deposition occurs preferentially at transcriptionally active sites are still not entirely clear [9] but the substitution with H3.3 may be the only way to eliminate methylated H3 since there are no histone demethylases in eukaryotic cells [41]. Moreover, *in vitro* (human) and *in vivo* (*Drosophila*) findings underlined how the majority of H3.3 N-tail PTMs are associated with an active transcriptional

state (e.g., K4me2, K36me); at steady state, H3.3 has a two-fold enrichment in acetylation with respect to H3.1 especially when in nucleosomes [9, 14, 34].
Indeed, DNA exposure is necessary for H3.3 incorporation to occur but H3.3 enrichment has been found on more than just promoters and body of active genes; a subset of repressed genes and silent chromatin also exhibited H3.3 enrichment suggesting a complex role for this variant [5].

Different chaperones and complexes are responsible for H3.3 incorporation in different loci; while HIRA is accountable for H3.3 deposition in both active and inactive genes, death domain-associated protein (DAXX) together with alpha-thalassemia/mental retardation X-linked syndrome protein (ATRX) deposits this variant at pericentric heterochromatin and telomeric regions. Apparently, the single Met90Gly substitution is the major determinant of the DAXX-H3.3 interaction [5, 42]. As for H2A.Z, the presence of H3.3 in the nucleosome might facilitate activating and/or repressive complexes binding partly explaining the dual nature of H3.3 involvement in transcription.

In 1985, Brush and colleagues identified in chicken two different genes (now addressed as *H3f3a* and *H3f3b*) coding for H3.3 whose transcripts and proteins were called H3.3A and H3.3B by them [19]. As for chickens, in humans both *H3f3a* and *H3f3b* possess the same number of exons and introns (four and three, respectively), however *H3f3b* introns are smaller [19, 43]. Additionally, *H3f3a* exhibits an oligodeoxyadenylated (oligo(dA)) tract in the 3' end close to the post-transcriptional polyadenylation (poly(A)) site. Even if *H3f3b* does not contain the oligo(dA) region, it possesses a canonical poly(A) signal sequence at +1494, absent in *H3f3a*. Both isoforms exhibit long 3' and 5' untranslated regions (UTRs) but 3' UTR of H3.3A is longer [19, 43, 44]. Moreover, contrary to *H3f3b* which possesses a classical promoter (one TATA box and six CCAAT boxes) for RNA pol II situated far from the coding sequence, *H3f3a* promoter has an incomplete TATA box (ATA), no CCAAT boxes but four GC-rich domains that may represent the consensus motives for specific protein 1 (SP1) which is a TF responsible for the regulation of many house-keeping genes [43].

Despite the different promoter organization, localization (*H3f3a* is on chromosome 1 and *H3f3b* on chromosome 17 in humans) and gene sequence (restricted to silent nucleotides), *H3f3a* and *H3f3b* code for identical proteins in embryonic and differentiated cells [19, 44, 45]. To further complicate H3.3 picture, in humans, three termination signals in the 3' region generate three different H3.3B transcripts which however, as H3.3A, produce the same proteins [43].

H3f3b is phylogenetically more ancient than *H3f3a* (which first appeared in Sarcopterygii) and more similar to the ancestral H3.3. It is noteworthy that the retention of the two genes implies a functional relevance of both of them [45]. This observation is supported by the fact that, even if the encoded proteins are exactly identical, mutations in one gene rather than the other can be related to different cancer types suggesting a differential mechanism of regulation and role; in brainstem gliomas the Lys27Met mutation has been identified in *H3f3a* but not in *H3f3b*; on the contrary in chondroblastoma the mutation Lys36Met occurs more frequently in *H3f3b* [45, 46]. Moreover, retrovirus-mediated disruption of *H3f3a* in E13.5 mice induces 50% of death in homozygous condition, and surviving mutants exhibit reduced growth rate and fertility along with neuromuscular deficits [47]. *H3f3b* null mutants present a more severe phenotype with respect to *H3f3a*. Homozygotes are inviable at birth and heterozygotes show growth-deficits. The simultaneous mutation of both genes results in early primary oocyte death suggesting the critical role exerted by H3.3 during development [48].

H3.3A and H3.3B have been detected in several adult tissues such as gonad, kidney and brain, with different ratios of expression; for instance, in kidney H3.3A is less abundant than H3.3B [43]. In the brain, H3.3A seems to be the more abundant isoform but the precise region-specific expression pattern of the two isoforms is still not fully elucidated. Moreover, it remains unclear if these two isoforms have a cell-type specific expression pattern.

1.6. Histone variants and neuroplasticity

Neuronal plasticity, the brain's ability to change in response to physiological or pathological internal or external stimuli, can be mediated by changes in gene expression which, in turn, can be regulated by changes in chromatin organization. Chromatin involvement in neurodevelopment and in age- or experience-dependent brain modifications is a new field of study named "neuroepigenetics" [49]. Since histones are stable proteins with a relatively slow turnover, the regulation of transcription was mainly attributed to PTMs and ATP-dependent remodelers [50].

Recent analyses have however highlighted, in active regions, a rapid rate of incorporation of new histone variants suggesting that histone dynamics may influence gene expression changes [50, 51]. H3.3, along with H2A.Z, is the principal variant that has been associated with neuroplastic changes. While H2A.Z presence is negatively correlated with stimulus-induced transcription but positively associated with steady state basal gene expression (for instance, it seems to be a negative regulator of hippocampal memory consolidation) [52, 53], all data implicate H3.3 (and especially H3.3B) as a stimulus-responsive

variant [50, 54]. In fact, emerging evidence underlines the importance of H3.3 turnover in neuronal function and brain plasticity [54]. It is noteworthy that an increase in H3.3 protein levels may occur even without a rise in H3.3 mRNA levels pointing to post-transcriptional processes, besides transcriptional regulation, for the regulation of H3.3 content [19].

In some tissues H3.3 represents the majority of H3 proteins [20]; H3.3 is the minor part of total H3 in the chromatin of mouse embryonic neurons whereas canonical H3s are highly represented [6]. After birth, H3.3 accumulates and by 2 years of age it constitutes more than 94% of total H3 neuronal pool [50]; this increment seems to occur from 14 to 72 years of age in humans. In astrocytes, H3.3 age-related accumulation is slower than in neurons; in fact, this variant represents only the 80% of total H3 pool in 2 year-old mice. Even if H3.3 becomes the predominant form of H3 in the adult brain, its incorporation remains dynamic: in 4 weeks, more than 30% of total H3.3 is actively exchanged and replaced. Histone turnover is faster in early life and slower, but still present, in adult life [50]. Deal and colleagues [51], using an innovative technique for nucleosome turnover estimation called "covalent attachment of tags to capture histones and identify turnover" or "CATCH-IT", in *Drosophila*, demonstrated that bodies of active genes and *cis*-regulatory elements possess the highest rate of H3.3 turnover. In line with Deal findings, three different H3.3 turnover rates (slow, intermediate and rapid) have been observed *in vivo* for mammals. While slow turnover is associated with telomeric regions and intermediate turnover is typical of gene bodies, rapid turnover occurs in enhancers and promoters and is associated with the presence of transcriptionally positive N-tail marks (e.g., H3K4me, H3K4me3, H3K9ac, H3K27ac) and H2A.Z variant [55]. Disrupting H3.3 turnover by reducing its soluble nuclear pool by means of chained microRNAs (miRs) targeting both H3.3 genes in Cornu Ammonis 1 (CA1) neurons has been proved to hinder learning and memory; in fact, KD mice showed impairments in the novel object recognition and fear conditioning tasks. In mouse cultured astrocytes, H3.3 turnover rate seems to be similar to that of neurons and to be able to regulate transcription; however, contrary to neurons, H3.3 KD-induced alterations are rescued by canonical histones in dividing cells such as astrocytes [50].

Apparently, while H3.3 removal from the nucleosome seems to be mediated by the proteasome, H3.3 dynamics upon neuronal activation are HIRA-dependent and involved in activity-dependent gene expression, synaptic connectivity and therefore plasticity [50]. On the contrary, DAXX/ATRX-mediated turnover of H3.3, in heterochromatic regions, may act as protection against repetitive element expansion and silence transposable elements [49]. Moreover, Michod and colleagues [56] demonstrated DAXX-

mediated H3.3 deposition in regulatory regions of some immediate early genes (e.g., brain derived neurotrophic factor (BDNF), c-Fos, Arc), upon neuronal activation with KCl.

H3.3 isoforms contribution to neuroepigenetics is apparently uneven; only H3.3B but not H3.3A expression and incorporation seems to be stimulated by neuronal activation; this is consistent with an acceleration in H3.3 turnover (half-life of 0.7 days in KCl-treated cells compared to 3.5 days in controls). Chronic exposure to an enriched environment (EE), a common model of induced neuronal plasticity, has been proved to increase mRNA levels and incorporation of H3.3B but not H3.3A in mouse hippocampus (Hip) [50]. On the contrary, H3.3A but not H3.3B mRNA levels are increased in the nucleus accumbens (NAc) of depressed subjects and in a rodent model of depression (i.e., chronic social defeat stress, CSDS). Chronic treatment with antidepressant, as well as EE, completely reverses H3.3 increment. In agreement with this, mice subjected to early life maternal separation, which has been demonstrated to favor depressive like behaviors, exhibit rapid H3.3 accumulation in the NAc. Knocking-down the soluble H3.3 pool in NAc by means of miRs targeting both H3.3 genes confers resilience to CSDS and inhibits aberrant transcriptional plasticity. It remains unclear which cell type (e.g., D1- or D2-expressing neurons, glia, etc.) is majorly affected by these alterations in H3.3 dynamics inside the NAc [57].

Because of the little differences among RC and RI H3 proteins, it is really challenging to obtain a highly specific antibody (Ab) to correctly study H3.3 and, even more difficult, to discriminate H3.3 isoforms in order to target H3.3A and H3.3B separately; the generation of tagged animals may be a very useful tool to this purpose. In fact, to study H3.3B expression in oocytes and pre-implantation embryos, Wen and colleagues [58], using the zinc-finger genome editing approach, generated a knock-in (KI) mouse where the last exon of the endogenous *H3f3b* is fused with the small hemagglutinin (HA) peptide and a fluorescent reporter. Tagged mice have been used ever since to study H3.3 expression in different developmental periods, cellular types and conditions. Ozato's group [59] generated KI HA-tagged mice for both *H3f3a* and *H3f3b* by homologous recombination and demonstrated the expression of both genes in lymphocytes and myeloid cells derived from the spleen and thymus as well as in splenic macrophages, natural killer and dendritic cells. Using HA-tagged mice for H3.3, McNally and colleagues [60] have been able to prove that not only H3.3 turnover blockade but also increased dynamics, as previously seen for NAc and depression, are able to negatively affect brain function; in fact, overexpression of this variant, in adult mouse excitatory neurons of the forebrain, induces deficits in contextual memory and motor learning.

Chromatin alterations have been found in some neurological disorders associated with aberrant external stimuli (e.g., addiction and social stress) [49]; for instance, chronic drug abuse alters histone acetylation pattern in reward-associated brain circuits [61]. By means of transgenic mice expressing the tagged H3.3 variant in the NAc (Calmodulin-dependent protein kinase II, CAMKIIα, promoter) only in adulthood (thanks to the tetracycline transactivator system), Wimmer and colleagues [62] determined the transcriptional changes occurring after chronic cocaine (Coc) administration. This analysis revealed H3.3 enrichment near genes involved in dendrite formation, neurogenesis, neural differentiation and morphine addiction.

Though our knowledge on histone variants and the role exerted by them is still in its infancy, H3.3 relevance in neuroplasticity is becoming more clear every day; in fact, normal and aberrant H3.3 dynamics (diminished, increased or altered) have been implicated in neuronal transcription, neuronal deficits and neurological disorders. All data implicate H3.3, and in particular *H3f3b* isoform, as the stimulus-responsive gene but further experiments, with the help of tagged animals, are necessary to elucidate H3.3 isoform contribution to the functions and neuroplasticity of different brain circuits.

1.6.1. Environmental enrichment, microglia and neuroplasticity

EE is a widely used model to mimic positive environmental stimulation and therefore to favor neuroplastic changes. The presence of frequently changed toys, wheels and tunnels and the large number of animals in the EE cages provide a complex stimulation enhancing aspects like learning, memory, physical exercise and sociability all at the same time; cerebral cortex (CTX) and Hip are the brain areas most affected by the EE. In the post-developmental and adult brain, exposure to EE has been proved to elicit different plastic responses such as increased Hip long-term potentiation (LTP), dendritic arborization, synaptogenesis, neurogenesis and gliogenesis. Moreover, EE favors nerve growth factor (NGF), BDNF and glial-cell-derived neurotrophic factor (GDNF) release [63, 64].

The central focus of neuroplasticity are certainly neurons but they are not the only cell population in the central nervous system (CNS) to be involved in plastic changes; for instance, the very abundant astrocytes, making close contacts with neuronal synapses and releasing neurotrophic factors and neuroactive compounds, are known for stimulating synaptic growth and maintenance and promoting formation of spine contacts; they can therefore modulate different aspects of neuroplasticity [65].

Also another glial population, namely microglia, is involved in synaptic maturation and synaptic pruning dependent on neuronal-activity. In the adult brain, microglia represent almost the 10% of total cells and, deriving from yolk sac erythro-myeloid progenitors, do not share a common origin with other brain populations; they represent the immune cells of the brain but, considering them as just the resident macrophages of the CNS parenchyma, is highly reductive [66-68]. While, the role of these cells in inflammation under pathological conditions has been extensively studied, in the last few years, microglial function in physiological conditions is becoming a very popular subject. Apparently, in the normal brain, ramified microglia called “resting” are not dormant but are continuously screening the CNS. This scanning process stops when an injury/infection occurs leading to morphological changes and migration towards the site of the lesion. Since resting microglia are not inactive, it is more proper to talk about a shift of activity states (from surveying to reactive microglia) than of microglial activation. This is why, the common phenotypic distinction between M0 as resting microglia, M1 as pro-inflammatory phenotype and M2 as anti-inflammatory regenerative state is fading [68].

Microglia has been proved to support adult neurogenesis and oligodendrogenesis and neuroprotection both directly, through cellular contacts, and indirectly, through the secretion of neurotrophic factors [68]. Microglial cells are key factors in homeostasis maintenance, immunological surveillance and synapse remodeling [67] and a model of complex plastic stimulation, like EE, elicits the proliferation of this glial population. In fact, exposure to EE increases the number of both astrocytes and microglial cells in the dentate gyrus (DG) of the Hip [69]. In addition, the activity of wheel running stimulates microglia proliferation also in the CTX and especially in superficial layers without any evident induction of morphological changes [70].

It remains unclear whether microglia are key players or minor contributors in the neuroplasticity scenario and if histone dynamics in these cells might contribute to this particular role. Moreover, there are no direct proofs of H3.3 expression in these cells yet.

2. Aim of the work

Histone variants involvement in neuroplasticity is a subject of growing interest and H3.3 seems to be the variant majorly associated to plastic changes. Two distinct genes, namely *H3f3a* and *H3f3b*, code for identical H3.3 proteins. Due to the little differences among their sequences it has been really challenging to study them separately; this is why the knowledge concerning H3.3 isoforms is limited but the phylogenetic conservation of both genes, as well as the different phenotypes generated from knocking out one or the other isoform, suggest a relevant functional distinction between *H3f3a* and *H3f3b*. Recent data have identified *H3f3a* as the steady-state gene and *H3f3b* as the stimulus-responsive gene. To understand the functional role of H3.3 in the brain it is first necessary to investigate when and where the two H3.3 isoforms are expressed and what are their possible differences; to this purpose, we used HA-tagged H3.3A and H3.3B mice to investigate the two isoforms, and in particular their i) distribution in different brain areas by means of semi-quantitative immunohistochemistry (IHC) and ii) expression in different neuronal and glial populations by means of double immunofluorescence (IF) stainings. Additionally, we assessed H3.3A and H3.3B co-localization with another histone variant, namely H2A.Z, through stimulated emission depletion (STED) microscopy. Once gained insights of H3.3 isoforms regional and cellular basal expression, we investigated H3.3B expression changes in three different conditions known to be associated to neuroplastic changes, namely iii) EE iv) aging and v) sub-chronic Coc administration. On the basis of the previous analyses, H3.3B presence was evaluated in different cell types to investigate the effects of neuroplastic stimuli in all brain cellular populations. Moreover, tissue clearing coupled with light sheet microscopy was performed to assess H3.3B expression in the whole brain after EE exposure. Present studies will give the necessary background knowledge to generate region- and cell-specific conditional KO models that may allow the understanding of H3.3A and H3.3B contribution to the neuroplastic changes occurring in specific cerebral circuits upon physiological and pathophysiological stimulation.

3. Materials and methods

3.1. Animals

Using wild type (WT) C57BL/6 mice as genetic background, tagged KI H3.3A and H3.3B heterozygous mice were obtained by homologous recombination targeting the *H3f3a* (WT/HA-fH3.3A) and *H3f3b* (WT/HA-fH3.3B) locus, respectively. A TAP-tag sequence comprehensive of two different tags, namely HA (AA sequence: YPYDVPDYA) and Flag (DYKDDDDK), is present in both constructs as well as LoxP sequences for the future generation of conditional KO mice.

These mouse strains were generated by the "Institut Clinique de la Souris" Illkirch, France. Founders of mice colonies used in present experiments were kindly provided by Dr. Stefan Dimitrov from Grenoble Institute for Advanced Biosciences to the pathogen–free animal care facility at the École Normale Supérieure of Lyon (Plateau de Biologie Expérimentale de la Souris) where the experimental mice are currently bred. The study was performed following the national and European laws on animal experimentation.

Mice were housed in plastic cages under standard laboratory conditions (except indicated otherwise, like for EE), with a 22-24°C temperature, *ad libitum* food and water, 55% ± 10% humidity and 12/12 hours (hr) light/dark cycle (light on at 6.30 am). Heterozygous mice of different age and sex were used for different experimental procedures (more details below). KI mouse genotyping was performed on DNA templates extracted from tissue derived from fingertips biopsies as described below.

Genotyping. Mouse genomic DNA was extracted from 2 mm fingertip biopsies as follows. Samples were incubated overnight (O/N) at 56°C with 100 µl of lysis buffer (100 mM TrisHCL, pH 8; 200 mM NaCl; 5mM EDTA, pH 8; 0.2% SDS; milliQ H_20 and 0.5 mg/ml of Proteinase-K). Next, 100 µl of isopropanol were added and samples were centrifuged at 4°C for 10 minutes (min) at 15000xg. After supernatant removal, 500 µl of 70% ethanol (EtOH) were added and samples were centrifuged as before. Finally, supernatant was removed, samples were resuspended in 150 µl of milliQ H_20 and stored at 4°C.

The polymerase chain reaction (PCR) was performed to determine mice genotype, with the following protocol for both H3.3A and H3.3B tagged mice:

95°C 3 min - (95°C 1 min - 58°C 30 sec - 72°C 1 min) x 40 cycles - 72°C 10 min

Two different couples of primers, astride the endogenous and exogenous sequence, were used for H3.3A (Forward, Fw: TTTGCAGACGTTTCTAATTTCTACT, Reverse, Rev: ATATCGGATTCAACTA-AAACATAAC) and H3.3B (Fw: TCCTCATTCTACCACATGTTCA, Rev: TCAATCTAGGCCT-AAGACCAAA), respectively.

Finally, gel electrophoresis was performed using 2% agarose in 0.5x TAE (tris-acetate ethylenediaminetetraacetic Acid (EDTA)) stained with 0.3% ethidium bromide. For H3.3A: 333 bp WT allele, 303 bp KI allele. For H3.3B: 177 bp WT allele, 303 bp KI allele.

3.2. Immunohistological analyses

For IHC and IF stainings, H3.3A and H3.3B heterozygous mice were sacrificed as follows: animals were anesthetized with isoflurane and their blood was washed out through intracardial infusion of 50 ml of saline solution (Sal, 0.9% NaCl). Next, intracardial perfusion (70ml/7min) with ice-cold 4% paraformaldehyde (PFA) in phosphate buffered saline (PBS, Dulbecco) was performed. Brains were collected, postfixed in 4% PFA for 12 hr and rinsed in 30% sucrose-PBS for 2 days to prevent cryolesion formation. Samples were then frozen using dry ice and stored at -80°C until use. Coronal sections of 40 μm thickness were cut using a cryostat (JUNG CM 3000) and stored in a 50% glycerol-PBS solution at -20°C until use.

A 40 min-long antigen retrieval with citrate buffer (10mM Sodium Citrate, 0.05% Tween-20, pH = 6) at 98°C, followed by 20 min at room temperature (RT), is required for the detection of the nuclear tag so this step was performed prior to both IHC and IF, on H3.3A and H3.3B mouse samples. All reagents used were purchased by Sigma unless otherwise specified.

3.2.1. Immunohistochemistry

IHC was performed using a validated protocol [71-73] as follows. After the blocking of endogenous peroxidases (for 10 min with 10% H_20_2) and non-specific binding blocking with 0.1% bovine serum albumin (BSA), free-floating brain sections from both H3.3A and H3.3B tagged mice were incubated O/N (except for anti-murine osteosarcoma viral oncogene homolog B (FosB) which was incubated for 48 hr) at 4°C with rat anti-HA (see Ab list, Table 1) primary Ab diluted in 1 % normal serum (NS), 0.3% Triton X-100 and PBS. Incubation with the secondary biotinylated Ab was performed for 1 hr at RT; the secondary Ab was diluted in 1% NS, 0.2% Triton X-100 and PBS.

A 45 min incubation with Streptavidin-Horseradish Peroxidase (HRP) was carried out at RT and followed by the staining reaction with 0.05% diaminobenzidine (DAB) and 0.01% H_20_2.
Finally, sections were placed on gelatinized glass slides, dehydrated with increasing concentration of EtOH (50%, 70%, 90% and 100%) and 100 % xylene, coverslipped with Eukitt® mounting medium and visualized through optical microscopy (Nikon Eclipse CiL). All images, captured by Nikon DS-Fi3 digital camera, were acquired using a 10x objective (obj) under the same light conditions.

3.2.2. Double/triple immunofluorescence

IF was performed using a validated protocol [74, 75] as follows. Free-floating sections were incubated with 1% BSA to prevent non-specific binding, then slices were incubated O/N with anti-HA in combination with different cell-specific primary Abs (see Table 1). Anti-HA Abs from two different species (mouse or rat) were used based on the host species of other Abs. All primary Abs were diluted in 1% NS, 0.1% Triton X-100 and PBS. The incubation with secondary Abs (see table 1), diluted in 1% NS, 0.2% Triton X-100 and PBS, was carried out at RT for 1 hr. Next, slices were placed on gelatinized glass slides, air dried and coverslipped with 4′,6-diamidino-2-phenylindole (DAPI) diluted in 50% glycerol-PBS for confocal microscopy visualization (Leica TCS SP8). A 40x oil-immersion obj was used for all different IF, while the zoom was labeling-dependent. 4 µm z-stacks were acquired with a line and frame average of 1 and 2 as line accumulation.

STED microscopy, with one laser pulse exciting the fluorophore and the other pulse de-exciting any fluorophore near the excitation point, allows the generation of images with high resolution (maximum xy resolution: 30 nm). For the visualization with STED microcopy, the IF protocol described above was followed with minor modifications: mouse anti-HA and rabbit anti-H2A.Z were used as primary Abs while goat anti-mouse Alexa Fluor® 594 and goat anti-rabbit IgG ATTO 647N were used as secondary Abs. Labeled brain slices were mounted using Mowiol. Finally, samples were visualized using Leica SP8, STED with 100x oil-immersion obj and 6x zoom.

Table 1: List of primary and secondary Abs used for different applications.

Application	Primary Ab	Host	Dilution	Source	Cat. N°
IHC, IF, clearing, STED	anti-HA (clone 16B12)	mouse	1:1000	Thermo Fisher	A-21287
	anti-HA (clone 3F10)	rat	1:1000	Roche	11867423001
	Anti-FosB (H-75)	rabbit	1:250	Santa Cruz	sc-7203
	anti-CD206	rat	1:1000	Bio-Rad	MCA2235T
	anti-CR	rabbit	1:1000	Millipore	AB5054
	anti-DCX	guinea pig	1:500	Millipore	AB2253
	anti-GFAP	rabbit	1:2000	Dako	Z0334
	anti-glutamine synthetase	rabbit	1:1500	abcam	ab73593
	anti-H2A.Z	rabbit	1:200	abcam	ab188314
	anti-Iba1	rabbit	1:500	Wako	01919741
	anti-Ki67	rabbit	1:500	abcam	ab833
	anti-nestin	mouse	1:400	Millipore	MAB353
	anti-NeuN	rabbit	1:200	Millipore	ABN78
	anti-NeuN	mouse	1:200	Millipore	MAB377
	anti-NPY	rabbit	1:200	Millipore	AB9608
	anti-PENK	rabbit	1:400	Cell Signaling	87120
	anti-PV	rabbit	1:1000	abcam	ab11427
	anti-S100B	rabbit	1:100	Dako	Z0311
	anti-SS	rabbit	1:200	Millipore	MAB354
	anti-TH	rabbit	1:500	Millipore	AB152
	NeuroTrace™ 640/660 Nissl Stain	-	1:50	Thermo Fisher	N21483
FACS	anti-CD11b	rat	1:100	BD	553312
	anti-CD45 PE	rat	1:100	BD	553081
	anti-Flag Alexa Fluor 488	rabbit	1:100	R&D	IC8529G
	Secondary Ab				
IHC	Anti-Rabbit IgG biotinylated	donkey	1: 200	GE Healthcare	RPN1004
	anti-Rat IgG biotinylated	goat	1:200	GE Healthcare	RPN1005
	Streptavidin-HRP	-	1: 200	GE Healthcare	RPN1231
IF, clearing, STED	anti-guinea pig IgG Alexa Fluor® 633	goat	1:200	Thermo Fisher	A-21105
	anti-mouse IgG Alexa Fluor® 488	goat	1:200	Thermo Fisher	A-11001
	anti-mouse IgG Alexa Fluor® 594	goat	1:200	Thermo Fisher	A-32742
	anti-rabbit IgG Alexa Fluor® 488	goat	1:200	Thermo Fisher	A-11008
	anti-rabbit IgG Alexa Fluor® 594	goat	1:200	Thermo Fisher	A-11037
	anti-rabbit IgG ATTO 647N	goat	1:500	abcam	ab245992
	anti-rat IgG Alexa Fluor® 546	goat	1:200	Thermo Fisher	A-11081

3.3. Environmental enrichment

EE experiment was performed accordingly to a previously validated protocol [76, 77] as follows. P21 H3.3B female mice were housed for 4 weeks in standard (SE, n = 16) or enriched (EE, n = 18) cages. For SE, standard cages (20 x 30 x 13 cm) from the animal facility were used with two animals/cage while for EE 10 mice/cage were placed in big (50 x 35 x 30 cm) colored plastic cages (Habitrail), connected to a 50 cm labyrinth, with tunnels, wheels and toys which were changed every 2 days. One cohort of animals (SE = 9, EE = 9) was sacrificed and processed for histological analyses as described above while a second cohort (SE = 5, EE = 7) was processed for microglial isolation and fluorescence-activated cell sorting (FACS). Additionally, two mice for each condition, namely SE and EE, were stained and cleared for light sheet visualization.

3.4. Microglial isolation and fluorescence-activated cell sorting

For cortical microglia isolation SE and EE housed mice were intracardially perfused with 50 ml of ice-cold PBS, CTX was dissected out, cut into small pieces using scalpels and incubated for 1 hr at 37°C with DNAse I 34 Kunitz/ml, 0.144 mg/ml of type IV Collagenase (770 U/mg), 10% fetal bovine serum (FBS), and phenol red Hank balanced salt solution (HBSS, Gibco). After the enzymatic digestion, mechanical homogenization of the tissue was carried out using a syringe with a 20G needle. Then samples were centrifuged at 4°C for 10 min at 900xg. After supernatant removal, pellet was resuspended in 10 ml of 37% Percoll Solution, obtained diluting with PBS a Percoll™/PBS solution (10x PBS 1:9 Percoll™, GE Healthcare) that is considered as 100% stock. To form a gradient, 37% Percoll was underlaid with 2 ml of 70% Percoll solution and placed in a centrifuge with swinging-buckets rotating at 500xg with no breaks for 28 min at RT. After Percoll gradient, samples were kept on ice for all the following steps; the top myelin layer was removed and the 37%/70% interface was recovered and put into ice-cold PBS. In order to fix cells, samples were centrifuged for 10 min at 500xg at 4°C, and the pellet was incubated with 1 ml of 4% PFA for 15 min; this step is necessary to prevent cell damage that may derive from cell permeabilization, which in turn is required for the nuclear staining. Cells were next washed, centrifuged (as before) and resuspended in 500 µl of the staining buffer (SB, made of 0.8% BSA, 0.25 µl/ml RNasin® Plus Promega, PBS). Cells were centrifuged again at 400xg for 3 min and then stored at 4°C without removing the supernatant. On the following day, cells were incubated for 30 min on ice with the permeabilization buffer (PB, made by 0.002% Triton X-100 and 1:100 rat anti-mouse CD16/CD32 Ab from BD, diluted in SB). Next, samples were centrifuged at 400xg for 3 min at 4°C and the pellet was resuspended in 100µl of Ab incubation mix (Ab diluted in SB).

Three different primary Abs, already conjugated with the fluorophore, were used at the same time to stain microglial cells (anti-CD11b allophycocyanin (APC) and anti-CD45 phycoerythrin (PE) Abs) and cells expressing the H3.3B variant (anti-Flag Alexa Fluor® 488 Ab). After 45 min of incubation samples were centrifuged as before, the pellet was resuspended in SB and moved to FACS tubes (Sarsted). This protocol, specific for microglia isolation and FACS nuclear antigen staining, was kindly provided by Dr. Nàdia Villacampa from Deutsches Zentrum fur Neurodegenerative Erkrankungen (DZNE, Bonn, Germany).

FACS analysis was performed immediately after the staining using the BD FacsAria II with continuous flow to detect all cells. For the gating choice and compensations, unstained samples, single stainings and FMO (fluorescence minus one) controls were used. First cells were selected according to their size (forward scatter, FSC > ~ 50k) and to their structural complexity/granularity (side scatter, SSC < ~ 200k). SSC height (H) versus pulse width (W) was used to remove doublets and debris. Next, only cells positive for both CD45 and CD11b (microglia) were considered. In this microglial population, cells with no or low (fluorescence < ~ $10^{3.5}$) H3.3B expression ($Flag^{low}$) and cells with high (fluorescence > ~ $10^{3.5}$) H3.3B expression ($Flag^{high}$) were counted. The % of cells for each population ($Flag^{low}$ and $Flag^{high}$), with respect to total microglial cells, was measured during 3 min of flow with a fixed flow rate (30 µl/min).

3.5. Tissue clearing and light sheet microscopy

To assess H3.3B staining in the whole brain, animals (2 SE and 2 EE mice) were perfused with ice-cold 4% PFA as described above, brains were collected, cut into two hemispheres (no post-fixation) and kept for 7 days at 4°C in PBS with 0.02% sodium azide (NaN_3). Samples were then stained and made transparent in 40 days using iDISCO+ protocol as follows. After dehydration with increasing methanol (MeOH) concentration (20%, 40%, 60%, 80%, 100%) samples were incubated with 33.33% MeOH-66.66% dichloromethane (DCM); all steps were performed for 1 hr at RT except for the last incubation which occurred O/N. On the following day, samples were washed in 100% MeOH at RT and then bleached with 100% MeOH-5% H_2O_2 O/N at 4°C. Hemibrains were then re-hydrated with decreasing MeOH concentration (80%, 60%, 40%, 20%), washed in PBS (all these steps were performed for 1 hr at RT) and permeabilized with 80% PTx.2 (0.2% Triton X-100-PBS), 2% glycine, 20% dimethyl sulfoxide (DMSO) and 0.02% NaN_3 for 2 days at RT. Next, non-specific binding was blocked by incubating samples for 3 days at RT with 1% NS, 1% DMSO and 0.02% NaN_3 diluted in PTx.2.

On the 8th day, hemibrains were incubated with the mouse anti-HA primary Ab for 3 weeks at 37°C; Ab was used at a concentration of 1:250 diluted in 3% NS, 5% DMSO and PTwH (0.2% Tween-20, 0.01mg/ml Heparin, 0.02% NaN_3, PBS). After 1 day of washes with PTwH, secondary Ab incubation was carried out for 8 days at 37°C using the anti-mouse IgG Alexa Fluor® 594 Ab 1:100 diluted in 5% NS and PTwH. Samples were washed for 1 day in PTwH at RT, dehydrated with increasing concentrations of MeOH (20%, 40%, 60%, 80%, 100%, 1hr/step at RT) and incubated for 3 hr with 33.33% MeOH-66.66% DCM. Finally, tissue clearing was performed incubating samples in 100% dibenzyl ether (DBE).

Samples were stored at RT in DBE and then visualized using LaVision UltraMicroscope II light sheet microscope with a 2x Olympus obj. Hemibrain mosaic photos were acquired using a 1.6x zoom and 4µm as step size. ImageJ software was used to stitch the images together while Arivis Vision4D allowed the 3D reconstruction of hemibrains.

Background subtraction, size-filtering, cell-distribution and cell-count analyses were carried out using Python scripts kindly provided by Dr. Amandine Cornil, Université Libre de Bruxelles, and modified by Dr. Paolo Pozzi, University of Modena and Reggio Emilia. Briefly, samples were analyzed using the following pipeline: images from the light sheet microscope showed objects of about 10-20 µm diameter (3-7 pixels), over a diffuse background of unspecific signal. In order to enhance the contrast of these objects over background, a median filter of 13 pixels across was applied to the image, and the filtered image obtained was subtracted from the raw image, resulting in a strong enhancement in the contrast of structures of approximate nucleus size, co-located with the objects observable in the raw image. In order to obtain a heatmap of nucleus-like object density, filtered images were binarized with a threshold manually determined on a per-image base, and a mean filter of size 20 pixels was applied, to compute the local density of pixels in nucleus-like objects.

3.6. Sub-chronic cocaine administration

Sub-chronic Coc treatment was performed using a validated protocol [78, 79] as follows. H3.3B tagged male mice of 2 months of age received 1 daily intra-peritoneal (i.p.) injection of Sal (n = 7) or Coc (n = 9) for 4 consecutive days. A relatively high dose of Coc, i.e., 20mg/Kg, was used. On the 5th day, 12 hr after the last injection, mice were sacrificed, perfused with 4% PFA and processed for histological analyses as previously described.

3.7. Image analysis and statistical analysis

For all experimental procedures, mice were encoded by numbers and all analyses were performed blind to the treatment in order to avoid biases. The % of area occupied by HA positive cells and the intensity of the signal (object mean grey value (MGV) subtracted from the background MGV) of these cells were analyzed using the particle analyzer function on ImageJ. For each area, the same size parameter ($pixel^2$: 30-infinity) but different thresholds (calculated from the peak of the MGV distribution corresponding to the background staining) were used in order to count only the population of positive objects thus distinguishing positive cells from the background. For each analysis, the mean value of four sections/area was considered.

In the EE experiment, H3.3B changes were qualitatively evaluated in all brain areas but analyzed only in EE affected areas such as CTX (when not specified, CTX stands for motor and somatosensory cortex) and Hip, where different subfields were analyzed: hilus, DG, CA1 and Cornu Ammonis 3 (CA3). For the CTX and hilus, a -15 MGV threshold was applied while -25 and -20 MGV thresholds were used for DG and CA1, and CA3, respectively.

In the sub-chronic Coc administration procedure, H3.3B changes were evaluated in the NAc core and shell areas majorly influenced by Coc treatment and with an observed increment of FosB positive cells. Here a -10 MGV threshold was used.

All data were analyzed by means of unpaired *t* test using Graphpad Prism; Welch's correction was applied in case of unequal standard deviations (SDs) between the groups. Differences have been considered significant with p value (p) < 0.05. All graphical data are expressed as mean ± standard error of the mean (SEM).

4. Results

4.1. H3.3A and H3.3B regional distribution

To assess H3.3A and H3.3B distribution by IHC, coronal brain sections from 4 month-old mice of both sexes (4 males and 4 females for each isoform) were incubated with rat anti-HA Ab. Semi-quantitative analysis of H3.3 isoforms regional expression was obtained by assigning two different scores related to the density of positive cells and the intensity of the signal, respectively (Table 2). The first score ranges from 0 (none) to 3 (all) and is estimated with respect to the density of cells/region visualized in Paxinos and Franklin's mouse atlas by hematoxylin and eosin staining. The second score is based on the estimation of signal intensity of a target area in comparison with signal intensity in the other brain areas and ranges from absent (-) to very intense (++). The main brain regions and subregions have been analyzed including the principal white matter tracts.

No sex-related differences have been observed (data not shown) so, hereafter, we will discuss the data without mentioning the sex of the animals. The proportion of the expression of the two H3.3 isoforms in different regions was not homogeneous (Fig. 3): for instance, in the CTX, H3.3A signal was more intense than H3.3B signal (a, b); this pattern was detected also in the striatum (caudate-putamen, CPu; c, d), whereas the lateral septum (LS; c, d) showed the opposite pattern. Generally speaking, H3.3A had a widespread distribution whereas H3.3B exhibited a more uneven expression. For instance, the latter isoform was highly expressed in some Thal (e.g., reticular Thal, Rt; i, j) and hypothalamic (Hyp; e.g., arcuate nucleus, Arc; e, f) nuclei where, on the contrary, H3.3A expression was comparable to that of most areas. In the DG (g, h), and particularly in the Hip granular layer (gr), both H3.3A and H3.3B were expressed in all cells but at very low intensity; similarly, the two isoforms were expressed by all cells in the gr of the cerebellum (CBX; k, m) where, however, H3.3A expression was more intense. On the contrary, in the CBX molecular layer (mol) H3.3B was more expressed than H3.3A. The habenula (Hb; g, h) exhibited a very high H3.3B expression.

H3.3A was expressed not only in grey matter regions but also in the main white matter tracts such as the corpus callosum (CC; c, d), confirming again the overall widespread expression of this isoform. On the contrary, H3.3B was nearly (e.g., in the CC) or completely (e.g., in the fimbria and anterior commissure) absent in white matter areas. Since most of the cellular nuclei in white matter tracts belong to glial cells, H3.3A presence and H3.3B absence in these areas may be due to a different cell-type expression of the two isoforms.

Brain Area			H3.3A		H3.3B	
			Positive cells	Intensity	Positive cells	Intensity
Cerebral cortex	Cingulate ctx		2	+	2	+
	Motor ctx		2	++	2	+
	Somatosensory ctx		2	++	2	+
	Piriform ctx		2	++	2	+
	Entorhinal ctx		2	+	2	++
Hippocampal formation	CA1 field		1	+	1	+/-
	CA3 field		1	+	1	++
	Dentate gyrus	Granular cell layer	3	+/-	2	+/-
		Hilus/subgranular zone	2	+/-	2	+
	Subiculum		1	+	1	++
Basal ganglia	Caudate-Putamen		2	++	2	+/-
	N. accumbens		2	+	2	+/-
	Islands of Calleja		3	+	3	++
	Ventral pallidum		2	+/-	2	+
Septum/ basal forebrain	Lateral septum	ventral	1	+/-	3	++
		intermediate	1	+/-	2	+
		dorsal	0	-	0	-
	Bed n. of the stria terminalis		1	+/-	2	++
Amygdala	Central		1	+/-	3	+
	Basolateral		1	+/-	1	+
	Basomedial		1	+/-	2	+
	Medial		1	+/-	2	+
	Cortical		1	+/-	2	+
Thalamus	Paraventicular n.		1	+/-	2	+
	Centromedian n.		1	+/-	0	-
	Anteroventral n.		2	+/-	2	+
	Reticular n.		2	+/-	3	++
	Ventrolateral		2	+/-	2	+
	Ventral posterolateral n.		2	+	2	+
	Ventral posteromedial n.		2	+/-	2	+
	Ventromedial n.		2	+/-	1	+
	Laterodorsal n. (ventrolateral part)		2	+	3	++
	Posterior nn.		2	+	1	+
	Parafascicular n.		1	+/-	2	++
	Lateral geniculate nn.	Ventral part	2	+	3	++
		Dorsal part	2	+	2	++
	Medial geniculate nn.	Ventral part	2	+	3	+
		Dorsal part	2	+	3	+
Hypothalamus	Preoptic region		1	+	2	++
	Suprachiasmatic n.		1	+/-	2	++
	Anterior n.		1	+	2	++
	Lateral hypothalamus		2	+	2	++
	Arcuate n.		2	+/-	3	++
	Ventromedial n.		1	+	2	++
	Tuberomammillary n.		1	+	2	++
	Mammillary n.		2	+	2	++
Subthalamus	Subthalamic n.		2	+	2	++
	Zona incerta		2	+	3	++
Epithalamus	Medial habenula		3	+	3	++
Midbrain	Anterior pretectal n.		2	+	1	+
	Olivary pretectal n.		2	+	1	+
	Superior colliculus		2	+	2	++
	Inferior colliculus		2	+/-	2	+
	Periaqueductal grey		1	+/-	1	+
	Raphe	Cap	1	+/-	2	++
		Median	1	+/-	2	++
		Dorsal	1	+/-	2	++
	Substantia nigra	Pars compacta	1	+	2	+
		Pars reticulata	1	+	1	+
	Interpeduncular n.		1	+	3	++
	Deep mesencephalic n.		2	+/-	2	+
Pons	Reticular formation		1	+/-	2	+
	Principal sensory n. of the trigeminal nerve		1	+/-	2	+
	N. of the lateral lemniscus		2	+/-	2	+
	Dorsal tegmentum		2	+/-	2	++
Cerebellum	Molecular layer		2	+	2	++
	Purkinje cells		2	+	1	+/-
	Granular layer		3	+	3	+/-
Main white matter tracts	Corpus callosum		2	+	1	+/-
	Anterior commissure		3	+	0	-
	Fimbria - fornix		2	+	0	-

Table 2: Regional distribution of H3.3A and H3.3B isoforms. For all the listed brain regions, abundance of HA positive cells is scored 0 = none, 1 = few, 2 = many, 3 = all, and intensity of the signal is scored - = absent, +/- = very low, + = low, ++ = high. Abbreviation: n = nucleus, nn = nuclei.

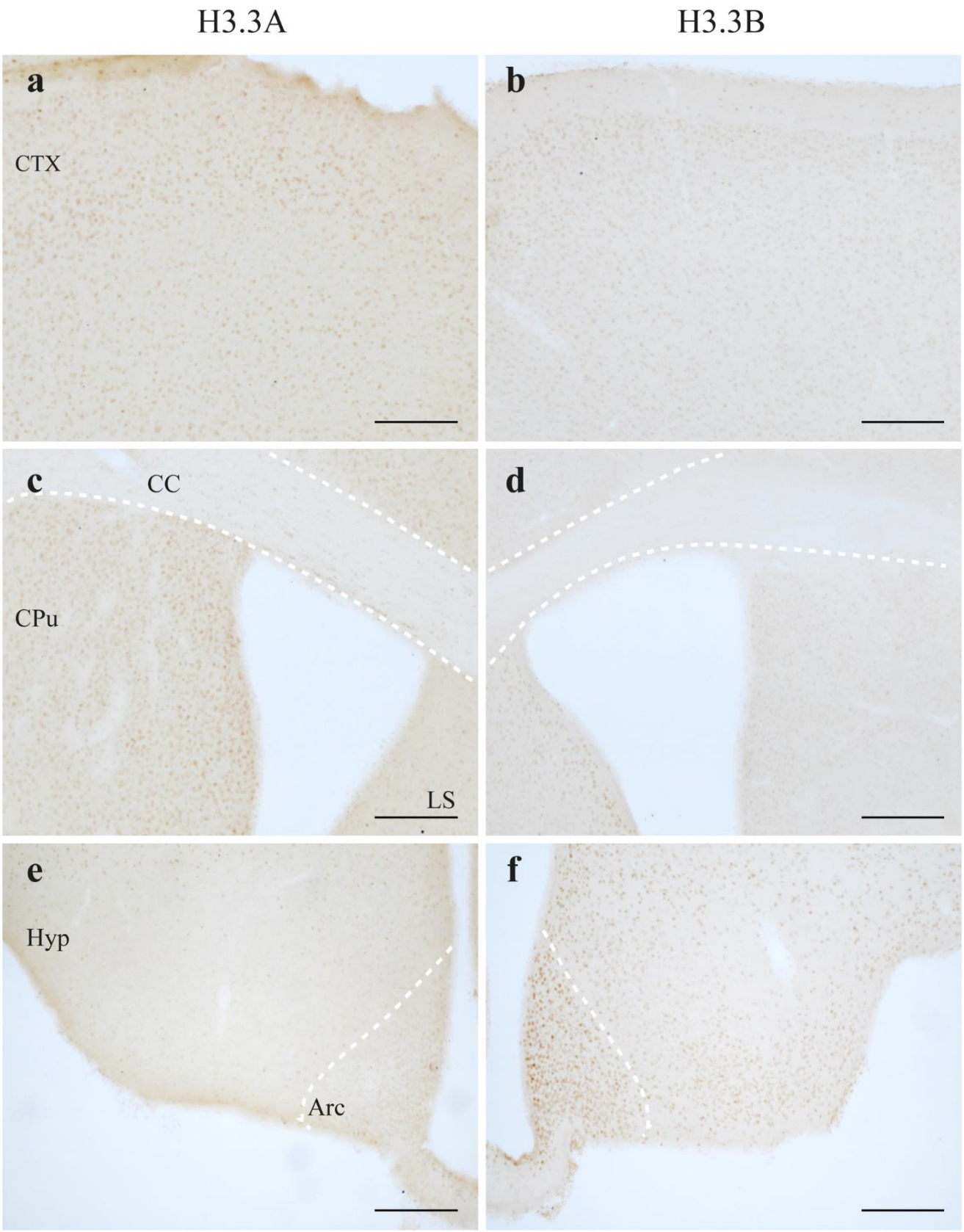

Fig. 3: Optical microscopy images of adult H3.3A and H3.3B tagged mouse brain sections, labeled with anti-HA. For both H3.3A (left column) and H3.3B (right column) animals, different areas are reported: CTX (a, b), CC, CPu and LS (c, d), Hyp nuclei including Arc (e, f). Scale bar: 200 μm.

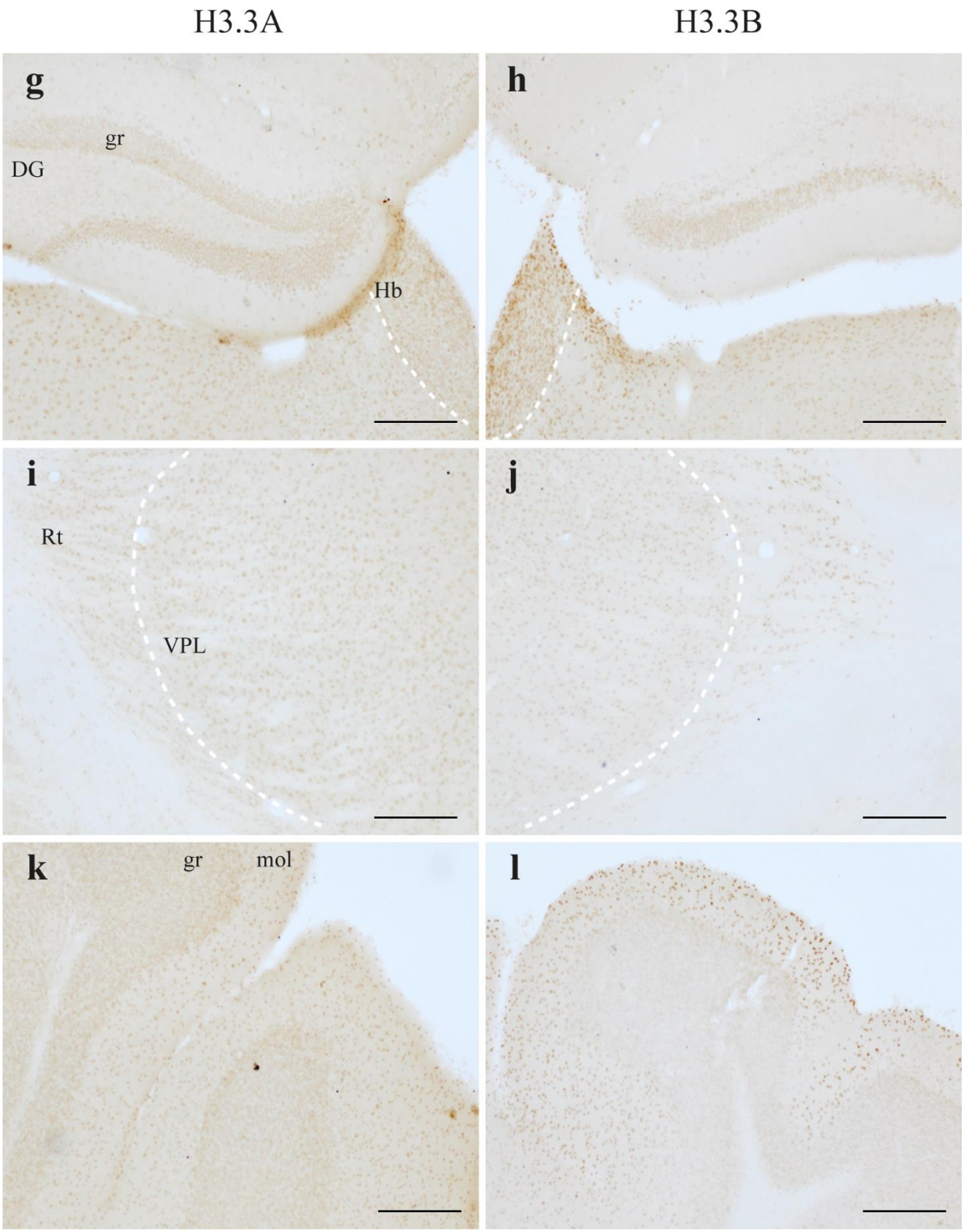

Fig. 3 (cont'd): Optical microscopy images of adult H3.3A and H3.3B tagged mouse brain sections, labeled with anti-HA. For both H3.3A (left column) and H3.3B (right column) animals, different areas are reported: DG and Hb (g, h), Rt and ventral posterolateral (VPL) Thal nuclei (i, j) and CBX gr and mol (k, l). Scale bar: 200 µm.

4.2. H3.3A and H3.3B cellular expression

In order to understand if H3.3A and H3.3B are preferentially expressed by different cell types, we performed double/triple IF with anti-HA in combination with different cell-specific Abs. IF was performed using the same animals used for IHC unless otherwise specified. Many brain areas have been analyzed but here, only the principal or most different regions are reported. In all IF panels anti-HA, i.e., the H3.3 variant, is green while the cell-type marker is red or purple.

4.2.1. Neuronal cells

First, we assessed H3.3 isoform expression in neurons by using anti-Neuronal Nuclei (NeuN) Ab combined with anti-HA Ab in H3.3A and H3.3B tagged animals. Three representative areas namely the CTX (a, d), CPu (b, e) and CC (c, f) are reported in Fig. 4; in the CC (c, f; between dashed lines), where NeuN staining was absent, H3.3A was more abundant than H3.3B, confirming IHC data. In all the analyzed areas, neurons were positive for both H3.3A (a-c) and H3.3B (d-e) but in some cells the signal was more intense.

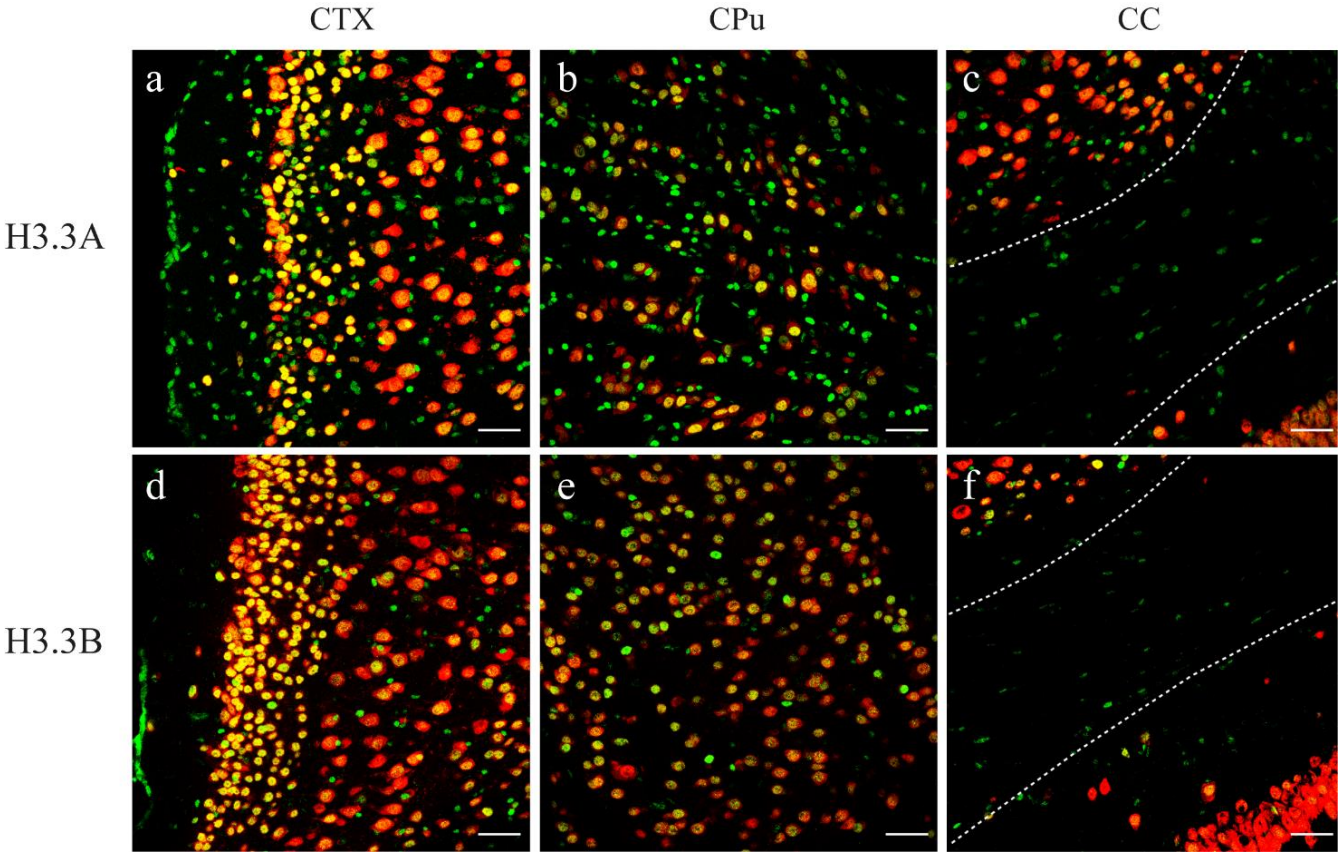

Fig. 4: Confocal microscopy images of adult H3.3A and H3.3B tagged mouse brain sections labeled with anti-HA (green) and anti-NeuN (red). NeuN positive cells in the CTX (a, d) and CPu (b, e) express both H3.3A (a, b) and H3.3B (d, e), being HA signal more intense in some cells than in others; in the CC, highlighted by dashed lined, more NeuN$^-$ cells are positive for H3.3A (c) than for H3.3B (f). Zoom: 1.28x; scale bar: 50 µm.

To further explore H3.3 signal heterogeneity observed among the NeuN-stained neuronal populations, different Abs have been used to investigate H3.3 isoforms expression in several mature neuronal types.

Dopaminergic neurons. H3.3 isoforms expression in dopaminergic (DA) neurons (Fig. 5) was evaluated using an Ab directed against tyrosine hydroxylase (TH), key enzyme in the synthesis of DA. All TH^+ DA neurons expressed both H3.3A (a-c) and H3.3B (d-f); while in Arc there were no remarkable differences between H3.3A (a) and H3.3B (d) expression, HA positivity in midbrain DA neurons was slightly higher in H3.3B tagged mice, especially in the substantia nigra (SN; e) and ventral tegmental area (VTA; f), compared to H3.3A tagged mice (b, c).

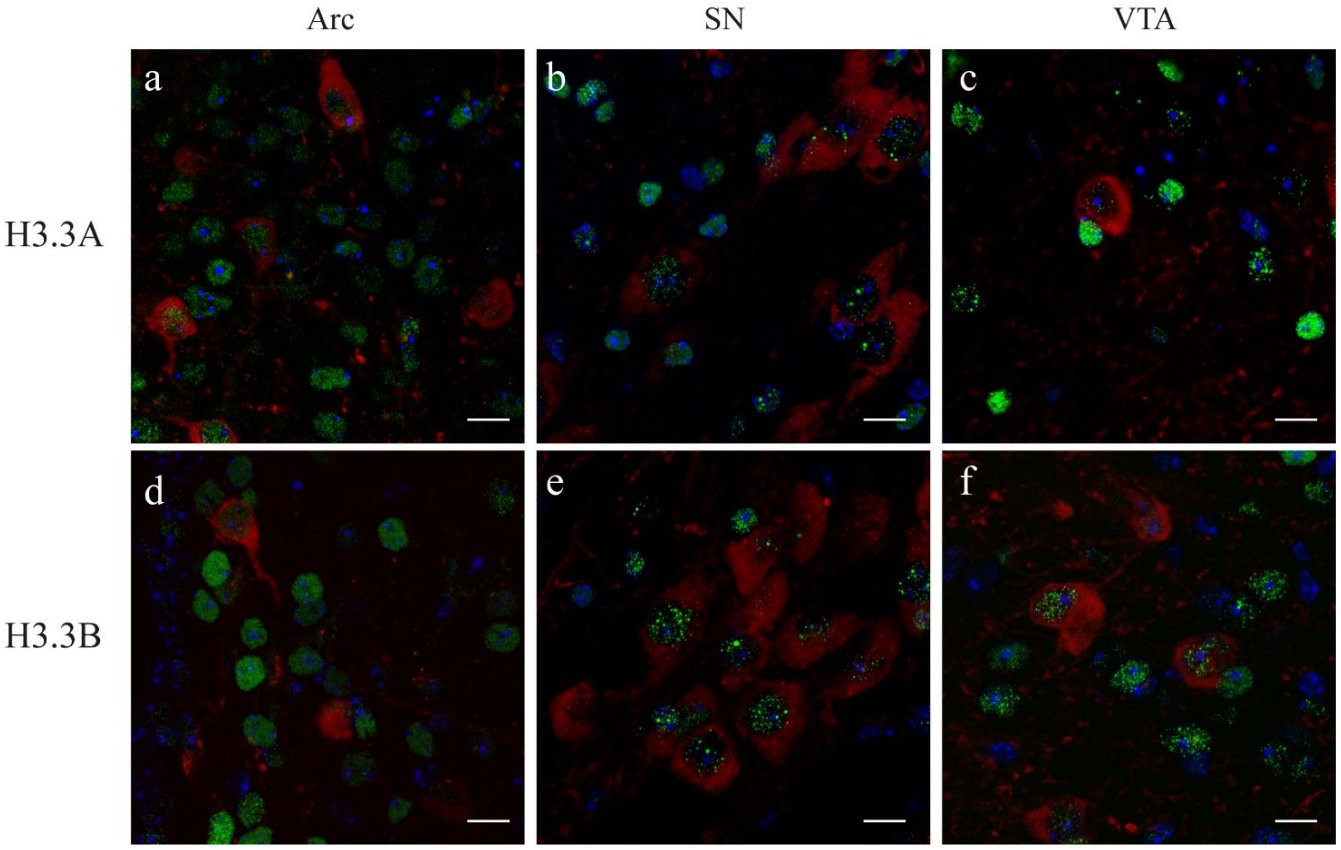

Fig. 5: Confocal microscopy images of adult H3.3A and H3.3B tagged mouse brain sections labeled with DAPI (blue), anti-HA (green) and anti-TH (red). TH^+ cells are more positive for H3.3B (d-f) than for H3.3A (a-c) in SN (b, e) and VTA (c, f). In the Arc TH^+ neurons exhibit similar positivity for both isoforms. Zoom: 3x; scale bar: 10 µm.

Interneurons. In the adult brain there are several classes of interneurons distinguishable on the basis of electrophysiology, localization and expression of particular markers. Major interneuronal populations comprise parvalbumin- (PV) and somatostatin- (SS) expressing cells [80]. To further elucidate H3.3A and H3.3B expression in neuronal subtypes we performed double IF for HA and the principal markers of some interneuronal populations.

PV, a calcium-binding protein, is expressed by the largest subgroup of cortical GABAergic inhibitory interneurons; PV^+ cells, do not express other interneuron markers such as neuropeptide Y (NPY) and calretinin (CR), so that anti-PV Ab identifies a precise population of interneurons [81]. From our analysis emerged that PV^+ cells express both H3.3A and H3.3B in almost all analyzed areas (Fig. 6) such as CTX (a, d) and striatum (b, e); in the DG (c, f) both H3.3 isoforms were expressed by PV^+ cells but to a lesser extent. Globally, there were no remarkable differences between the expression of the two isoforms in this cell type.

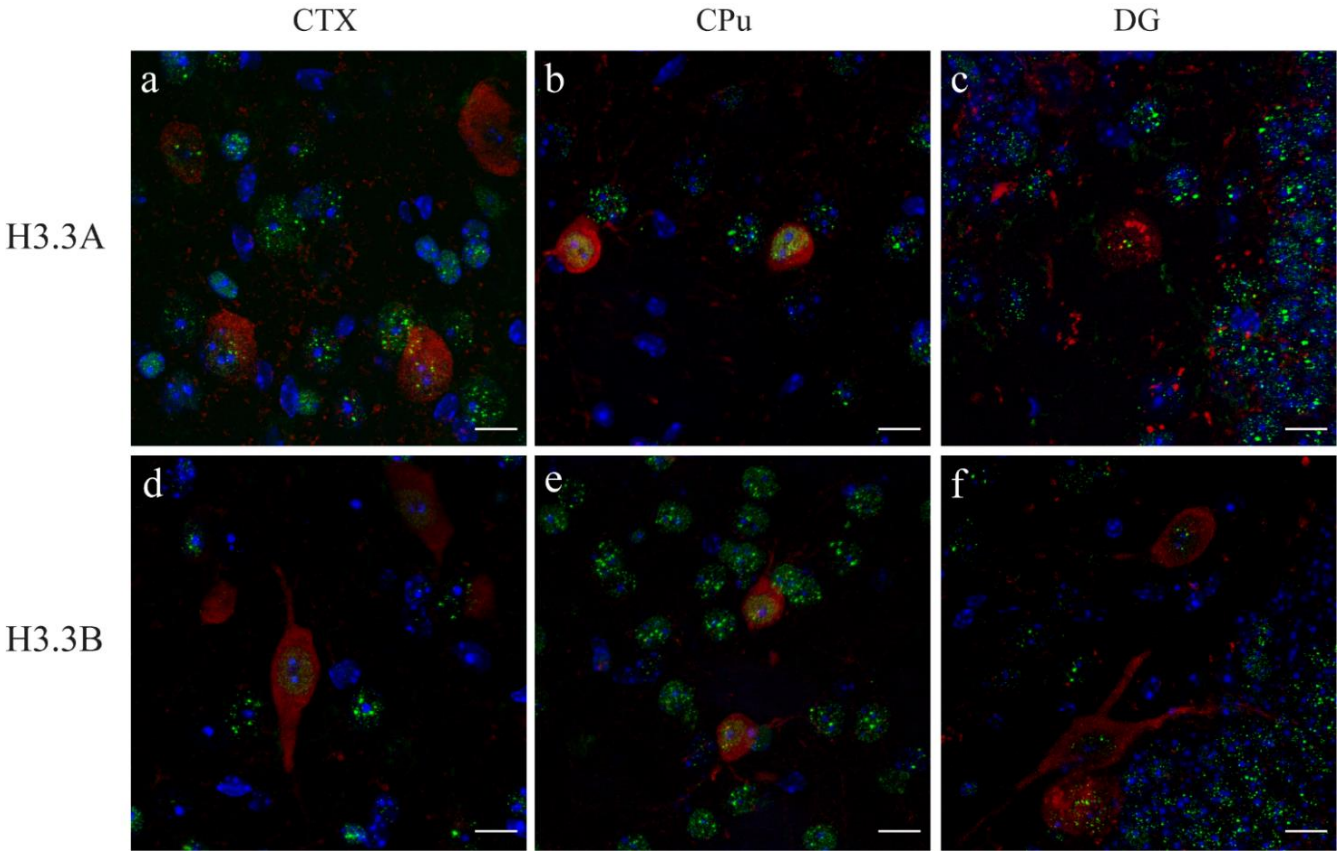

Fig. 6: Confocal microscopy images of adult H3.3A and H3.3B tagged mouse brain sections labeled with DAPI (blue), anti-HA (green) and anti-PV (red). No notable differences can be observed in the expression level between H3.3A (a-c) and H3.3B (d-f) in PV^+ cells; in CTX (a, d) and CPu (b, e) H3.3 isoforms are highly expressed whereas DG (c, f) shows low HA positivity. Zoom: 3x; scale bar: 10 µm.

SS^+ cells are a distinct class of GABAergic interneurons which is separated from PV^+ cells [81]. Using an Ab against SS we observed a comparable expression of H3.3A and H3.3B in this cell type (Fig. 7) in all analyzed areas such as the CTX (a, d) and the DG (c, f). Only in the striatum (CPu, b, e) H3.3B was more expressed than H3.3A in SS^+ interneurons. Globally, in SS^+ cells HA immunoreactivity (ir) was lower with respect to PV^+ cells.

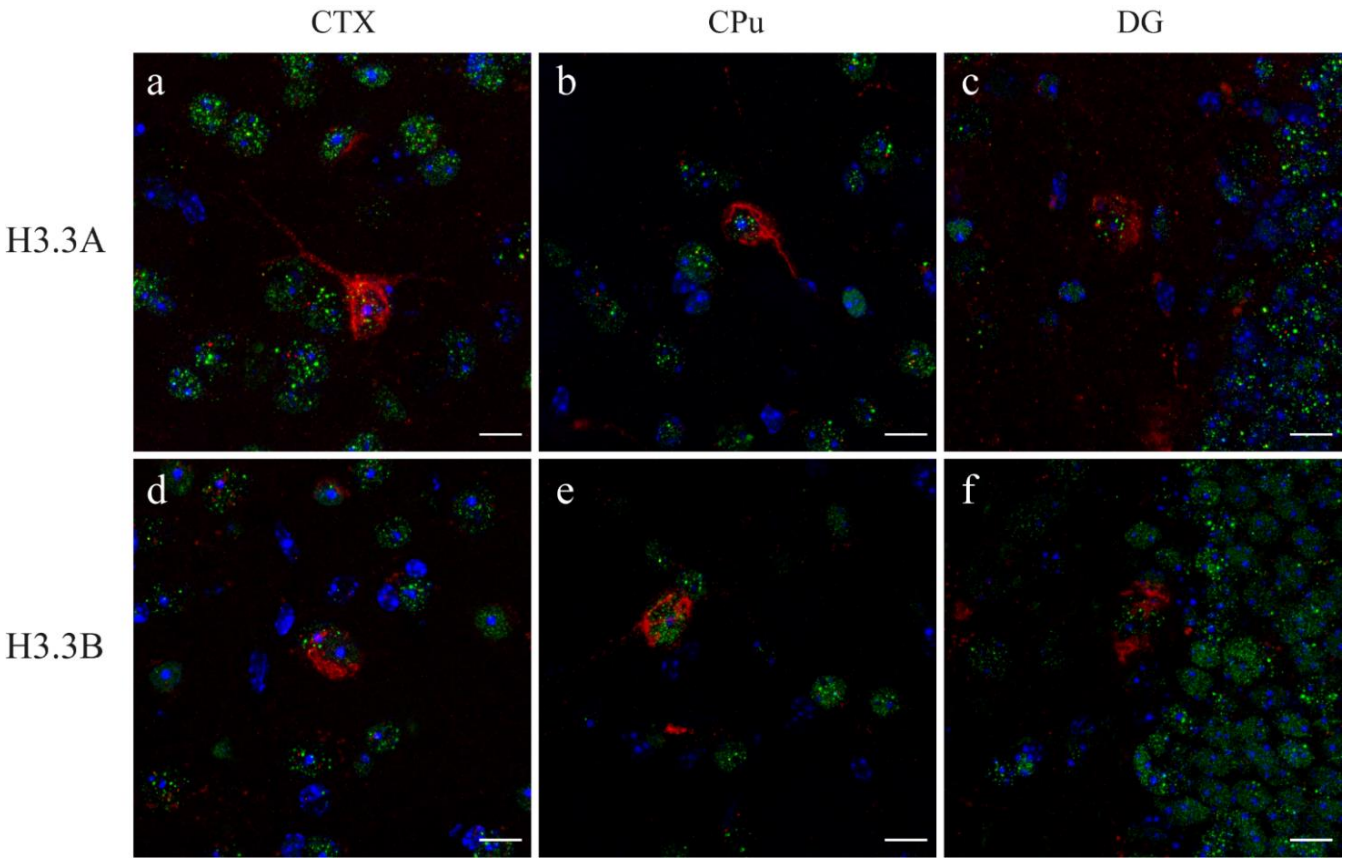

Fig. 7: Confocal microscopy images of adult H3.3A and H3.3B tagged mouse brain sections labeled with DAPI (blue), anti-HA (green) and anti-SS (red). SS^+ cells exhibit low but comparable HA ir in both H3.3A (a-c) and H3.3B (d-f) tagged mice in the majority of analyzed brain regions such as CTX (a, d) and DG (c, f) but not in the CPu (b, e) where H3.3B is more expressed than H3.3A. Zoom: 3x; scale bar: 10 µm.

The 20% or the 7% of SS^+ cells can also be CR^+ or NPY^+, respectively. In fact, most interneurons are a heterogeneous population expressing a combination of different markers in different proportions. Markers such as SS, CR and NPY can identify distinct or partially overlapping cellular populations; for instance, CR^+ cells have a 10% overlap with NPY^+ cells [81]. While NPY is a neuropeptide, CR, as PV, is a calcium-binding protein highly expressed in the CTX where it represents the 10-30% of total GABAergic interneurons [82].

To continue investigating H3.3 isoform expression in mouse interneurons we labeled brain sections with Abs against CR (Fig. 8) or NPY (Fig. 9). CR^+ cells are a heterogeneous population but globally speaking H3.3B was more expressed than H3.3A, especially in the anterior cingulate cortex (aCg; a, c) while in the dorsal CTX (b, d) the expression of the two isoforms was comparable.

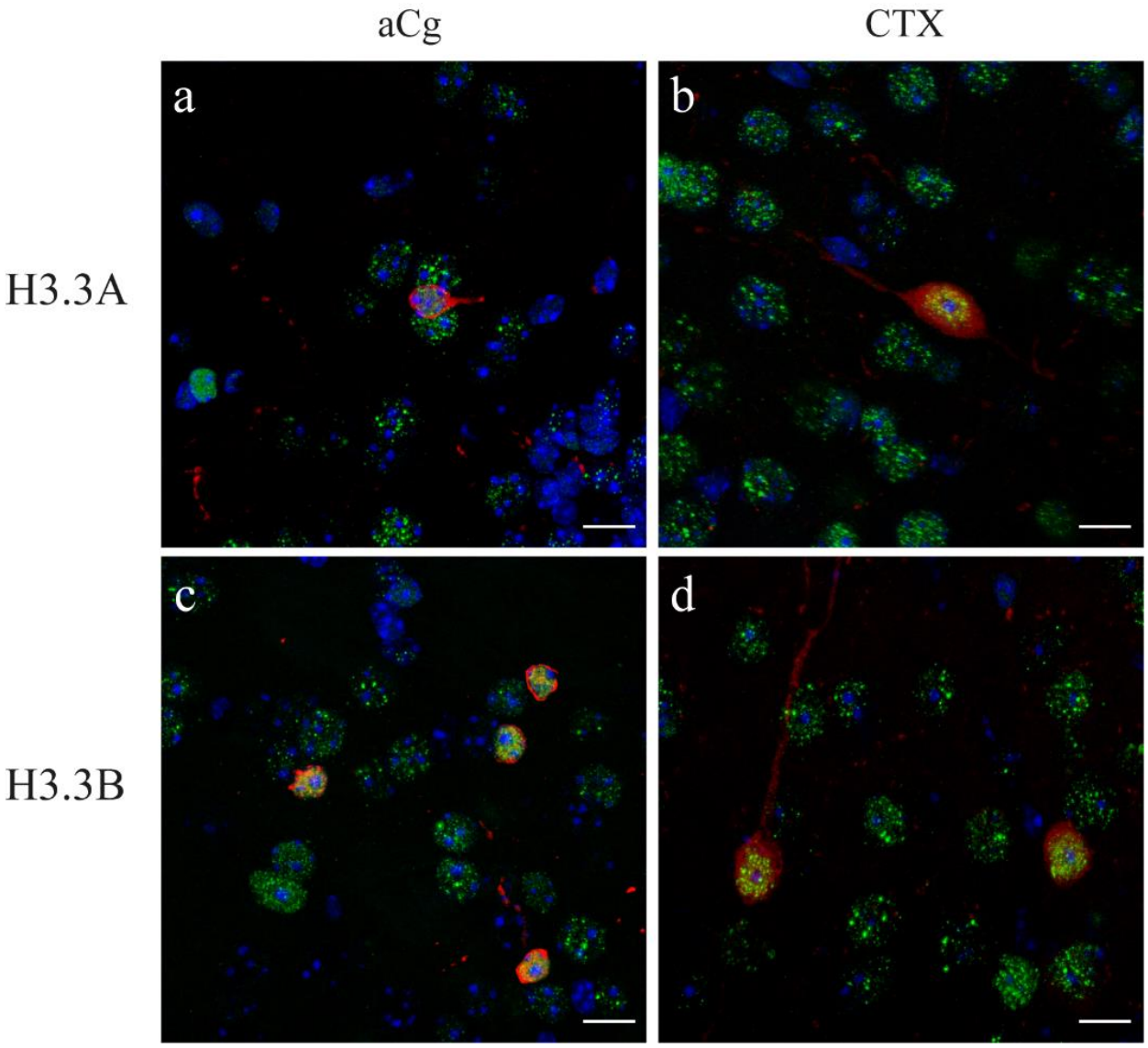

Fig. 8: Confocal microscopy images of adult H3.3A and H3.3B tagged mouse brain sections labeled with DAPI (blue), anti-HA (green) and anti-CR (red). CR^+ cells exhibit high HA ir in both H3.3A (a, b) and H3.3B (d, e) tagged mice in the majority of analyzed brain regions and especially in the dorsal CTX (b, d). In the aCg (a, c) H3.3B is higher than H3.3A. Zoom: 3x; scale bar: 10 µm.

Compared to other interneuron classes, H3.3A (a-c) and H3.3B (d-f) expression in NPY^+ cells (Fig. 9) was more inhomogeneous. In fact, in the CTX HA ir was high in both H3.3A (a) and H3.3B (b) tagged mice. In the Hip, and especially in the DG, NPY^+ cells exhibited low levels of H3.3A (c) but were positive or negative for H3.3B (f). In the striatum, H3.3A levels in NPY^+ interneurons were comparable to other regions (b) while H3.3B signal was very high (e) as already observed for SS^+ cells.

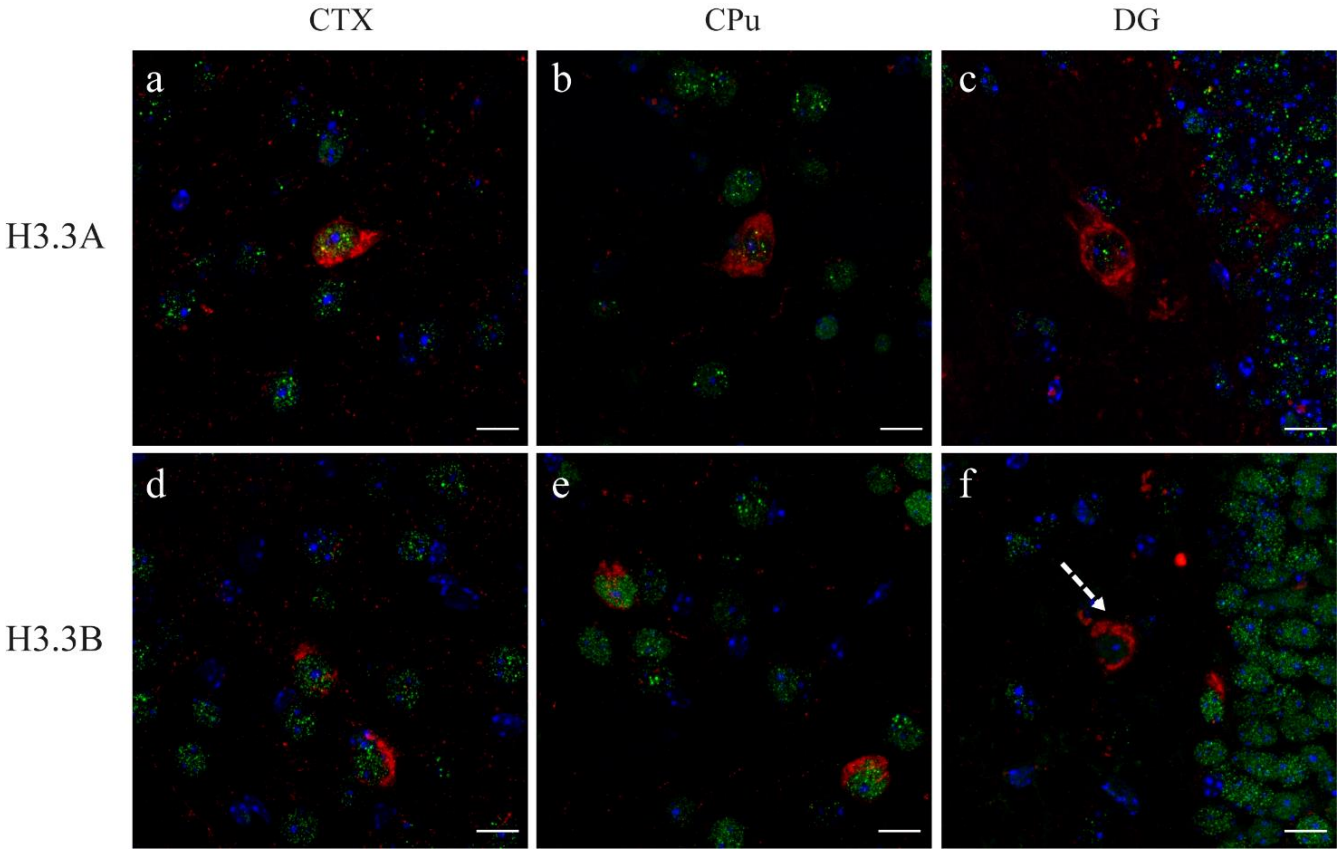

Fig. 9: Confocal microscopy images of adult H3.3A and H3.3B tagged mouse brain sections labeled with DAPI (blue), anti-HA (green) and anti-NPY (red). In NPY^+ cells H3.3A expression is high in the CTX (a) but low in CPu (b) and DG (c). On the contrary, H3.3B is highly expressed in the CPu (e), less expressed in the CTX (d) and present or absent in the DG (f). Dashed arrow indicates NPY^+ cells negative for HA ir. Zoom: 3x; scale bar: 10 µm.

Overall, all tested types of interneurons exhibited both H3.3A and H3.3B even if to a different extent. PV^+ and CR^+ cells presented high levels of both isoforms whereas in SS^+ interneurons, with CPu as an exception, H3.3 isoforms expression was low. Finally, in the striatum NPY^+ and SS^+ cells expressed higher H3.3B levels than H3.3A levels.

Neuronal differentiation stages. Once assessed the expression of both isoforms in mature neurons, we investigated H3.3A and H3.3B expression at different stages of neuronal differentiation to assess the starting point in H3.3 variants expression during adult neurogenesis. To this purpose, brain sections from young (2 month-old) H3.3A and H3.3B tagged mice were labeled using anti-Ki67 Ab which specifically recognizes cycling/proliferating cells and anti-nestin and anti-doublecortin (DCX) Abs for the identification of two subsequent stages of neuronal maturation (Fig. 10). Two different triple IF experiments were performed: one using anti-HA, anti-Ki67 and anti-DCX Abs and the other using anti-HA, anti-Ki67 and anti-nestin Abs. Interestingly, proliferating cells positive for Ki67, but not for immature neuron markers, expressed H3.3A (a) but not H3.3B (d). Only part of immature nestin$^+$ neurons, which are not proliferating (Ki67$^-$), expressed H3.3A and H3.3B: in particular, in the sub-granular zone (SGZ) at the interface between DG gr and hilus, nestin$^+$ neurons expressed both H3.3A and H3.3B whereas nestin$^+$ neurons located more internally in the gr were negative for both isoforms (b, e). Finally, non-cycling (Ki67$^-$) DCX$^+$ cells were positive for both H3.3A and H3.3B (c, f).

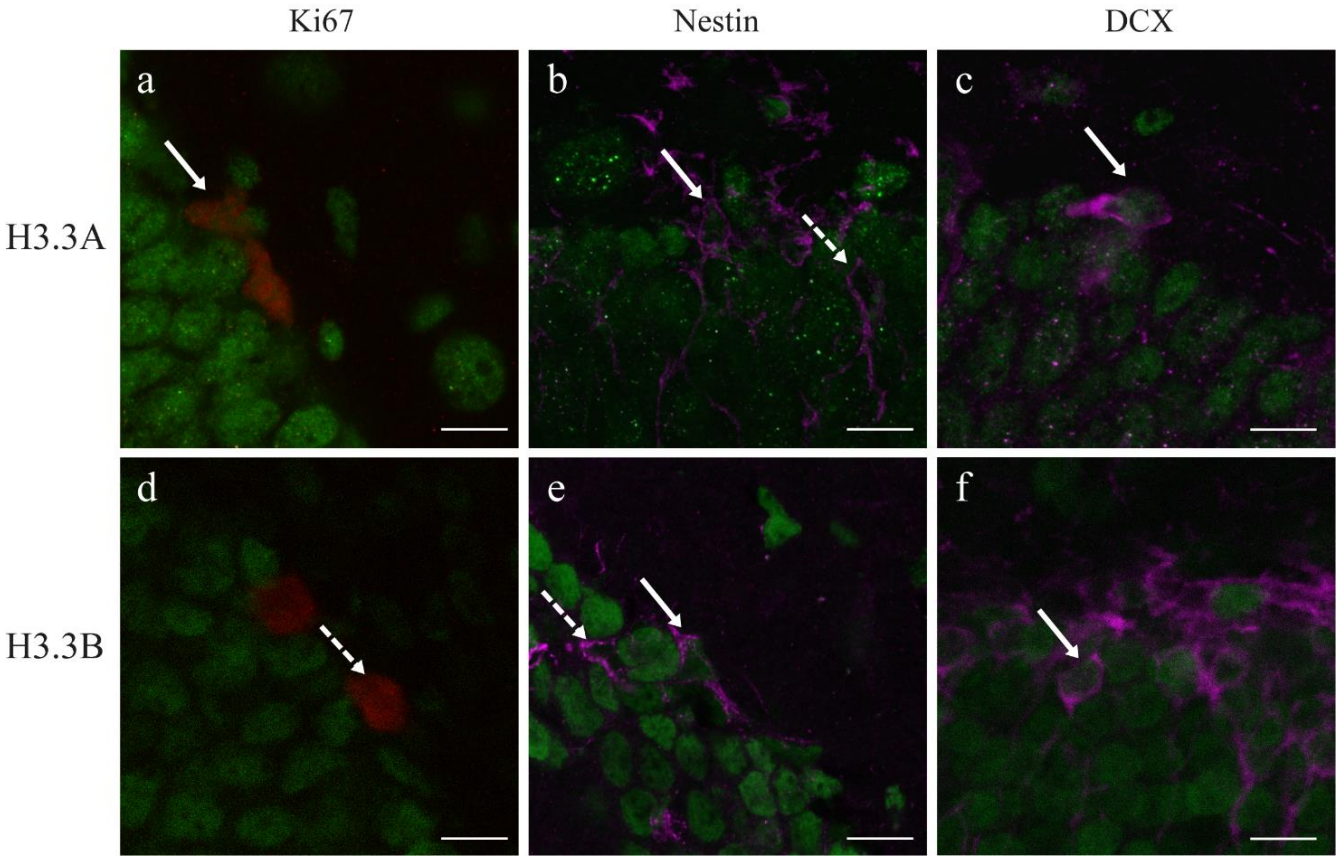

Fig. 10: Confocal microscopy images of young H3.3A and H3.3B tagged mouse brain sections labeled with anti-HA (green), anti-ki67 (red) and nestin (b, e) or DCX (c, f) neuronal maturation markers (purple). Ki67$^+$ cells are positive for H3.3A (a) but not H3.3B (d). Nestin$^+$ cells in the SGZ, but not those inside gr, are positive for both isoforms (b, e). DCX$^+$ cells express both H3.3A (c) and H3.3B (f). Full arrows indicate examples of double positive cells while dashed arrows point to HA$^-$ cells. Zoom: 4.5x; scale bar: 10 µm.

4.2.2. Glial cells

The differential expression of H3.3 isoforms in white matter tracts led us to investigate their presence in glial cells. Double IF stainings for HA and glial cell-specific markers were performed on adult H3.3A and H3.3B tagged mice (4 males and 4 females, of 4 months of age, for each isoform). Glial fibrillary acidic protein (GFAP) and ionized calcium-binding adapter molecule 1 (Iba1) expression were used as astrocytic and microglial markers, respectively. Additionally, S100 calcium-binding protein B (S100B) was employed to identify a subpopulation of mature astrocytes and precursors of oligodendrocytes.

S100B-expressing cells. Almost all S100B$^+$ cells (Fig. 11) were highly positive for H3.3A in both white (e.g., CC; a) and grey (e.g., CA3; b) matter regions. On the contrary, in the mixed population of S100B$^+$ cells, H3.3B expression was low or absent (c, d).

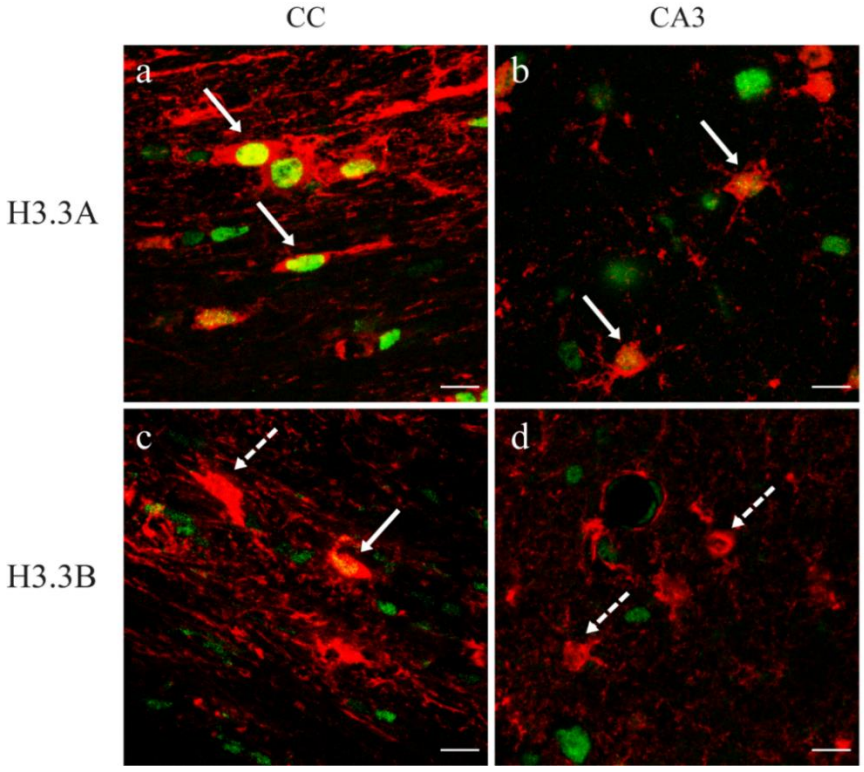

Fig. 11: Confocal microscopy images of adult H3.3A and H3.3B tagged mice brain sections labeled with anti-HA (green) and anti-S100B (red). In the CC S100B$^+$ cells are highly positive for H3.3A (a) but slightly positive or negative for H3.3B (c). Accordingly, in the CA3 all S100B$^+$ cells are positive for H3.3A (b) and negative for H3.3B (d). Full arrows indicate examples of double positive cells while dashed arrows point to HA$^-$ cells. Zoom: 4 x; scale bar: 10 µm.

Astrocytes. In line with the expression pattern of S100B$^+$ cells, GFAP$^+$ astrocytes (Fig. 12) showed H3.3A positivity in both white (c) and grey matter (a, e, g) whereas extremely low or absent H3.3B expression was observed in all the analyzed areas (b, d, f, h).

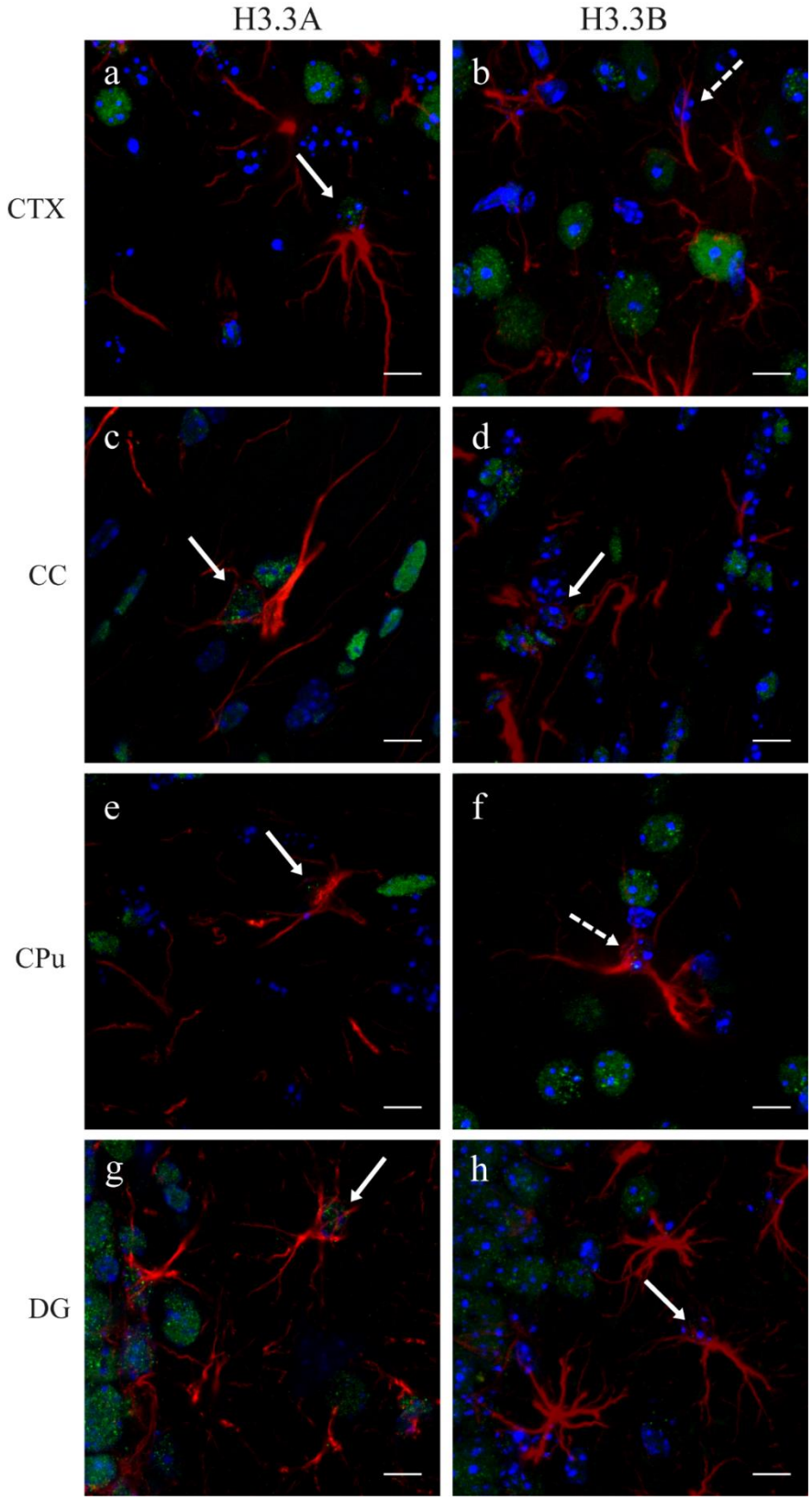

Fig. 12: Confocal microscopy images of adult H3.3A and H3.3B tagged mouse brain sections labeled with DAPI (blue), anti-HA (green) and anti-GFAP (red). $GFAP^{+}$ cells express H3.3A in both white (c) and grey matter (a, e, g). H3.3B is nearly absent or absent in all the analyzed areas (b, d, f, h). Full arrows indicate examples of double positive cells while dashed arrows point to HA^{-} cells. Zoom: 4 x; scale bar: 10 µm.

H3.3A isoform expression in $GFAP^+$ and $S100B^+$ glial cells, where H3.3B was nearly absent, confirmed the IHC data on the widespread distribution of H3.3A and the low expression of H3.3B in the white matter tracts.

Microglia. Interestingly, almost the totality of microglial cells ($Iba1^+$), in all the analyzed areas, was negative not only for H3.3B but also for H3.3A (Fig. 13). In fact, in both white (c, d) and grey matter (a, b, e-h) HA signal did not co-localize with $Iba1^+$ cell nuclei in both H3.3A (a, c, e, g) and H3.3B (b, d, f, h) tagged mice. Very rare slightly positive cells were observed in dorsal cortical areas and Arc. As mentioned before, microglial cells, unlike other glial populations in the adult brain, derive from yolk sac progenitors and not from common neural progenitors, so the absence of H3.3A in this glial population is not entirely surprising.

4.2.3. H3.3 and H2A.Z co-expression

It is known from literature that both H3.3 and H2A.Z tend to destabilize the nucleosome; these two variants have been proved to co-localize in frequently disrupted genomic sites in chickens; in fact, double-variant nucleosomes are highly unstable [5, 83]. To observe H3.3A or H3.3B co-localization with H2A.Z we labeled brain sections from 4 month-old H3.3A and H3.3B tagged mice using anti-HA Ab combined with anti-H2A.Z Ab. High resolution images were obtained using STED microscopy (Fig. 14). In all the analyzed areas, both H3.3A (a) and H3.3B (b) co-localized with H2A.Z but not in all nuclei: some cells were double-positive while other cells were positive only for H3.3 or H2A.Z. Super-resolution allowed the visualization of both variants inside the nucleus, where apparently H3.3 isoforms (red) and H2A.Z (blue) were dispersed and did not tend to form specific chromatin domains (a, b). Unfortunately, co-localization within the same nucleosome could neither be demonstrated nor excluded since the size of the antibodies (~10-20 nm each), along with STED resolution (~30 nm), prevents the visualization of a single nucleosome (~11 nm). With this approach, we can only state that, inside the nucleus, both H3.3A and H3.3B can be found in close proximity to H2A.Z.

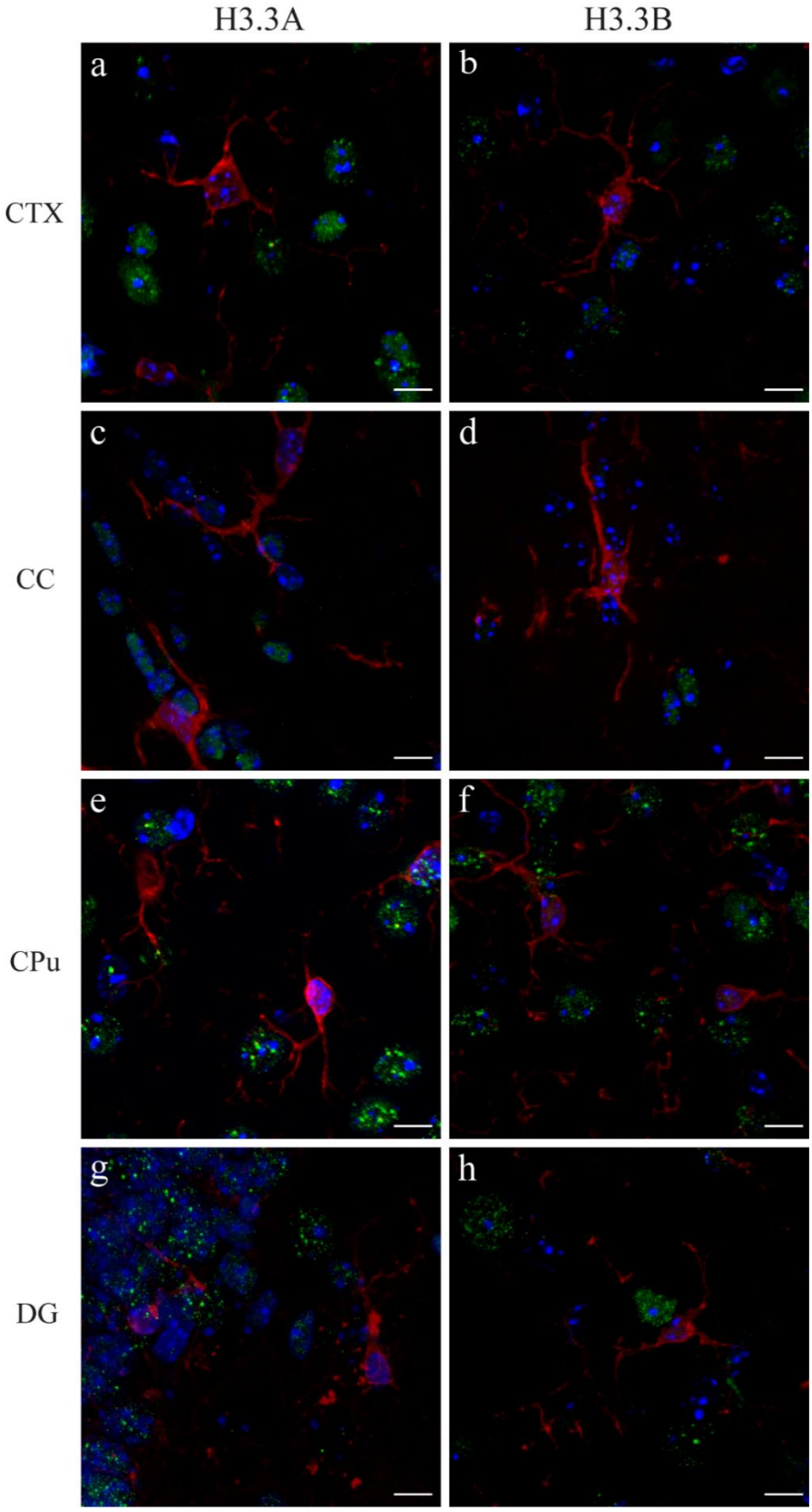

Fig. 13: Confocal microscopy images of adult H3.3A and H3.3B tagged mouse brain sections labeled with DAPI (blue), anti-HA (green) and anti-Iba1 (red). Almost the totality of microglial cells is negative for both H3.3A (a, c, e, g) and H3.3B (b, d, f, h) in white (c, d) and grey matter (a, b, e-h). Zoom: 4 x; scale bar: 10 µm.

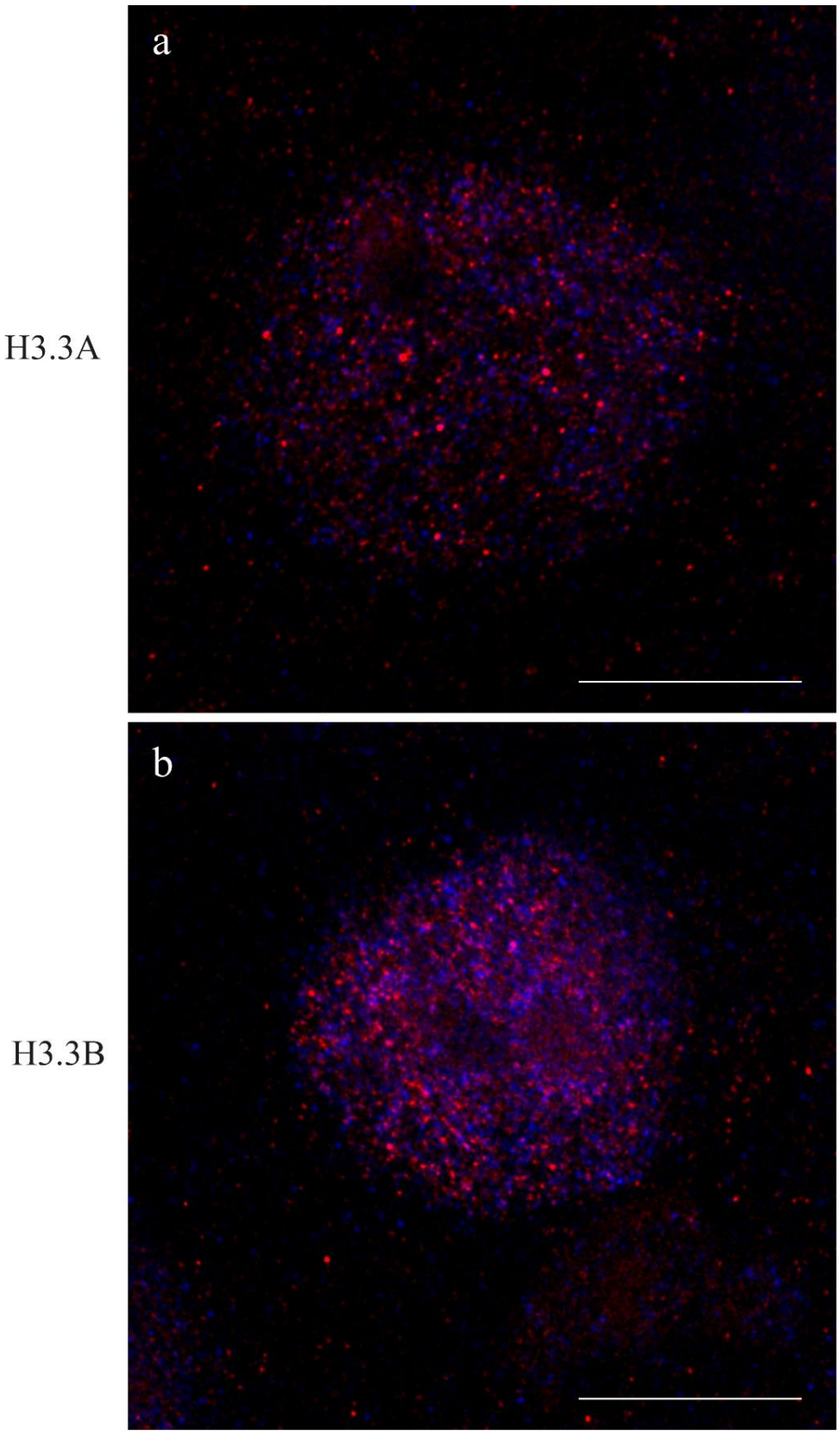

Fig. 14: Super-resolution images of cell nuclei stained with anti-HA (red) and anti-H2A.Z (blue) in H3.3A and H3.3B tagged mice. Inside the nucleus, both H3.3A (a) and H3.3B (b) can be found close to H2A.Z. Scale bar: 5 µm

4.3. H3.3B expression changes after exposure to an enriched environment

After assessing H3.3 basal presence in different brain areas and cellular types, we investigated the possible changes arising from two completely different stimuli such as the exposure to an EE and sub-chronic Coc treatment. Due to the more heterogeneous region-specific distribution and cellular expression of H3.3B, with respect to H3.3A, and to literature data describing the former as the stimulus-responsive variant, only H3.3B was chosen for these subsequent analyses. Moreover, since no sex differences have been observed in basal variant expression, to avoid EE-associated male aggression previously observed in C57BL/6 mice in our laboratory, only females underwent EE/SE experiment while males were used for Coc treatment.

After 4 weeks of exposure to SE (n = 9) or EE (n = 9), 2 month-old H3.3B tagged mice were processed for IHC and labeled using anti-HA Ab (Fig. 15). Different brain areas such as CTX and Hip, known from literature to be primarily affected by EE, were analyzed; the number of H3.3B expressing cells and the intensity of their signal, indicated respectively as % of area occupied by HA^+ cells and MGV after background subtraction, were evaluated using ImageJ particle analyzer. In CA3 (h) and DG (f) Hip subregions, but not in CA1 (g), a significant increase in the number of H3.3B expressing cells could be observed in EE housed mice (b) with respect to SE housed mice (a). Additionally, a trend for significance could be observed in the CTX (c, d). SE and EE animals did not exhibit any significant differences as concerns signal intensity (data not shown).

Moreover, to evaluate H3.3B expression changes after exposure to an EE in the whole brain, hemispheres obtained from two SE and two EE housed mice were stained using anti-HA Ab, cleared and visualized by means of a light sheet microscope; 3D images were reconstructed using Arivis Vision4D (Fig. 16, a). Z-stack images (b) were size-filtered and background-corrected using Python (c, d), then positive nuclei density was estimated binarizing filtered images with a manually-determined threshold and visualized by means of heatmaps (e, f) using ImageJ. While no remarkable differences could be observed in the CPu, CC and CBX, and in general in subcortical regions, mice subjected to EE (f) exhibited a higher density of nuclei positive to HA, compared to SE (e) animals, in the CTX, CA3 and DG confirming the IHC data. The method employed here allows only a qualitative estimation; a precise count to determine the number of positive cells in different atlas-aligned brain regions, will be performed in the future.

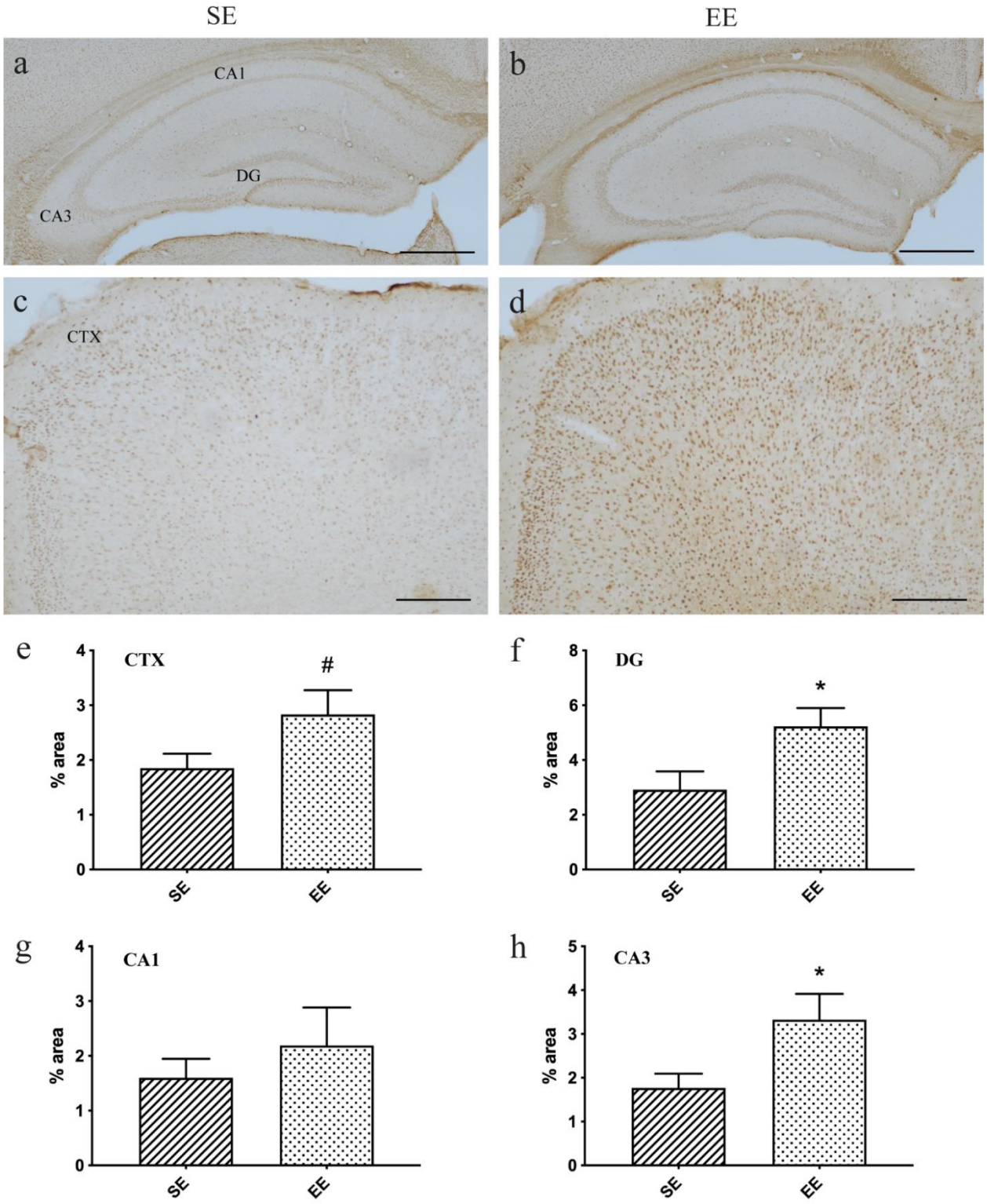

Fig. 15: a-d) Optical microscopy images of brain sections of H3.3B tagged mice, housed in SE or EE, labeled with anti-HA. Representative images of the Hip (a, b) and its subregions and CTX (c, d) of SE (a, c) and EE (b, d) mice. Scale bar a,b: 500 µm; c, d: 200 µm. **e-h) % of area occupied by HA^+ cells of SE and EE mice in different brain regions**. In the DG (f) and CA3 (h), but not in CA1 (g), the % of area covered by HA^+ cells is significantly higher (*) in EE housed animals with respect to SE housed animals. In the CTX only a trend towards a significant effect (#) can be observed (e). All data are plotted as mean ±SEM. Statistical analyses were performed by *t* test with Welch's correction when the two groups had unequal SDs; CTX p=0.0843 (e), DG p=0.0337 (f), CA1 p=0.4662 (g) and CA3 p=0.0416 (h).

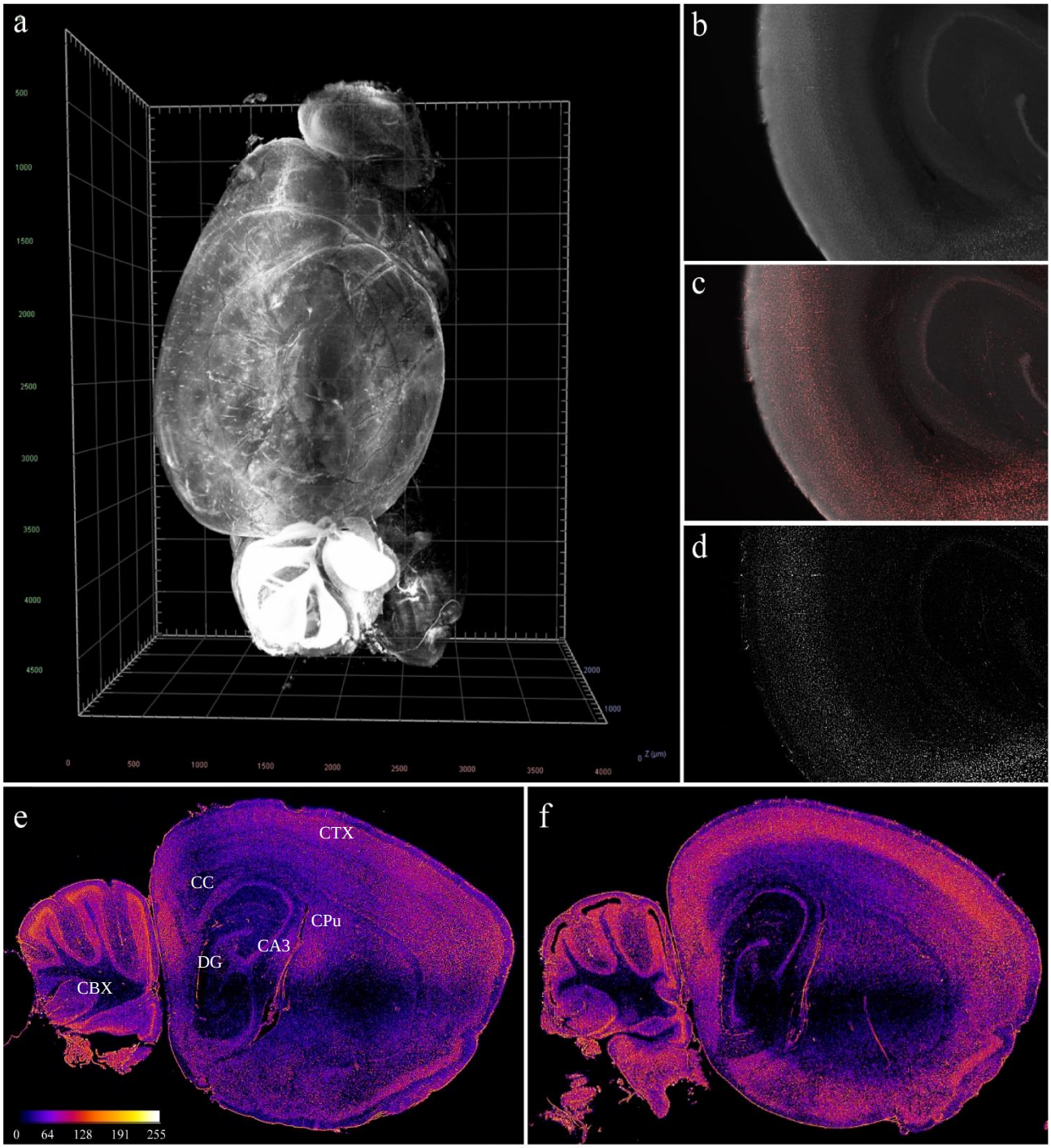

Fig. 16: a) 3D reconstruction of a clarified H3.3B tagged mouse hemibrain. Arivis Vision 4D software was used to reconstruct Z-stack sagittal images acquired with a light sheet microscope. Scale grid: 5000 x 4000 µm. **b-d) Background correction and filtering of light sheet images.** Raw images with high background noise (b) were filtered to enhance cells (red) over nonspecific signal (c). Finally, filtered images (d) were obtained subtracting enhanced contrast images to the raw ones. **e, f) Heatmaps of HA^+ cells density obtained from SE and EE H3.3B tagged mice clarified hemibrains.** Filtered images of comparable sagittal sections, representative for HA labeling in SE (e) and EE (f) animals, were binarized to generate heatmaps. The nuclei density is represented by different colors in arbitrary units ranging from absence (0, black) to highest density (255, white). In CTX, DG and CA3, the density of H3.3B positive cells is higher in EE mice, while in CC, CPu and CBX H3.3B expression in EE animals is comparable to that of SE animals.

Next, in order to understand if EE exposure could stimulate changes in H3.3B cellular expression pattern, double IF stainings were performed using anti-HA Ab in combination with Abs directed against different neuronal (Fig. 17) and glial (Fig. 18 and Fig. 19) cell populations.

First, fluorescent Nissl staining (NeuroTrace^{TM}) was used to mark both adult and immature neurons at the same time (Fig.17, a, d). The number of HA^{-} neurons was higher in the DG of SE mice (a) compared to EE mice (d), especially in the superficial layer of gr in contact with the hilus. So, the exposure to EE increased H3.3B expression in particular in the internal gr, the part of the gr containing immature neurons. Proliferating cells expressing Ki67 were, however, negative for H3.3B even after EE (data not shown).

Changes in H3.3B expression were then evaluated in SS^{+} (b, e) and NPY^{+} (c, f) interneurons, where histone basal expression was not very high; however, no remarkable differences were observed between SE (b, c) and EE (e, f) animals.

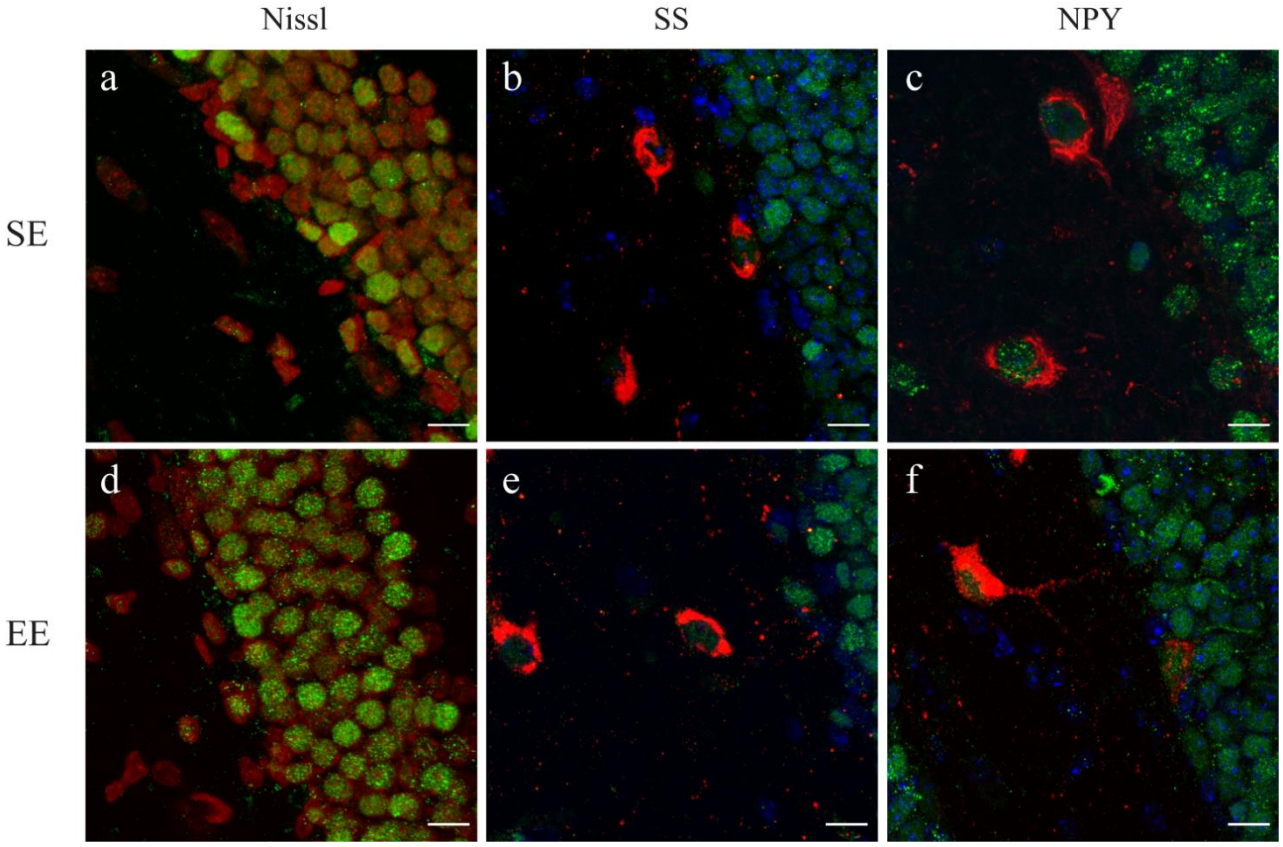

Fig. 17: Confocal microscopy images of the DG of H3.3B tagged mice, housed in SE or EE, labeled with DAPI (blue), anti-HA (green) and different neuronal markers (red). While no evident changes in H3.3B expression are observed in SS^{+} (b, e) and NPY^{+} (c, f) interneurons after EE, Nissl fluorescent staining (a, d) revealed an increase in the number of H3.3B expressing neurons in the gr of the DG consequent to EE exposure (d). Zoom: 3x; scale bar: 10 µm.

Next, we evaluated the effects of EE on GFAP$^+$ and S100B$^+$ cells (Fig. 18), where H3.3B was barely expressed in basal condition. While H3.3B expression in astrocytes remained low (a, b), S100B-expressing cells were more positive for HA in EE mice (d) compared to SE animals (c) in all analyzed areas.

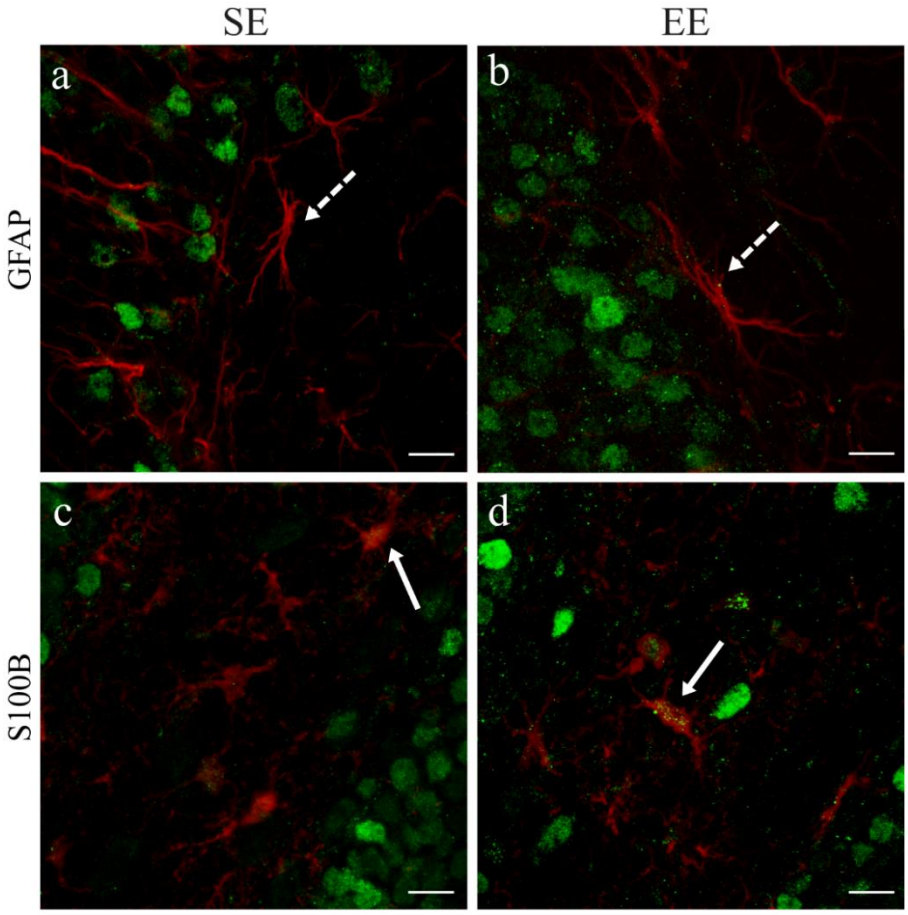

Fig. 18: Confocal microscopy images of DG in H3.3B tagged mice, housed in SE or EE, labeled with DAPI (blue), anti-HA (green) and different glial markers (red). No evident changes in H3.3B expression are observed, in GFAP$^+$ cells, between SE (a) and EE (b) mice, while S100B$^+$ cells show higher HA signal in EE (d) animals with respect to SE (c) animals. Full arrows indicate examples of double positive cells while dashed arrows point to HA$^-$ cells. Zoom: 4x; scale bar: 10 µm.

Finally, H3.3B expression was assessed in microglial cells (Fig. 19). In basal conditions, this histone variant was basically absent in Iba1$^+$ cells; this was confirmed in SE mice (a, c, e, g). After a 4 week exposure to EE, an increase in double positive cells (Iba1$^+$/HA$^+$) could be observed, especially in the dorsal Cg (d) where almost the totality of microglial cells expressed H3.3B. This EE-dependent increment of H3.3B-expressing microglia could be also found in the Arc (b), and to a lesser extent in the LS (h). In all other analyzed regions such as in the lacunosum molecular layer (LMol; f) no differences have been observed between SE and EE mice.

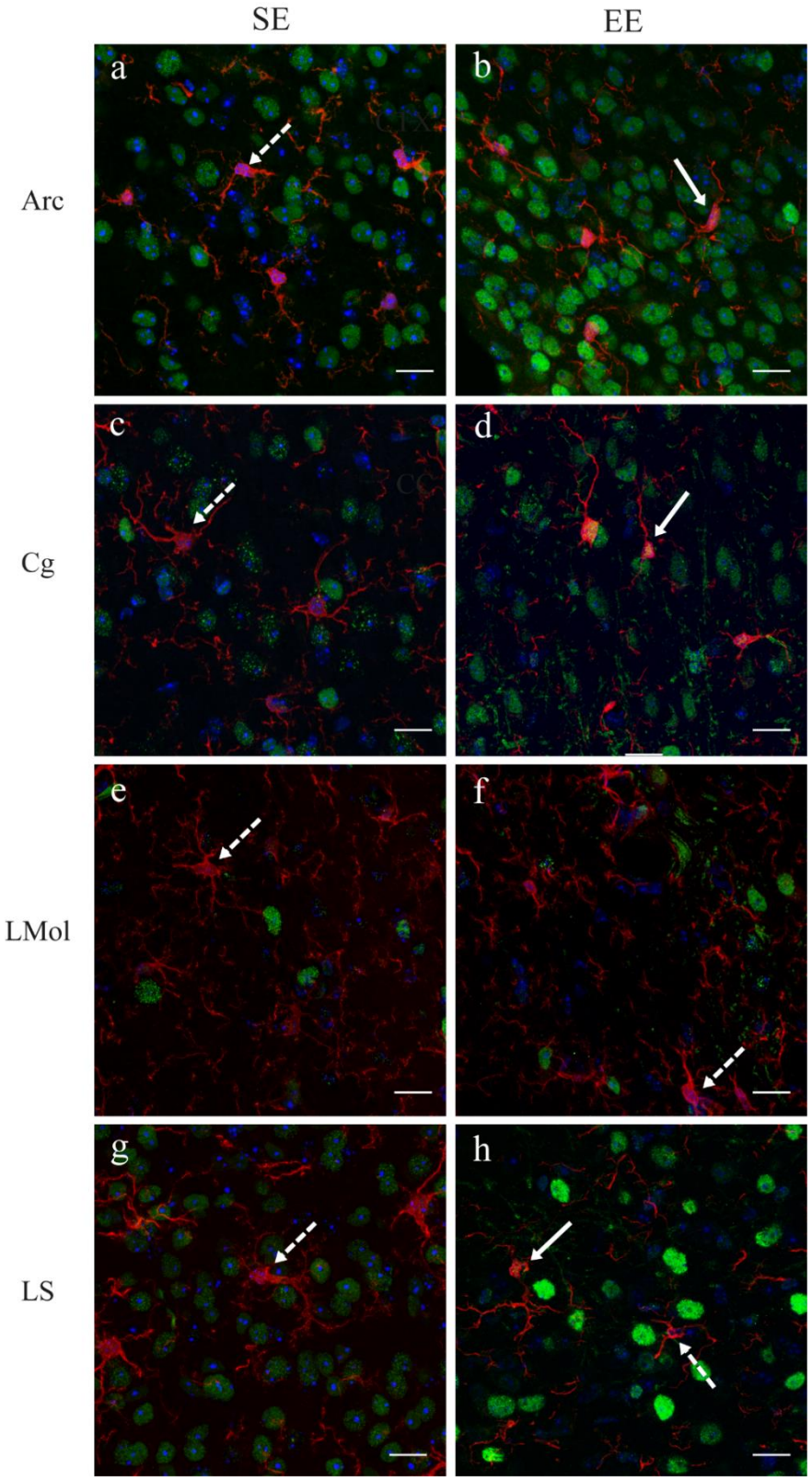

Fig. 19: Confocal microscopy images of SE or EE H3.3B tagged mice brain sections labeled with DAPI (blue), anti-HA (green) and anti-Iba1 (red). In SE housed mice (a, c, e, g) almost the totality of microglial cells is negative for H3.3B in all the analyzed areas. Exposure to EE increases the number of H3.3B expressing microglia especially in the Cg (d) and to a lesser extent in Arc (b) and LS (h). In the LMol (f) no increment can be observed. Full arrows indicate examples of double positive cells while dashed arrows point to HA^- cells. Zoom: 4 x; scale bar: 10 µm.

To understand if H3.3B$^+$ and H3.3B$^-$ microglial cells belong to specific subpopulations, two different M1 and M2 microglial-state markers were used. The M1 pro-inflammatory phenotype was assessed by using an Ab directed against triggering receptor expressed on myeloid cells 2 (TREM2); however, no TREM2$^+$ cells were detected in any brain regions (data not shown) in both SE and EE animals. The M2 anti-inflammatory phenotype was marked by means of anti-cluster of differentiation 206 (CD206) Ab along with anti-Iba1 Ab (Fig. 20). In H3.3B tagged mouse brain very few cells expressed CD206 (purple) even in CTX (a, d) and Arc (b, e); additionally, it appears that this is not a very specific marker, since also most meningeal and perivascular cells usually express CD206. Therefore, we assessed H3.3B expression also in meninges (Men; c, f). CD206$^+$ cells, often expressed H3.3B even under standard conditions (a-c); this H3.3B expression could be observed both when Iba1 (red) and CD206 co-localize (e.g., b) and when they do not (e.g., c). In EE animals (d-f) there were no clear changes in the number of H3.3B$^+$/CD206$^+$ cells and Iba1$^+$/CD206$^-$/H3.3B$^+$ could be observed (d); these data indirectly suggest that the H3.3B expression increment in microglia does not correlate with the classical pro-/anti-inflammatory phenotypic distinction.

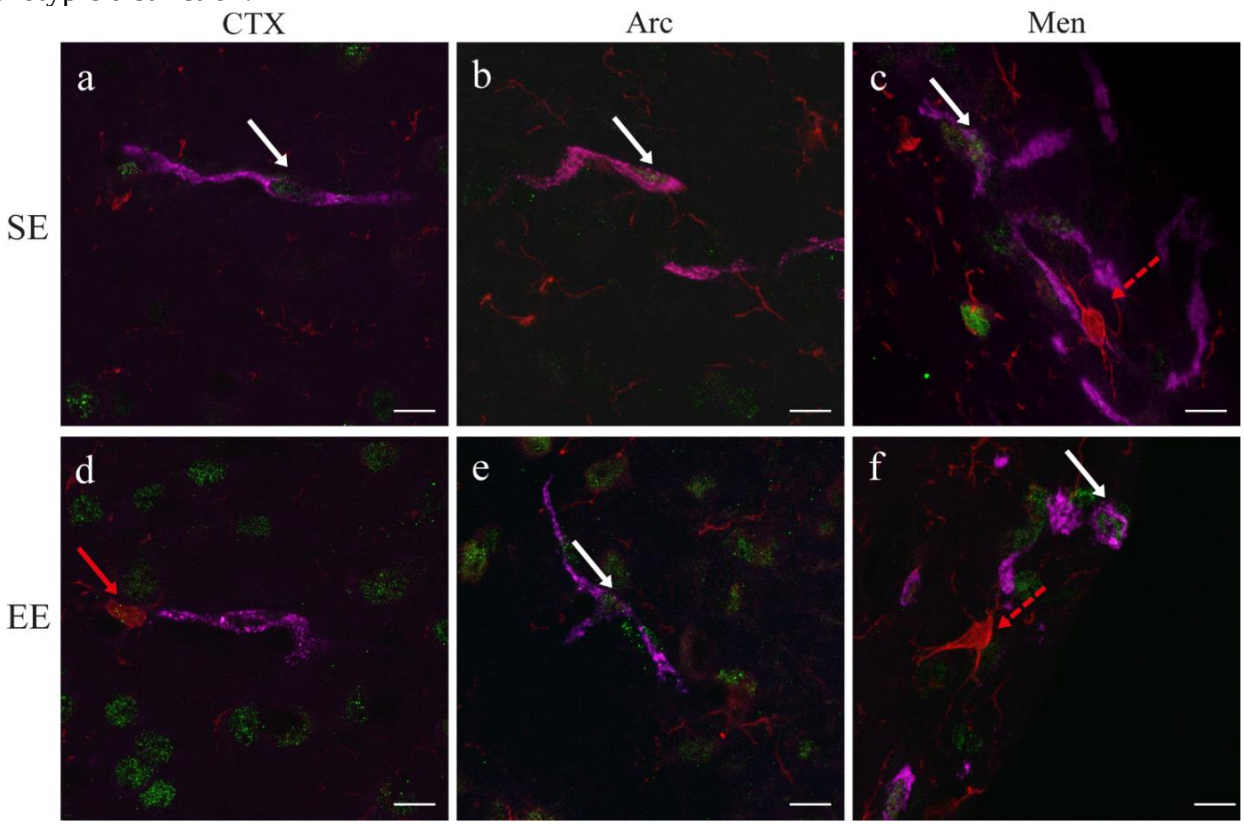

Fig. 20: Confocal microscopy images of SE or EE H3.3B tagged mouse brain sections labeled with anti-HA (green), anti-Iba1 (red) and anti-CD206 (purple). In both SE (a-c) and EE (d-f) mice single CD206$^+$ or double CD206$^+$/Iba1$^+$ cells usually express H3.3B. No differences concerning the number of CD206$^+$ cells can be observed between the two different housing conditions in CTX (a, d), Arc (b, e) and Men (c, f). Full white arrows indicate examples of CD206$^+$/HA$^+$ cells while white dashed arrows point to CD206$^+$/HA$^-$ cells; full red arrows indicate examples of Iba1$^+$/HA$^+$ cells while red dashed arrows point to Iba1$^+$/HA$^-$ cells. Zoom: 4 x; scale bar: 10 µm.

Microglia, with few exceptions, did not express H3.3B in 2 and 4 month-old animals (as seen in SE and unstimulated animals, see above) whereas, after 4-week EE exposure, a quite high number of microglial cells showed positivity for HA staining. As previously mentioned, in astrocytes H3.3 accumulation is slower when compared to neurons [50]; therefore, to assess whether H3.3B expression in $Iba1^+$ cells, consequent to EE, is specifically dependent on EE or is just the acceleration of a physiological aging process, we performed a double IF staining with anti-HA and anti-Iba1 (Fig. 21) Abs in young (2 month-old: a-c), young adult (6 month-old; d-f) or adult (1 year-old; g-i) mice (n = 4/group). Interestingly, with rare exceptions in CTX and Arc (as described above), microglial cells of young, young adult and adult mice did not express H3.3B, barring the physiological accumulation hypothesis.

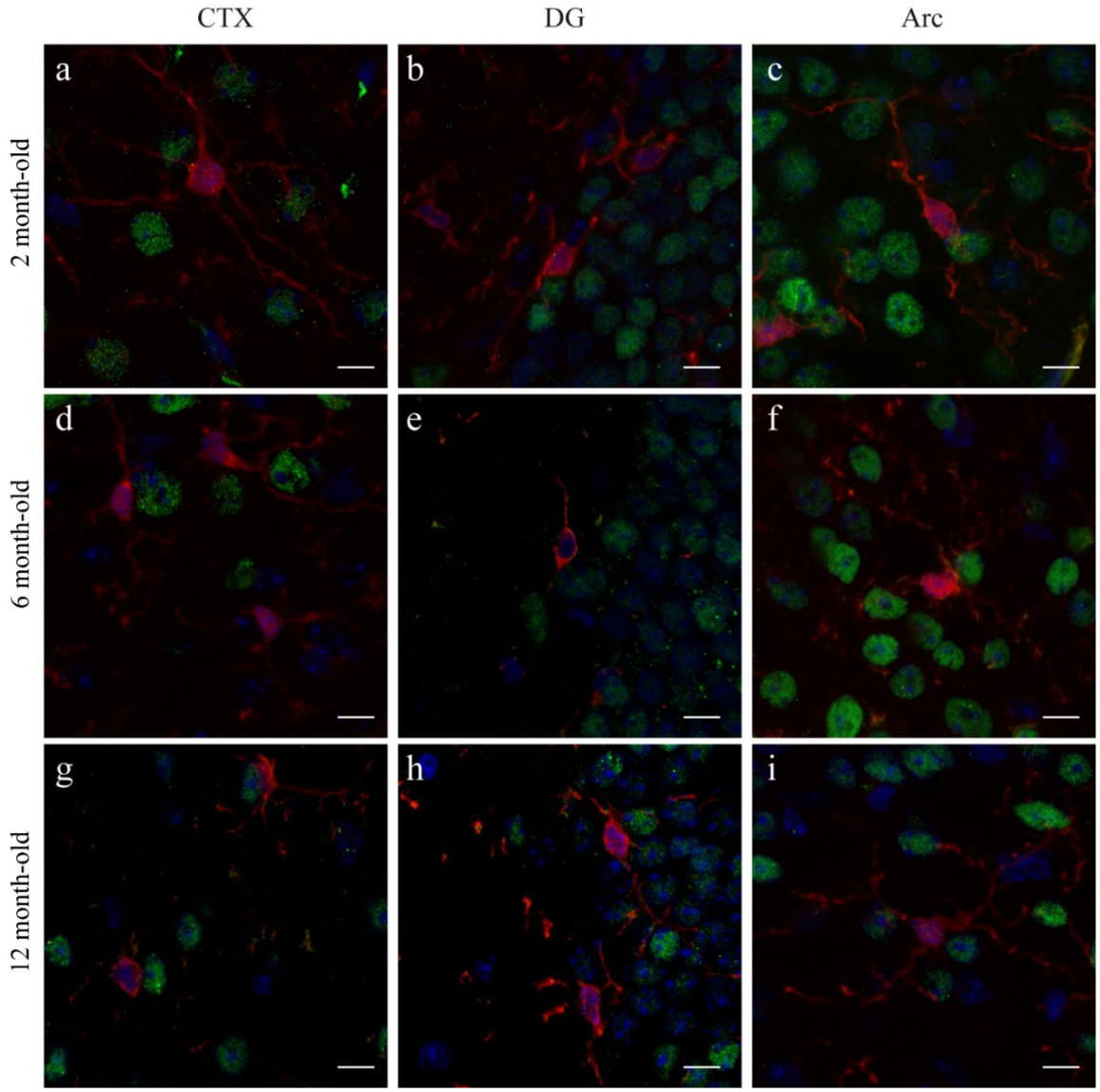

Fig. 21: Confocal microscopy images of young, young adult and adult H3.3B tagged mice brain sections labeled with DAPI (blue), anti-HA (green), anti-Iba1 (red). In all the analyzed areas such as CTX (a, d, g), DG (b, e, h) and Arc (c, f, i) almost no double $Iba1^+/HA^+$ cells can be observed in H3.3B tagged mice at any ages: 2 month-old (a-c), 6 month-old (d-f) and 12 month-old (g-i) animals. Zoom: 4 x; scale bar: 10 µm.

To further study the EE-derived increment of H3.3B-expressing microglia in the CTX observed with double IF stainings, a second cohort of H3.3B tagged mice housed in SE or EE was perfused and processed for microglia isolation. The whole CTX was dissected out and microglial cells were isolated using a 37%/70% Percoll gradient and labeled using fluorescent Abs directed against CD11b and CD45; fluorescent anti-Flag Ab was used to detect H3.3B expression (Fig. 22). Then, FACS was used to separate and count cortical microglial cells with no or low H3.3B expression, called Flag low, from microglia characterized by high H3.3B presence, called Flag high, in both SE (a) and EE (b) animals. The % of Flag high cells ($CD11b^{+}/CD45^{+}/Flag^{high}$), on total microglial population ($CD11b^{+}/CD45^{+}$), was significantly higher in cortical samples from EE mice compared to those from SE mice (c) confirming IF data, although, due to the different sensitivity of the two methods, the number of triple positive cells, in both housing conditions, was higher in FACS study than expected from IF study.

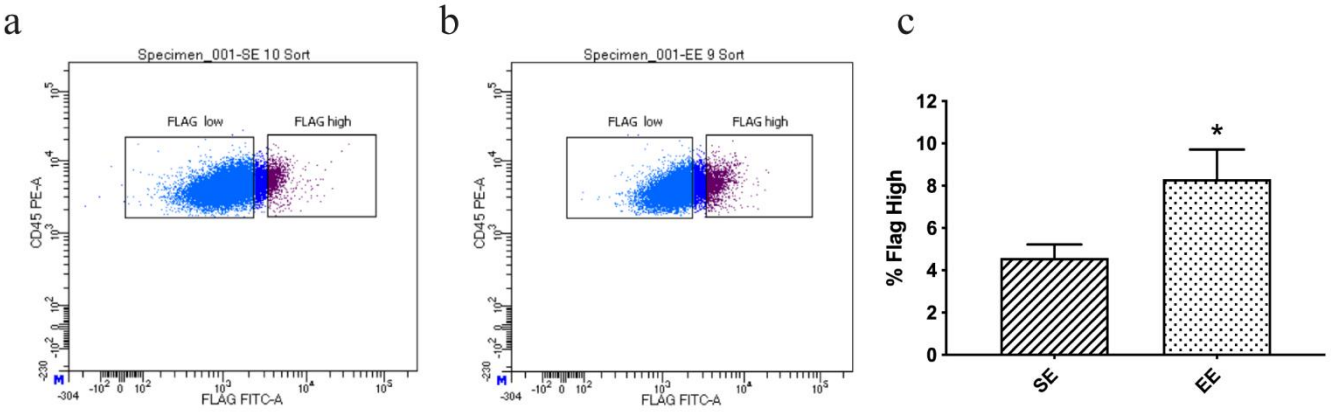

Fig. 22: a, b) FACS plots of cortical microglia of H3.3B tagged mice, housed in SE or EE. In the total microglia population (light blue + blue + purple), previously selected for CD11b/CD45 positivity, two subpopulations were separated based on H3.3B expression (i.e., anti-Flag fluorescence, in the plot x axis): Flag low (light blue), with absent or low Flag expression and Flag high (purple), with fluorescence > ~ $10^{3.5}$; the first plot (a) is representative of tagged mice housed in SE while the second of mice housed in EE (b). **c) % of Flag high microglia of SE and EE housed H3.3B tagged mice**. Cells were counted while sorted; the % of $CD11b^{+}/CD45^{+}/Flag^{high}$ was calculated over the total $CD11b^{+}/CD45^{+}$ population for both SE and EE mice. The % of Flag high microglia is significantly (*) higher in the CTX of EE housed mice. All data are plotted as mean ±SEM. Statistical analysis was performed by *t* test with Welch's correction for unequal SDs; p=0.0461.

Sorted cells will be processed for future RNA-seq analyses to identify a possible specific differential expression profile of Flag high and Flag low microglial cells.

4.4. H3.3B expression changes after sub-chronic cocaine treatment

As emerged from our basal regional distribution analysis, H3.3B signal in the NAc is not high; in this area, an H3.3B increment has been reported in depressed subjects [57] and an H3.3 enrichment has been observed near genes induced by chronic Coc administration [62]. Until now, no specific analysis was conducted on H3.3B isoform expression in the NAc of Coc-treated mice. Therefore, 2 month-old H3.3B tagged male mice were subjected to sub-chronic Coc (n=9), i.e., 4 days of a daily i.p. injection of 20 mg/Kg Coc, or Sal (n=7) treatment.

First, to understand whether Coc treatment were effective, IHC staining using anti-FosB Ab was performed; in fact, FosB is a TF whose expression is stimulated in some brain areas, such as the NAc, by Coc administration [84]. FosB is not very stable and treated mice, sacrificed 12 hr after the last Coc injection, showed a relatively limited amount of $FosB^+$ cells in the NAc. However, the number of $FosB^+$ cells was significantly higher in Coc-treated mice with respect to Sal-treated mice (Fig. 23).

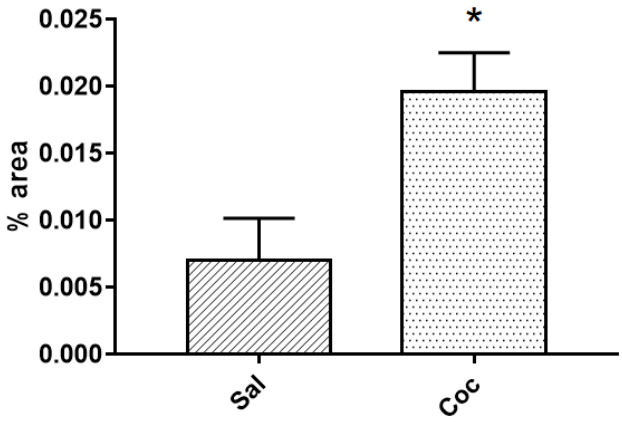

Fig. 23: % of area occupied by $FosB^+$ cells in H3.3B tagged mice brain sections after 4 days of treatment with Sal or Coc. Coc-treated mice exhibit higher FosB ir with respect to Sal-treated mice. All data are plotted as mean ±SEM. Statistical analysis was performed by *t* test. p= 0.0161.

Next, anti-HA Ab was used to determine H3.3B expression changes consequent to Coc treatment (Fig. 24); in the NAc of Coc-treated mice (b), compared to Sal-treated mice (a), a significant increase of $H3.3B^+$ cells (% of area; c) as well as signal intensity (MGV; d) could be observed.

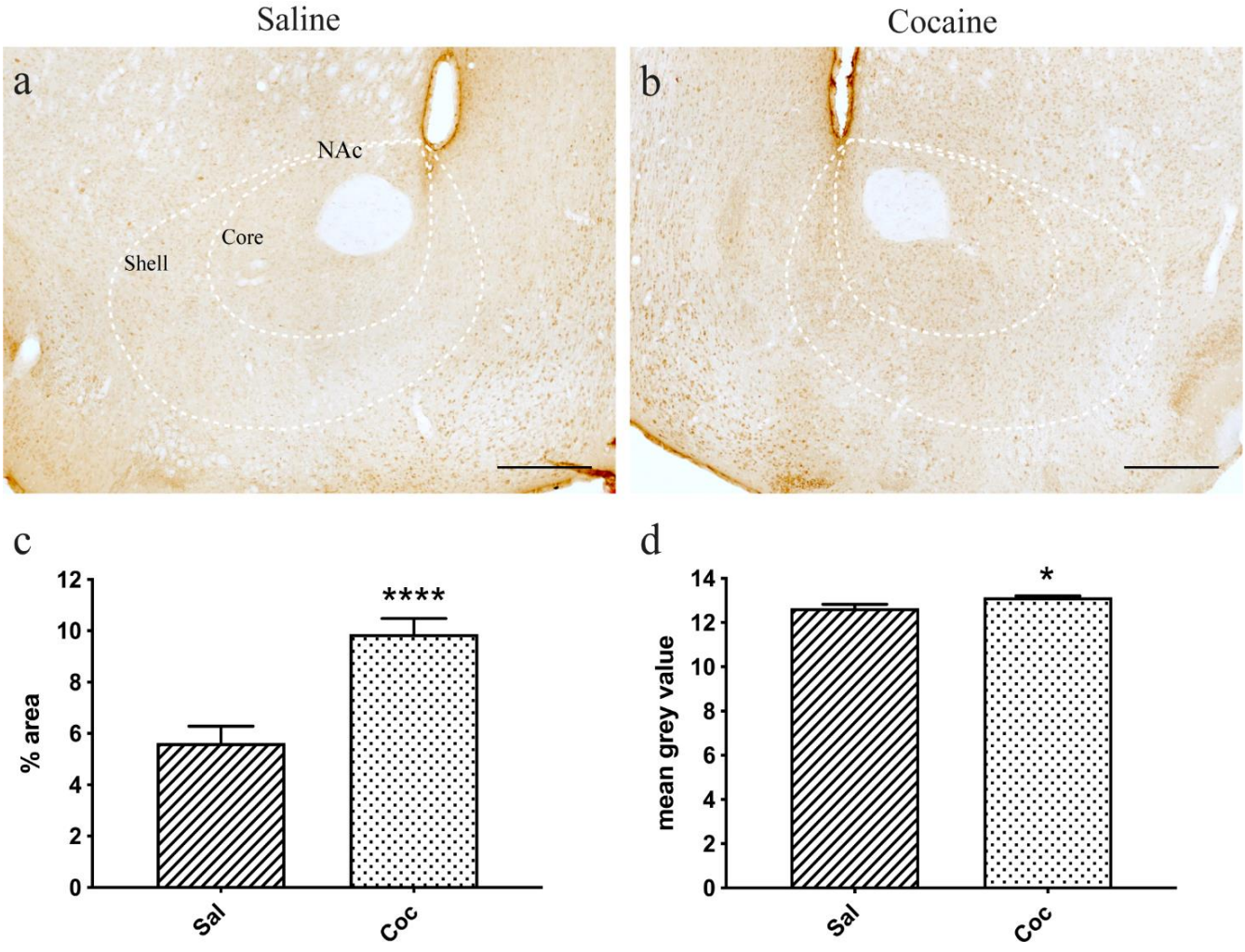

Fig. 24: a, b) Optical microscopy images of HA-labeled NAc of H3.3B tagged mice after 4 days of Sal or Coc treatment. Representative images of the NAc and its subregions (core and shell) of Sal (a) and Coc (b) treated mice. Scale bar: 300 µm. **c) % of area occupied by HA^+ cells in the NAc of Sal and Coc-treated mice.** Coc treatment significantly (****) increases the area positive for HA ir; p = 0.0018. **d) Corrected MGV of HA^+ cells in the NAc of Sal and Coc-treated mice**. Coc treatment significantly (*) increases the signal intensity of HA-expressing cells; p=0.0135. All data are plotted as mean ±SEM. Statistical analyses were performed by *t* test.

Triple IF staining was performed labeling Sal- and Coc-treated mouse brain sections with anti-HA, anti-NeuN and anti-proenkephalin (PENK) Abs to specifically mark H3.3B histone, neuronal nuclei and DA D2 receptor-expressing striatal neurons, respectively. In the NAc, sub-chronic Coc treatment did not significantly change the number of $PENK^{+}/H3.3B^{+}$ cells (data not shown).

On the contrary, analyzing NeuN labeling (Fig. 25), a higher number of non-neuronal cells expressing H3.3B ($NeuN^{-}/HA^{+}$) could be observed after sub-chronic Coc treatment (b) in the NAc; the count (c), performed on 5 µm z-stacks of a 28x28 µm field, revealed a mean of 16.5 cells/field for Coc-treated mice compared to only 4.7 cells/field for Sal-treated mice.

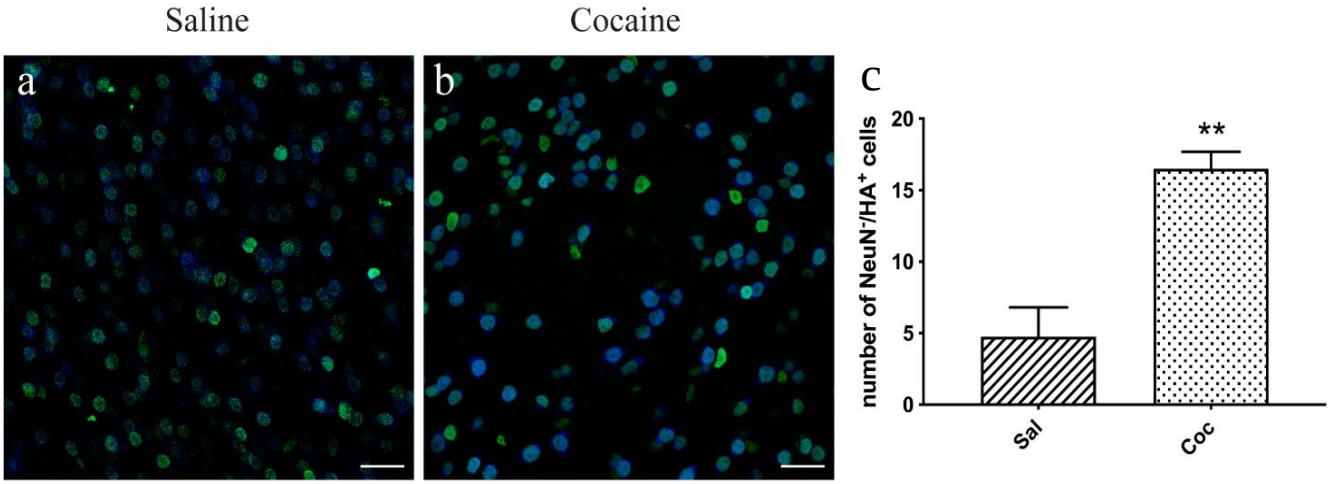

Fig. 25: a, b) Confocal microscopy images of H3.3B tagged mouse NAc labeled with anti-NeuN (blue) and anti-HA (green) after 4 days of Sal (a) or Coc (b) treatment. Zoom: 1.28x; scale bar: 50 µm. **c) Number of non-neuronal cells expressing H3.3B in Sal or Coc-treated H3.3B tagged mice.** The number of $NeuN^{-}/HA^{+}$ cells is significantly (**) higher in Coc-treated animals with respect to Sal-treated mice; p= 0.0048. All data are plotted as mean ±SEM. Statistical analyses were performed by *t* test with Welch's correction for unequal SDs.

Finally, double IF stainings were performed to assess H3.3B expression in specific glial cell populations after sub-chronic Coc treatment. HA expression in astrocytes and microglia, marked with anti-glutamine synthetase (GS) and anti-Iba1 Abs respectively, was evaluated in the NAc where these cells basally did not express H3.3B isoform (Fig. 26). No differences could be observed between the two treatments: in the NAc, microglia (a, b) and astrocytes (c, d) were globally negative for H3.3B.

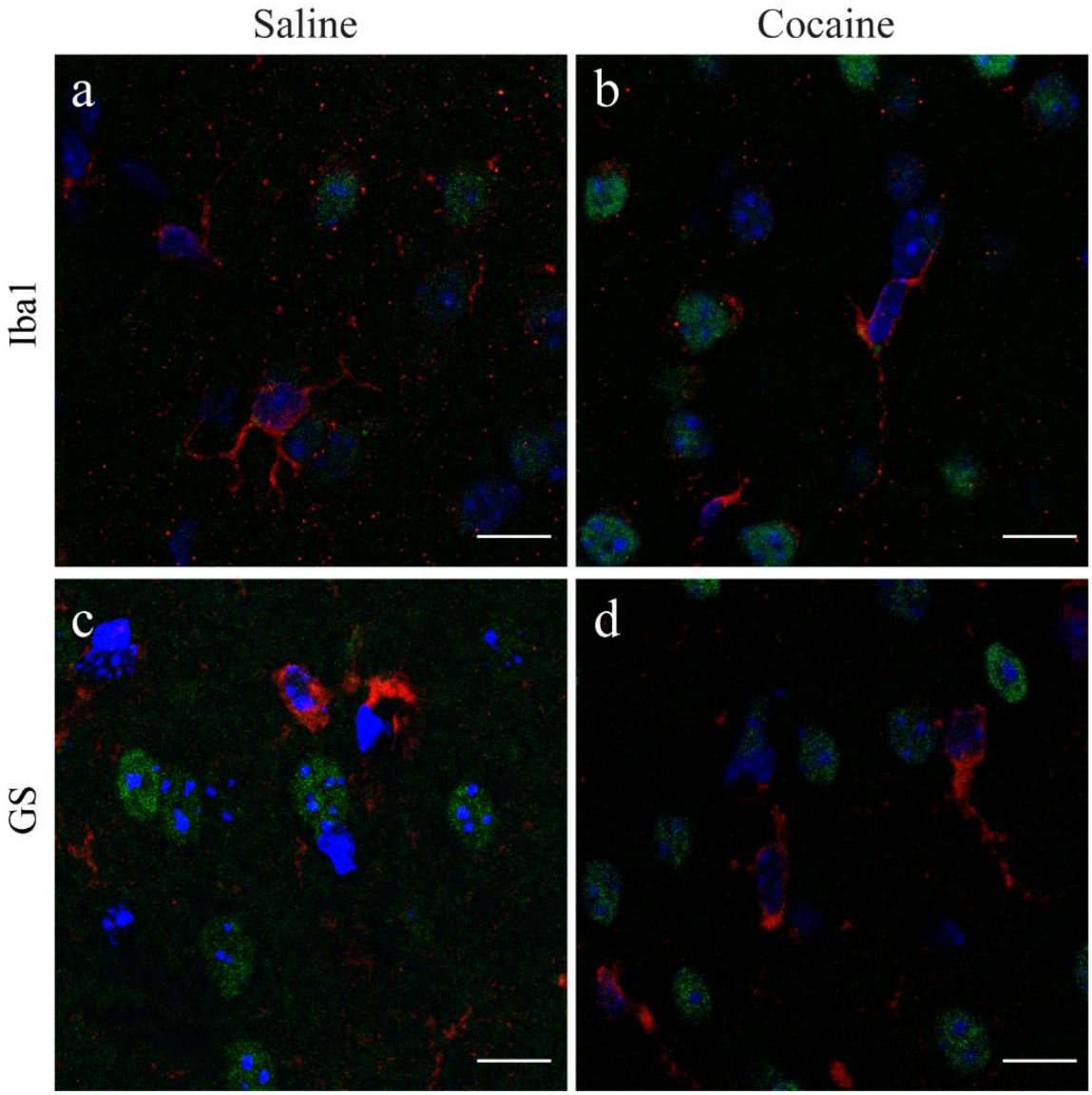

Fig. 26: Confocal microscopy images of Sal- or Coc- treated H3.3B tagged mouse NAc labeled with DAPI (blue), anti-HA (green) and anti-Iba1 (a, b; red) or anti-GS (c, d; red). Almost no double $Iba1^+/HA^+$ cells can be observed in H3.3B tagged mice after either Sal (a) or Coc (b) treatment. No differences can be observed in GS^+ cells (c, d) as well. Zoom: 4 x; scale bar: 10 µm.

5. Discussion

It is well established that chromatin structure, organization and dynamics are crucial for cell physiology and their changes are linked to the insurgence and progression of many diseases [8]. Structural changes, mediated by PTMs of N-tails, chromatin remodelers or variant incorporation into nucleosome, generate domains important for both transient gene expression/repression and epigenomic perpetuation of gene activity states [9, 55]. Modifications of N-tails and HFDs, first discovered in early eukaryotes, have been extensively studied, and seem unable to alter nucleosomes structure in a relevant way; several lines of evidence implicate variants incorporation and turnover in facilitating different chromatin states [6, 18]. Histone variants functions are not just redundant of those of canonical histones: in fact, some histone variants have developed specific features to exert specific functions. For instance, the RI incorporation of variants is a key feature to regulate transcription outside the cell cycle and especially, in adult life, in tissues with non-dividing cells such as the brain [34].

Emerging data underline the importance of variants, and especially of H3.3 deposition and/or turnover, in neuronal function and brain plasticity [54]; while different H2A variants are expressed in the brain, in most mammals H3.3 is the only H3 variant expressed in this organ (CENP-A is also present but it has different functions) implying its crucial involvement in neural function [85]. Even if H3.3 is very similar to canonical H3.1 and H3.2, possessing only four and five different AAs respectively, it displays unique features regarding its gene organization and localization, expression, chaperone-directed deposition and PTMs [58]. Being found in both active and silent genes, H3.3 role is however controversial and has not been fully elucidated yet. Additionally, two different genes named *H3f3a* and *H3f3b*, located on chromosome 1 and 7 respectively, code for H3.3 proteins (H3.3A and H3.3B) with the same AA sequence [45, 19, 44]; for this reason, a tagged mouse model is very useful to study the two isoforms independently. The retention of both genes through evolution, the different relative abundance in adult tissues, the diverse association to tumors and the different KO phenotype, imply a different regulation and a functional distinction between the two isoforms [43, 45].

The aim of present work has been to elucidate some aspects of the differential regional and cellular expression of the two H3.3 isoforms in the mouse CNS in various physiological conditions, namely, aging and exposure to an EE, and sub-chronic Coc treatment.

In order to understand the possible different contribution given by the two isoforms to brain function, we first assessed H3.3A and H3.3B region- and cell type-specific expression pattern using KI heterozygotes tagged (Flag-HA) mice for H3.3A (WT/fH3.3A) or H3.3B (WT/fH3.3B). H3.3A and H3.3B regional distribution is not homogeneous. In fact, while H3.3A has a widespread distribution both in grey and white matter, H3.3B expression is nearly absent in white matter tracts. On the contrary the latter isoform is more abundant in some Thal (e.g., Rt) and Hyp (e.g., Arc) nuclei as well as in other restricted areas such as the Hb. This heterogeneity cannot be easily traced back to known anatomical or functional features of these regions. For instance, given the links of H3.3B incorporation to neuronal activity, areas with higher or more precocious expression of H3.3B variant might be those where more intense neuronal activity or plastic changes occur. Neuronal activity is, broadly speaking, correlated with blood flow that continuously supplies neural cells with energetic precursors. Regional measures of local blood flow with imaging techniques have relatively modest resolution in the mouse; yet a rank order of macroregions can be built on the basis of available data [86-89]: Thal > CTX = Hip > CPu >> CC. This regional rank order broadly fits with the density and intensity of $H3.3B^{+}$ cells. Looking at some instances of specific regions, in the Hip formation, DG gr and CA3 pyramidal layer have sparse and diffuse neuronal activity respectively, while most interneurons have high spiking activity; this relative pattern of activity is coherent with the pattern of H3.3B expression. The Rt, where very intense H3.3B labeling was observed, is endowed with rather peculiar morpho-functional features. It is the only Thal nucleus containing GABA neurons that are connected between them by large numbers of gap-junctions and are therefore highly synchronized [90]. Other regions with predominant GABA neurons are the CPu and pallidal regions, that have however relatively modest expression of H3.3B. Another region with high H3.3B expression is the medial Hb, that is not particularly rich in gap junctions but has high spontaneous tonic firing [91]. Overall, while some correlation can be built between activity-related markers and H3.3B expression, no univocal attribution of H3.3B preferential expression to a specific activity marker or other cell feature could be found.

As regards cell type expression, H3.3A and H3.3B presence in neurons had already been documented but no information concerning other cell types was available [43, 57]. Maze [50] reported H3.3 expression in both neurons and astrocytes without distinguishing between the two isoforms. Indeed. present IHC analysis of the two isoforms that showed different signal intensity in different brain areas and H3.3A preferential presence in white matter tracts, suggested a cell-type specific expression. Therefore, we decided to evaluate H3.3A and H3.3B cellular expression, using tagged mice, through

triple and double IF using anti-HA Ab with different cell-type Abs, first in neurons then in glial cells. $NeuN^+$ cells showed high but variable positivity for both isoforms confirming literature data [50]. However, analyzing selected neuronal populations, neuron-specific differential expression of H3.3A and H3.3B has emerged; with some area-related exceptions, DA neurons (TH-expressing cells) were more positive for H3.3B than for H3.3A. PV- as well as SS-expressing interneurons were positive for both H3.3A and H3.3B without striking differences between the two isoforms although SS^+ cells showed lower HA ir compared to PV^+ cells, in mice of both genotypes. Similarly to PV^+ neurons, CR^+ interneurons were highly positive for both isoforms but, in the prefrontal CTX, expression of H3.3B was higher than that of H3.3A. Finally, NPY^+ interneurons showed comparable H3.3A and H3.3B expression in CTX, where both were highly expressed, and DG, where both were poorly expressed, but different expression in the striatum where H3.3B was more abundant than H3.3A. Overall, also when selected neuronal populations are investigated no general rule for H3.3 variant expression can be identified.

Being RI variants, H3.3 isoforms can be incorporated into chromatin potentially throughout all cell cycle; however, in cycling cells, contrary to differentiated cells, H3.3 should be diluted by canonical H3s [5, 6, 50]. So, having established the widespread expression of H3.3 isoforms in mature neurons, we wished to investigate H3.3A and H3.3B expression in cycling cells ($Ki67^+$) and immature neurons of the adult brain. The analysis was carried out in the DG, one of the two main regions where neurogenesis occurs in adult CNS [92, 93]. Immature post-mitotic neurons showed no differences regarding H3.3A and H3.3B expression; in the SGZ, nestin-expressing immature neurons were positive for both isoforms while most cells into the DG gr were negative. DCX^+ cells, which are more mature than $nestin^+$ cells, expressed both H3.3A and H3.3B. Interestingly, cycling/proliferating cells ($Ki67^+$) expressed H3.3A but not H3.3B underlining once again a differential regulation between the two isoforms.

Finally, H3.3 expression was evaluated in three different glial populations namely astrocytes ($GFAP^+$), a subpopulation of mature astrocytes and oligodendrocyte precursors ($S100B^+$) and microglia ($Iba1^+$); astrocytes as well as $S100B^+$ cells exhibited higher levels of H3.3A than H3.3B confirming the evidence, obtained by the analysis at regional level, of H3.3A, but not H3.3B, expression in white matter regions. On the other hand, almost the totality of microglial cells was negative for both isoforms; the peculiarity of microglia is, however, not entirely surprising considering its different embryonic origin with respect to the other CNS cell populations [67].

It has been shown, in chickens, that H3.3/H2A.Z double-variant nucleosomes are very unstable [83] independently from their PTMs. Double-variant nucleosomes are enriched at frequently disrupted sites such as NDRs and regulatory elements. Since the presence of either H3.3 or H2A.Z can facilitate genome receptivity to both activating and repressive complexes, a cross-talk between these two variants or a reciprocal influence in their dynamics, when they are expressed in the same nucleosome, is highly probable [5]. By means of super-resolution STED microscopy we investigated separately H3.3A and H3.3B co-localization with H2A.Z. Not all H2A.Z expressing cells were positive for H3.3 and vice versa; however, double expressing-cells were found in both H3.3A and H3.3B tagged animals. Inside their nuclei H3.3 isoforms and H2A.Z were in close proximity but their co-localization in distinct chromatin domains could not be demonstrated, possibly for technical limitations (see above). These data confirm the possible co-presence of H3.3 and H2A.Z in the adult mouse brain while they show no differences between the two isoforms.

In basal conditions in 4 month-old mice, H3.3A and H3.3B exhibited a quite different region- and cell type-specific expression pattern; however, it remained to be elucidated whether their differences persist, flatten or burst under the thrust of external stimuli. Both chromatin modifying mechanisms and variants have been proved to respond to environmental stimulation [33]. The environment is able to induce measurable changes in the adult brain. EE is a commonly used model of induced plasticity which mimics the exposure to environments rich in physical, social and psychological stimulations [63, 64, 70]. Chromatin dynamics, and in particular H3.3 turnover, seem to be essential for gene expression changes in the brain and consequently for neuronal plasticity [85]. H3.3 regulation in neurons seems to be experience-mediated. In fact, Maze and colleagues [50] demonstrated an increase in H3.3, and particularly in H3.3B, mRNA levels and turnover in mouse Hip consequent to chronic EE exposure. These changes were reported in both neuronal ($NeuN^+$) and non-neuronal ($NeuN^-$) cells without discriminating different cellular populations and subpopulations. In the present study, environmental influence on H3.3B expression was assessed by IHC and double IF stainings in H3.3B tagged mice housed for 4 weeks in SE or EE. Chronic EE exposure significantly increased H3.3B expression in the DG and CA3 but not in CA1; in the CTX a trend could be observed while no evident changes occurred in subcortical brain areas in line with Maze's results. Tissue clearing and light sheet microscopy allowed a more global vision of EE-derived changes confirming these data.

For the first time, H3.3B expression changes after EE exposure have been evaluated in different cell types. While the scattered increased signal in projection neuron layers of the Hip and large cells of CTX (i.e., pyramidal neurons), in both IHC and IF experiments, point to an increased expression of H3.3B in cortico-hippocampal glutamatergic projection neurons, in GABAergic interneurons (SS- and NPY-expressing cells) no remarkable differences could be observed in any of the analyzed brain areas. Remarkably, in the internal part of DG gr and SGZ more neurons expressed H3.3B in EE housed mice compared to SE housed mice. EE exposure is known to increase the number of newborn neurons in the SGZ, the neurogenetic area of the Hip [63, 64]; however, since H3.3B is not expressed in proliferating ($Ki67^+$) neuronal precursors, HA^+-Nissl stained cells in EE H3.3B tagged mice are probably newborn immature neurons.

The EE has also been proved to affect glial cells, increasing gliogenesis as well as the number of ramifications of astrocytes and favoring neurotrophic factors release [69, 94]. All these processes could be directly or indirectly linked to neuroplasticity. On the contrary EE does not seem able to affect oligodendrogenesis [70]. H3.3B tagged mice housed in EE cages did not exhibit altered HA expression in astrocytes when compared to SE animals, whereas S100B-expressing population showed increased H3.3B expression consequent to EE chronic exposure. Since S100B does not identify a specific population but a mixed one comprising both precursors of oligodendrocytes and some subtypes of differentiated astrocytes, the $S100B^+$ population affected by EE might be a subclass of astrocytes not identified by GFAP marker or oligodendrocyte precursors.

The major difference observed between SE and EE animals is H3.3B expression in microglial cells. In fact, while basally almost all $Iba1^+$ cells were negative for H3.3B, EE housed mice showed an increment in double positive cells, especially in CTX and Arc. EE is known to stimulate microglia proliferation in the CTX and Hip [69, 70] but, since H3.3B is apparently not expressed by proliferating cells, these double positive cells must be post-mitotic immature or fully differentiated cells. We used TREM2 and CD206 markers to understand whether H3.3B expression increment is linked to a particular microglial phenotype (M1 and M2 respectively). However, while no M1 pro-inflammatory $TREM2^+$ cells were detected in any of the two housing conditions, the M2 anti-inflammatory $CD206^+$ cells that were detected had similar H3.3B expression. Therefore, the increment in H3.3B expression in microglia observed in EE housed mice is not linked to any of the two classical macrophagic phenotypes.

Both in neurons and in glial cells, though at slower rate in the latter case, H3.3 accumulation increases throughout life [50]. We therefore hypothesized that EE might accelerate a physiological increase in microglial H3.3B expression occurring during aging. However, we proved that this is not the case, since microglial cells are negative for H3.3B in 1 year-old mice, as in 2 month-old mice. The EE-derived increment in H3.3B expression in microglia has been confirmed with a different approach extracting $CD11b^+/CD45^+$ cells from H3.3B tagged mouse CTX and separating them with FACS. The % of microglial cells with high levels of H3.3B ($CD11b^+/CD45^+/Flag^{high}$) was significantly higher in EE housed mice with respect to SE housed mice. Microglia is a very heterogeneous population: parenchymal microglia are different from perivascular and meningeal microglia. Microglial subpopulations can be distinguished by their expression profile; for instance, neurotrophin-3 is expressed only in microglia from the CTX, globus pallidus and medulla [68]. Moreover, in perivascular tracts and meninges immunological surveillance is operated by bone-marrow-derived cells such as dendritic cells and border-associated macrophages (BAMs) able to infiltrate the parenchyma when a damage occurs [67]. That $H3.3B^+$ microglia in EE mice belong to a specific subclass remains a distinct possibility though the presence of $H3.3B^+$ infiltrating macrophages, that is rather unlikely in a physiological stimulation condition such as EE, cannot be excluded.

Sub-chronic Coc treatment, which is another neuroplastic stimulation model quite different from EE, was studied in H3.3B tagged mice. A H3.3 response to Coc had already been reported by Wimmer and colleagues [62], who demonstrated H3.3 enrichment near promoters of genes induced by chronic Coc treatment. This study, however, did not discriminate between the two isoforms and tagged H3.3 expression was restricted to NAc CaMKIIα expressing neurons excluding the effects on other cell types. Under basal conditions, H3.3B is not very abundant in the NAc while, after 4 days of treatment with Coc 20 mg/Kg, a significant increment in H3.3B expressing cells and signal intensity could be observed. Coc treatment stimulated H3.3B expression in both major NAc subregions (core and shell). We directly demonstrated that Coc treatment does not increase H3.3B expression in D2 expressing $PENK^+$ neurons. That a Coc-induced increase in H3.3B expression occur in D1 expressing neurons, that are indeed exquisitely sensitive to Coc treatments [95-98], remains a hypothesis to be investigated. Coc-treated mice exhibited a higher number of non-neuronal cells expressing H3.3B ($NeuN^-/HA^+$) with respect to Sal-treated animals. However, from a preliminary analysis, Sal and Coc-treated mice showed no significant differences in H3.3B expression in $Iba1^+$ microglial cells or GS^+ astrocytes. Other populations of non-neuronal cells have not been investigated yet.

Despite possessing an identical AA sequence, different regional and cellular expression of H3.3A and H3.3B points out their differential regulation and therefore involvement in distinct functions. Our data confirm the emerging evidence identifying H3.3B as the stimulus-responsive isoform. While H3.3A has a widespread distribution and is expressed in almost all cell types, H3.3B expression is more limited and is strongly affected by neuroplastic stimulations. The promoter organization of the two isoforms might be essential in explaining why H3.3A is homogeneously expressed in basal condition while and H3.3B is heterogeneously expressed and sensitive to stimuli. In fact, while *H3f3a* promoter contains SP1 recognition motives typical of housekeeping genes, *H3f3b* gene possesses sequences typical of inducible promoters [43]. While the causes of H3.3 isoform differential expression at the cell type level are still unclear, all available data including present results point to the importance of H3.3B expression in non-neuronal cells upon physiological and pharmacological stimulation and suggest that future mechanistic studies on H3.3 induction and downstream regulation of H3.3 target genes in these cells might help decipher glial cell contribution to neuroplasticity.

References

[1] K. E. Van Holde, "Chromatin. Series in molecular biology," *Springer-Verlag, New York. Journal of Molecular Recognition*, 1989.

[2] T. J. Richmond and C. A. Davey, "The structure of DNA in the nucleosome core," *Nature*, vol. 423, p. 145-150, 2003.

[3] M. R. Hübner, M. A. Eckersley-Maslin and D. L. Spector, "Chromatin Organization and Transcriptional Regulation," *Current Opinion in Genetics & Develeopment*, vol. 23, p. 89–95, 2013.

[4] H. A. Cole, F. Cui, J. Ocampo, T. . L. Burke, T. Nikitina, V. Nagarajavel, N. Kotomura, V. B. Zhurkin and D. J. Clark, "Novel nucleosomal particles containing core histones and linker DNA but no histone H1," *Nucleic Acids Research*, vol. 44, p. 573–581, 2016.

[5] C. M. Weber and S. Henikoff, "Histone variants: dynamic punctuation in transcription," *Genes & Development*, vol. 28, p. 672–682, 2014.

[6] H. S. Malik and S. Henikoff, "Phylogenomics of the nucleosome," *Nature Structural Biology*, vol. 10, p. 882-891, 2003.

[7] C. L. Woodcock and S. Dimitrov, "Higher-order structure of chromatin and chromosomes," *Current Opinion in Genetics & Development*, vol. 11, p. 130–135, 2001.

[8] C. L. Woodcock, "Chromatin architecture," *Current Opinion in Structural Biology*, vol. 16, p. 213–220, 2006.

[9] J. Jin, Y. Cai, B. Li, R. C. Conaway, J. L. Workman, J. Weliky Conaway and T. Kusch, "In and out: histone variant exchange in chromatin," *Trends in Biochemical Sciences*, vol. 30, p. 680-687, 2005.

[10] H. S. Tims, K. Gurunathan, M. Levitus and J. Widom, "Dynamics of Nucleosome Invasion by DNA Binding Proteins," *Journal of Molecular Biology*, vol. 411, p. 430-448, 2011.

[11] D. Noble, "Conrad Waddington and the origin of epigenetics," *The Journal of Experimental Biology*, vol. 218, p. 816-818, 2015.

[12] R. Jaenisch and A. Bird, "Epigenetic regulation of gene expression: how the genome integrates intrinsic and environmental signals," *Nature Genetics*, vol. 33, p. 245–254, 2003.

[13] C. Dupont, D. R. Armant and C. A. Brenner, "Epigenetics: Definition, Mechanisms and Clinical Perspective," *Seminars in Reproductive Medicine*, vol. 27, p. 351–357, 2009.

[14] S. Henikoff, T. Furuyama and K. Ahmad, "Histone variants, nucleosome assembly and epigenetic inheritance," *Trends in Genetics*, vol. 20, p. 320-326, 2004.

[15] B. M. Turner, "Cellular Memory and the Histone Code," *Cell*, vol. 111, p. 285–291, 2002.

[16] B. D. Strahl and C. D. Allis, "The language of covalent histone modifications," *Nature,* vol. 403, p. 41-45, 2000.

[17] T. Jenuwein and C. D. Allis, "Translating the Histone Code," *Science,* vol. 293, p. 1074-1080, 2001.

[18] S. B. Hake and D. C. Allis, "Histone H3 variants and their potential role in indexing mammalian genomes: The ‘‘H3 barcode hypothesis’’," *PNAS,* vol. 103, p. 6428–6435, 2006.

[19] D. Brush, J. B. Dodgson, O.-R. Choi, P. Wilkins Stevens and J. D. Engel, "Replacement Variant Histone Genes Contain Intervening Sequences," *Molecular and Cellular Biology,* vol. 5, p. 1307-1317, 1985.

[20] R. S. Wu and W. M. Bonner, "Separation of Basal Histone Synthesis from S-Phase Histone Synthesis in Dividing Cells," *Cell,* vol. 27, p. 321-330, 1981.

[21] P. B. Talbert, K. Ahmad, G. Almouzni, J. Ausió, F. Berger, P. L. Bhalla, W. M. Bonner, W. Z. Cande, B. P. Chadwick, S. W. Chan, G. A. Cross, L. Cui, S. I. Dimitrov, D. Doenecke, J. M. Eirin-López, M. A. Gorovsky, S. B. Hake, B. A. Hamkalo, S. Holec, S. E. Jacobsen, K. Kamieniarz, ... and S. Henikoff, "A unified phylogeny-based nomenclature for histone variants," *Epigenetics & Chromatin,* vol. 5:7, 2012.

[22] C. C. Hentschel and M. L. Birnstiel, "The Organization and Expression of Histone Gene Families," *Cell,* vol. 25, p. 301-313, 1981.

[23] W. F. Marzluff, E. J. Wagner and R. J. Duronio, "Metabolism and regulation of canonical histone mRNAs: ife without a poly(A) tail," *Nature Reveiws Genetics,* vol. 9, p. 843–854, 2008.

[24] O. I. Kulaeva, D. A. Gaykalova, N. A. Pestov, V. V. Golovastov, D. G. Vassylyev, I. Artsimovitch and V. M. Studitsky, "Mechanism of chromatin remodeling and recovery during passage of RNA polymerase II," *Nature Structural & Molecular Biology,* vol. 16, p. 1272-1279, 2009.

[25] M. Hondele, T. Stuwe, M. Hassler, F. Halbach, A. Bowman, E. T. Zhang, B. Nijmeij, C. Kotthoff, V. Rybin, S. Amlacher, E. Hurt and A. G. Ladurner, "Structural basis of histone H2A–H2B recognition by the essential chaperone FACT," *Nature,* vol. 449, p. 111-116, 2013.

[26] A. K. Shaytan, D. Landsman and A. R. Panchenko, "Nucleosome adaptability conferred by sequence and structural variations in histone H2A–H2B dimers," *Current Opinion in Structural Biology,* vol. 32, p. 48–57, 2015.

[27] S. Chakravarthy and K. Luger, "The Histone Variant Macro-H2A Preferentially Forms “Hybrid Nucleosomes”," *Journal of Biological Chemistry,* vol. 281, p. 25522–25531, 2006.

[28] R. Zhang, M. V. Poustovoitov, X. Ye, H. A. Santos, W. Chen, S. M. Daganzo, J. P. Erzberger, I. G. Serebriiskii, A. A. Canutescu, R. L. Dunbrack, J. R. Pehrson, J. M. Berger, P. D. Kaufman and P. D. Adams, "Formation of MacroH2A-Containing Senescence-Associated Heterochromatin Foci and Senescence Driven by ASF1a and HIRA," *Developmental Cell,* vol. 8, p. 19–30, 2005.

[29] M. Bruno, A. Flaus, C. Stockdale, C. Rencurel, H. Ferreira and T. Owen-Hughes, "Histone H2A/H2B Dimer Exchange by ATP-Dependent Chromatin Remodeling Activities," *Molecular Cell,* vol. 12, p. 1599–1606, 2003.

[30] S. D. Farris, E. D. Rubio, J. J. Moon, W. M. Gombert, B. H. Nelson and A. Krumm, "Transcription-induced Chromatin Remodeling at the c-myc Gene Involves the Local Exchange of Histone H2A.Z," *The Journal of Biological Chemistry,* vol. 280, p. 25298–25303, 2005.

[31] C. Bönisch, K. Schneider, S. Punzeler, S. M. Wiedemann, C. Bielmeier, M. Bocola, H. C. Eberl, W. Kuegel, J. Neumann, E. Kremmer, H. Leonhardt, M. Mann, J. Michaelis, L. Schermelle and S. B. Hake, "H2A.Z.2.2 is an alternatively spliced histone H2A.Z variant that causes severe nucleosome destabilization," *Nucleic Acids Research,* vol. 40, p. 5951–5964, 2012.

[32] V. Sansoni, C. S. Casas-Delucchi, M. Rajan, A. Schmidt, C. Bönisch, A. W. Thomae, M. S. Staege, S. B. Hake, M. C. Cardoso and A. Imhof, "The histone variant H2A.Bbd is enriched at sites of DNA synthesis," *Nucleic Acids Research,* vol. 42, p. 6405–6420, 2014.

[33] J. Postberg, S. Forcob, W.-J. Chang and H. J. Lipps, "The evolutionary history of histone H3 suggests a deep eukaryotic root of chromatin modifying mechanisms," *BMC Evolutionary Biology,* vol. 10:259, 2012.

[34] A. Loyola and G. Almouzni, "Marking histone H3 variants: How, when and why?," *Trends in Biochemical Sciences,* vol. 32, p. 425-433, 2007.

[35] H. Tagami, D. Ray-Gallet, G. Almouzni and Y. Nakatani, "Histone H3.1 and H3.3 Complexes Mediate Nucleosome Assembly Pathways Dependent or Independent of DNA Synthesis," *Cell,* vol. 116, p. 51–61, 2004.

[36] E. Dunleavy, A. Pidoux and R. Allshire, "Centromeric chromatin makes its mark," *Trends in Biochemical Sciences,* vol. 30, p. 172-175, 2005.

[37] D. R. Foltz, L. E. Jansen, A. O. Bailey, J. R. Yates III, E. A. Bassett, S. Wood, B. E. Black and D. W. Cleveland, "Centromere-Specific Assembly of CENP-A Nucleosomes Is Mediated by HJURP," *Cell,* vol. 137, p. 472–484, 2009.

[38] J. Govin, C. Caron, S. Rousseaux and S. Khochbin, "Testis-specific histone H3 expression in somatic cells," *Trends in Biochemical Sciences,* vol. 30, p. 357-359, 2005.

[39] O. Witt, W. Albig and D. Doenecke, "Testis-specific expression of a novel human H3 histone gene," *Experimental Cell Research,* vol. 229, p. 301-306, 1996.

[40] S. M. Wiedemann, S. N. Mildner, C. Bönisch, L. Israel, A. Maiser, S. Matheisl, T. Straub, R. Merkl, H. Leonhardt, E. Kremmer, L. Schermelleh and S. B. Hake, "Identifcation and characterization of two novel primate-specifc histone H3 variants, H3.X and H3.Y," *The journal of Cell Biology,* vol. 190, p. 777–791, 2010.

[41] K. Ahmad and S. Henikoff, "The Histone Variant H3.3 Marks Active Chromatin by Replication-Independent Nucleosome Assembly," *Molecular Cell*, vol. 9, p. 1191–1200, 2002.

[42] E. Szenker, D. Ray-Gallet and G. Almouzni, "The double face of the histone variant H3.3," *Cell Research*, vol. 21, p. 421-434, 2011.

[43] D. Frank, D. Doenecke and W. Albig, "Differential expression of human replacement and cell cycle dependent H3 histone genes," *Gene*, vol. 312, p. 135–143, 2003.

[44] W. Albig, B. Bramlage, K. Gruber, H. G. Klobeck, J. Kunz and D. Doenecke, "The Human Replacement Histone H3.3B Gene (H3F3B)," *Genomics*, vol. 30, p. 264–272, 1995.

[45] B. M. Muhire, M. A. Booker and M. Y. Tolstorukov, "Non-neutral evolution of H3.3-encoding genes occurs without alterations in protein sequence," *Scientific Reports*, vol. 9:8472, 2019.

[46] C. Xiong, Z. Wen and G. Li, "Histone Variant H3.3: A versatile H3 variant in health and in disease," *Science China Life Sciences*, vol. 59, p. 245–256, 2016.

[47] C. Couldrey, M. B. Carlton, P. M. Nolan, W. H. Colledge and M. J. Evans, "A retroviral gene trap insertion into the histone 3.3A gene causes partial neonatal lethality, stunted growth, neuromuscular deficits and male sub-fertility in transgenic mice," *Human Molecular Genetics*, vol. 8, p. 2489–2495, 1999.

[48] M. C. W. Tang, S. A. Jacobs, D. M. Mattiske, Y. M. Soh, A. N. Graham, A. Tran, S. L. Lim, D. F. Hudson, P. Kalitsis, M. K. O'Bryan, L. H. Wong and J. R. Mann, "Contribution of the Two Genes Encoding Histone Variant H3.3 to Viability and Fertility in Mice," *PLoS Genetics*, vol. 11:2, 2015.

[49] W. Wenderski and I. Maze, "Histone turnover and chromatin accessibility: Critical mediators of neurological development, plasticity, and disease," *Bioessays*, vol. 38, p. 410–419, 2016.

[50] I. Maze, W. Wenderski, K.-M. Noh, R. C. Bagot, N. Tzavaras, I. Purushothaman, S. J. Elsasser, Y. Guo, C. Ionete, Y. L. Hurd, C. A. Tamminga, T. Halene, L. Farrelly, A. A. Soshnev, D. Wen, S. Rafii, M. R. Birtwistle, S. Akbarian, B. A. Buchholz, R. D. Blitzer, E. J. Nestler, Z.-F. Yuan, B. A. Garcia, L. Shen, H. Molina and C. D. Allis, "Critical Role of Histone Turnover in Neuronal Transcription and Plasticity," *Neuron*, vol. 87, p. 77–94, 2015.

[51] R. B. Deal, J. G. Henikoff and S. Henikoff, "Genome-wide kinetics of nucleosome turnover determined by metabolic labeling of histones," *Science*, vol. 328, p. 1161–1164, 2010.

[52] I. B. Zovkic, B. S. Paulukaitis, J. J. Day, D. M. Etikala and J. D. Sweatt, "Histone H2A.Z subunit exchange controls consolidation of recent and remote memory," *Nature*, vol. 515, p. 582–586, 2014.

[53] G. Stefanelli, A. B. Azam, B. J. Walters, M. A. Brimble, C. P. Gettens, P. Bouchard-Cannon, H.-Y. M. Cheng, A. M. Davidoff, K. Narkaj, J. J. Day, A. J. Kennedy and I. B. Zovkic, "Learning and Age-Related Changes in Genome-wide H2A.Z Binding in the Mouse Hippocampus," *Cell Reports*, vol. 22, p. 1124–1131, 2018.

[54] D. Bano, A. Piazzesi, P. Salomoni and P. Nicotera, "The histone variant H3.3 claims its place in the crowded scene of epigenetics," *Aging*, vol. 9, p. 602-614, 2017.

[55] D. C. Kraushaar, W. Jin, A. Maunakea, B. Abraham, M. Ha and K. Zhao, "Genome-wide incorporation dynamics reveal distinct categories of turnover for the histone variant H3.3," *Genome Biology*, vol. 14:10, 2013.

[56] David Michod, S. Bartesaghi, A. Khelifi, C. Bellodi, L. Berliocchi, P. Nicotera and P. Salomoni, "Calcium-Dependent Dephosphorylation of the Histone Chaperone DAXX Regulates H3.3 Loading and Transcription upon Neuronal Activation," *Neuron*, vol. 74, p. 122–135, 2012.

[57] A. E. Lepack, R. C. Bagot, C. J. Peña, Y.-H. E. Loha, L. A. Farrelly, Y. Lu, S. K. Powell, Z. S. Lorsch, O. Issler, H. M. Cates, C. A. Tamminga, H. Molina, L. Shen, E. J. Nestler and C. D. Allis, "Aberrant H3.3 dynamics in NAc promote vulnerability to depressive-like behavior," *PNAS*, vol. 113, p. 12562–12567, 2016.

[58] D. Wen, K.-M. Noh, A. D. Goldberg, C. D. Allis, Z. Rosenwaks, S. Rafii and L. A. Banaszynski, "Genome Editing a Mouse Locus Encoding a Variant Histone, H3.3B, to Report on its Expression in Live Animals," *Genesis*, vol. 52, p. 959–966, 2014.

[59] M. Bachu, T. Tamura, C. Chen, A. Narain, V. Nehru, N. Sarai, S. B. Ghosh, A. Ghosh, R. Kavarthapu, M. L. Dufau and K. Ozato, "A versatile mouse model of epitope-tagged histone H3.3 to study epigenome dynamics," *Journal of Biological Chemistry*, vol. 294, p. 1904–1914, 2019.

[60] A. G. McNally, S. G. Poplawski, B. A. Mayweather, K. M. White and T. Abel, " Characterization of a Novel Chromatin Sorting Tool Reveals Importance of Histone Variant H3.3 in Contextual Fear Memory and Motor Learning," *Frontiers in Molecular Neuroscience*, vol. 9:11, 2016.

[61] W. Renthal and E. J. Nestler, "Histone acetylation in drug addiction," *Seminars in Cell & Developmental Biology*, vol. 20, p. 387–394, 2009.

[62] M. E. Wimmer, B. Fant, S. E. Swinford-Jackson, A. Testino, D. V. Nest, T. Abel and R. C. Pierce, "H3.3 Barcoding of Nucleus Accumbens Transcriptional Activity Identifies Novel Molecular Cascades Associated with Cocaine Self-administration in Mice," *The Journal of Neuroscience*, vol. 39, p. 5247–5254, 2019.

[63] H. v. Praag, G. Kempermann and F. H. Gage, "Neural Consequences of Environmental Enrichment," *Nature Reviews*, vol. 1, p. 191-198, 2000.

[64] L. Baroncelli, C. Braschi, M. Spolidoro, T. Begenisic, A. Sale and L. Maffei, "Nurturing brain plasticity: impact of environmental enrichment," *Cell Death and Differentiation*, vol. 17, p. 1092–1103, 2010.

[65] A. J. Barker and E. M. Ullian, "Astrocytes and Synaptic Plasticity," *The Neuroscientist*, vol. 16, p. 40-50, 2010.

[66] M. W. Salter and S. Beggs, "Sublime microglia: expanding roles for the guardians of the CNS," *Cell,* vol. 158, p. 15-24, 2014.

[67] N. Villacampa and M. T. Heneka, "Microglia: You'll Never Walk Alone!," *Immunity,* vol. 48, p. 195-197, 2018.

[68] U.-K. Hanisch and H. Kettenmann, "Microglia: active sensor and versatile effector cells in the normal and pathologic brain," *Nature Neuroscience,* vol. 10, p. 1387-1394, 2007.

[69] L. L. Williamson, A. Chao and S. D. Bilbo, "Environmental enrichment alters glial antigen expression and neuroimmune function in the adult rat hippocampus," *Brain, Behavior, and Immunity,* vol. 26, p. 500–510, 2012.

[70] D. Ehninger and G. Kempermann, "Regional Effects of Wheel Running and Environmental Enrichment on Cell Genesis and Microglia Proliferation in the Adult Murine Neocortex," *Cerebral Cortex,* vol. 13, p. 845–851, 2003.

[71] J. A. Hill Jr, M. Zoli, J. P. Bourgeois and J. P. Changeux, "Immunocytochemical localization of a neuronal nicotinic receptor: the beta 2-subunit," *Journal of Neuroscience,* vol. 13, p. 1551-1568, 1993.

[72] A. Cintra, M. Zoli, L. Rosén, L. F. Agnati, S. Okret, A. C. Wikström, J. A. Gustaffsson and K. Fuxe, "Mapping and computer assisted morphometry and microdensitometry of glucocorticoid receptor immunoreactive neurons and glial cells in the rat central nervous system," *Neuroscience,* vol. 62, p. 843-897, 1994.

[73] M. Zoli, F. Ferraguti, J. A. Gustafsson, G. Toffano, K. Fuxe and L. F. Agnati, "Selective reduction of glucocorticoid receptor immunoreactivity in the hippocampal formation and central amygdaloid nucleus of the aged rat," *Brain Research,* vol. 545, p. 199-207, 1991.

[74] G. Rigillo, A. Vilella, C. Benatti, L. Schaeffer, N. Brunello, J. M. C. Blom, M. Zoli and F. Tascedda, "LPS-induced histone H3 phospho(Ser10)-acetylation(Lys14) regulates neuronal and microglial neuroinflammatory response," *Brain, Behavior and Immunity,* vol. 74, p. 277-290, 2018.

[75] A. Vilella, G. Tosi, A. M. Grabrucker, B. Ruozi, D. Belletti, M. A. Vandelli, T. M. Boeckers, F. Forni and M. Zoli, "Insight on the fate of CNS-targeted nanoparticles. Part I: Rab5-dependent cell-specific uptake and distribution," *Journal of Controlled Release,* vol. 174, p. 195-201, 2014.

[76] A. Zanardi, R. Ferrari, G. Leo, U. Maskos, J. P. Changeux and M. Zoli, "Loss of high-affinity nicotinic receptors increases the vulnerability to excitotoxic lesion and decreases the positive effects of an enriched environment," *FOSEB Journal,* vol. 21, p. 4028-4037, 2007.

[77] M. Grilli, S. Zappettini, A. Zanardi, F. Lagomarsino, A. Pittaluga, M. Zoli and M. Marchi, "Exposure to an enriched environment selectively increases the functional response of the pre-synaptic NMDA receptors

which modulate noradrenaline release in mouse hippocampus," *Journal of Neurochemistry,* vol. 110, p. 1598-1606, 2009.

[78] J. F. De Backer, S. Monlezun, B. Detraux, A. Gazan, L. Vanopdenbosch, J. Cheron, G. Cannazza, S. Valverde, L. Cantacorps, M. Nassar, L. Venance, O. Valverde, P. Faure, M. Zoli, O. De Backer, D. Gall, S. N. Schiffmann and A. de Kerchove d'Exaerde, "Deletion of Maged1 in mice abolishes locomotor and reinforcing effects of cocaine," *EMBO Reports,* vol. 19:9.

[79] L. Zanetti, A. de Kerchove D'Exaerde, A. Zanardi, J. P. Changeux, M. R. Picciotto e M. Zoli, «Inhibition of both alpha7* and beta2* nicotinic acetylcholine receptors is necessary to prevent development of sensitization to cocaine-elicited increases in extracellular dopamine levels in the ventral striatum,» *Psychopharmacology,* vol. 187, p. 181-188, 2006.

[80] D. Keller, C. Erö and H. Markram, "Cell Densities in the Mouse Brain: A Systematic Review," *Frontiers in Neuroanatomy,* vol. 12:83, 2018.

[81] X. Xu, K. D. Roby and E. M. Callaway, "Immunochemical characterization of inhibitory mouse cortical neurons: Three chemically distinct classes of inhibitory cells," *Journal of Comparative Neurology,* vol. 518, p. 389–404, 2010.

[82] B. Cauli, X. Zhou, L. Tricoire, X. Toussay and J. F. Staiger, "Revisiting enigmatic cortical calretinin-expressing interneurons," *Frontiers in Neuroanatomy,* vol. 8:52, 2014.

[83] C. Jin and G. Felsenfeld, "Nucleosome stability mediated by histone variants H3.3 and H2A.Z," *Genes & Development,* vol. 21, p. 1519-1529, 2007.

[84] P. A. Gajewski, G. Turecki and A. J. Robison, "Differential Expression of FosB Proteins and Potential Target Genes in Select Brain Regions of Addiction and Depression Patients," *PLoS ONE,* vol. 11:8, 2016.

[85] I. B. Zovkic and J. D. Sweatt, "Memory-Associated Dynamic Regulation of the ‘‘Stable’’ Core of the Chromatin Particle," *Neuron,* vol. 87, p. 1-4, 2015.

[86] L. M. Foley, A. M. I. O'Meara, S. R. Wisniewski, T. K. Hitchens, J. A. Melick, C. Ho, L. W. Jenkins and P. M. Kochanek, "MRI assessment of cerebral blood flow after experimental traumatic brain injury combined with hemorrhagic shock in mice," *Journal of Cerebral Blood Flow & Metabolism,* vol. 33, p. 129-136, 2013.

[87] H. Lei, Y. Pilloud, A. W. Magill and R. Gruetter, "Continuous arterial spin labeling of mouse cerebral blood flow using an actively-detuned two-coil system at 9.4T," *2011 Annual International Conference of the IEEE Engineering in Medicine and Biology Society,* p. 6993-6996, 2011.

[88] S. H. Han, J. H. Cho, H. S. Jung, J. Y. Suh, J. K. Kim, Y. R. Kim, G. Cho and H. Cho, "Robust MR assessment of cerebral blood volume and mean vessel size using SPION-enhanced ultrashort echo acquisition," *Neuroimage,* vol. 112, p. 382-389, 2015.

[89] K. Maeda, G. Mies, L. Oláh and K. A. Hossmann, "Quantitative measurement of local cerebral blood flow in the anesthetized mouse using intraperitoneal [14C]iodoantipyrine injection and final arterial heart blood sampling," *Journal of Cerebral Blood Flow & Metabolism,* vol. 20, p. 10-14, 2000.

[90] T. A. Zolnik and B. W. Connors, "Electrical synapses and the development of inhibitory circuits in the thalamus," *Journal of Physiology,* vol. 594, p. 2579-2592, 2016.

[91] H. W. Lee, S. H. Yang, J. Y. Kim and H. Kim, "The Role of the Medial Habenula Cholinergic System in Addiction and Emotion-Associated Behaviors," *Frontiers in Psychiatry,* vol. 10:100, 2019.

[92] R. M. Seaberg and D. van der Kooy, "Adult Rodent Neurogenic Regions: The Ventricular Subependyma Contains Neural Stem Cells, But the Dentate Gyrus Contains Restricted Progenitors," *Journal of Neuroscience,* vol. 22, p. 1784-1793, 2002.

[93] G.-l. Ming and H. Song, "Adult Neurogenesis in the Mammalian Brain: Significant Answers and Significant Questions," *Neuron,* vol. 70, p. 687–702, 2011.

[94] G. G. Viola, L. Rodrigues, J. C. Américo, G. Hansel, R. S. Vargas, R. Biasibetti, A. Swarowsky, C. A. Gonçalves, L. L. Xavier, M. Achaval, D. O. Souza and O. B. Amaral, "Morphological changes in hippocampal astrocytes induced by environmental enrichment in mice," *Brain Research,* vol. 1274, p. 47-54, 2009.

[95] K. W. Lee, Y. Kim, A. M. Kim, K. Helmin, A. C. Nairn and P. Greengard, "Cocaine-induced dendritic spine formation in D1 and D2 dopamine receptor-containing medium spiny neurons in nucleus accumbens," *PNAS,* vol. 103, p. 3399-3404, 2006.

[96] C. Baimel, L. M. McGarry and A. G. Carter, "The Projection Targets of Medium Spiny Neurons Govern Cocaine-Evoked Synaptic Plasticity in the Nucleus Accumbens," *Cell Reports,* vol. 28, p. 2256–2263, 2019.

[97] J. Bertran-Gonzalez, C. Bosch, M. Maroteaux, M. Matamales, D. Hervé, E. Valjent and J. A. Girault, "Opposing patterns of signaling activation in dopamine D1 and D2 receptor-expressing striatal neurons in response to cocaine and haloperidol," *Journal of Neuroscience,* vol. 28, p. 5671-5685, 2008.

[98] R. J. Smith, M. K. Lobo, S. Spencer and P. W. Kalivas, "Cocaine-induced adaptations in D1 and D2 accumbens projection neurons (a dichotomy not necessarily synonymous with direct and indirect pathways)," *Current Opinion in Neurobiology,* vol. 23, p. 546–552, 2013.

[99] D. P. Melters, J. Nye, H. Zhao and Y. Dalal, "Chromatin Dynamics in Vivo: A Game of Musical Chairs," *Genes (Basel),* vol. 6, p. 751-776, 2015.

[100] C. Huang and B. Zhu, "H3.3 turnover: A mechanism to poise chromatin for transcription, or a response to open chromatin?," *Bioessays,* vol. 36, p. 579-584, 2014.

AKNOWLEDGEMENTS

I would like to express my sincere gratitude to my tutor, Professor Michele Zoli, for giving me the chance to work in his research group and for guiding me with his knowledge and experience. A special thank to my co-relator (and Yoda master) Dr. Antonietta Vilella for helping and supporting me throughout my doctoral studies; she has been a friend and an inspiration. Thank you to all the people like Dr. Nàdia Villacampa and Dr. Amandine Cornil, and especially to Dr. Edwige Belotti, who helped me carry out my thesis project. I would also like to thank all the girls from the Lab, and Paolo, for all the fun, laughs and memories. And finally, to my great and supportive family, to my friends and to my Chimichanga, thank you, for everything.

"I feel a very unusual sensation - if it is not indigestion, I think it must be gratitude"

~ Benjamin Disraeli ~